The Dissertation Committee for Allison Paige Myers certifies that this is the approved version of the following dissertation:

Solution Characterization and Fabrication of Hydrogel Microstructures on an Optical Fiber

Committee:

Jason B. Shear, Supervisor

Jennifer S. Brodbelt

Lauren J. Webb

Keith J. Stevenson

Solution Characterization and Fabrication of Hydrogel Microstructures on an Optical Fiber

by

Allison Paige Myers

Dissertation

Presented to the Faculty of the Graduate School of

The University of Texas at Austin

in Partial Fulfillment

of the Requirements

for the Degree of

Doctor of Philosophy

The University of Texas at Austin

December 2018

Dedication

I dedicate this dissertation to Wayne Beeson, my chemistry teacher at Olympia High School. You taught me to love chemistry in 10^{th} grade, and I haven't looked back since. Without you, this dissertation may have never happened, and I cannot thank you enough.

Acknowledgements

I would like to thank my advisor, Dr. Jason Shear, for encouraging and allowing me the freedom and independence to adapt our fabrication technique to a new platform. I would also like to thank my committee members, Drs. Jennifer Brodbelt, Lauren Webb, and Keith Stevenson for their advice and collaboration throughout my time in graduate school. Thank you to fellow members of the Shear Lab, past and present, for sharing their knowledge and time with me, including Drs. Mike Robinson, Derek Hernandez, Maryam Ali, Janine Elliott, and current lab member Olja Simoska. Special thanks go to Mindy Fitzpatrick, for being a steadfast friend and supporter since we started grad school together, without you this experience would have been infinitely more difficult. A number of people behind the scenes also deserve significant recognition for their help in keeping lab, research, and life in general running smoothly, including Marvin Whiteley, Tim Hooper, Dwight Romanovicz, Betsy Hamblen, Danielle Nestler, Ann Harosimowitz, and building manager extraordinaires Steve Moore and Cory Konieczny. To Dr. Jim Holcombe, thank you for your guidance, mentorship, and therapeutic rounds of golf. To Natalie Czimskey, for being my writing partner in this crazy dissertation journey and adopting me into the Texas Drums football family. I would also like to give special thanks to Christie Harriss Applewhite, Dr. Jim Masson, Dr. Jennifer Shannon, and Dr. Priscilla Sierk - without your help and support I wouldn't be where I am today. Lastly, thank you to my parents, Garry and Doreen Myers, and my brother, Jeff Myers, for always cheering me on with as much voracity as we cheer on the Seattle Seahawks. I love you.

Abstract

Solution Characterization and Fabrication of Hydrogel Microstructures on an Optical Fiber

Allison Paige Myers, PhD

The University of Texas at Austin, 2018

Supervisor: Jason B. Shear

Sociomicrobiology has recently come to the forefront of bioanalytical research, primarily due to its physiological impact in the medical field. The interaction of bacterial cells in small, dense populations can reveal emergent properties of microbial communities, such as increased virulence and pathogenicity, as well as create a more accurate model for bacterial behavior in natural environments. Such systems are particularly relevant in mono- and polymicrobial communities, which exhibit social behaviors as well as the potential for symbiotic and/or adversarial interactions between species. The standard techniques for culturing bacteria lack the tools to provide adequate control over polymicrobial organization on a microscopic scale or to evaluate the spatiotemporal dynamics of bacterial interactions. Using our previously developed micro-3D printing platform, we can arrange cells in biocompatible, pico-liter sized containers, allowing us to overcome these prior spatial limitations. However, key questions still exist regarding the dynamics of

interactions between distinct cellular populations. This dissertation focuses on the development of a modified micro-3D printing platform that enables us to fabricate protein-based structures around bacteria on the tip of a moveable substrate. Fabricating structures on moveable substrates such as a glass rod or optical fiber allows us to precisely tune where bacterial clusters are located in relation to varying stimuli and enables delivery of fabricated structures to remote environments such as chronic wounds. However, several challenges were faced in the development of this technique, such as optimization of fabrication solutions, successful layering of hydrogels of varying composition on glass rods, and creation of a custom-built fabrication setup for fabrication on optical fiber tips. Development of these techniques enables us to better appreciate the intricacies of sociomicrobial behavior and interactions, allowing for a better understanding of microbial responses leading to antibiotic resistance, and directing a better approach towards the treatment of various microbial infections.

Table of Contents

List of Tables

List of Figures

Chapter 1: Introduction

1.1 SOCIOMICROBIOLOGY

Sociomicrobiology is a field that has become of primary interest to many researchers, largely due to its implication in certain illnesses and physiological complications such as cystic fibrosis (CF), [1-2] nosocomial infections, [3-5] and antibiotic resistance. [6-12] Through the production, release, and uptake of various signaling molecules, bacteria within small, highly dense populations (≥ 150 cells) can engage quorum sensing (QS), [13] a density-dependent process during which phenotypic changes lead to increased pathogenicity. [2, 6, 14-16] More specifically, QS is a process that initiates the regulation of bacterial gene expression through diffusible molecules known as autoinducers, or AIs for short. [17] Upon interaction between these diffusible molecules and bacterial receptor proteins, genes that typically remain dormant in low-density populations become expressed, triggering global phenotypic changes that can manifest themselves as resistance to immune-cell attack, [18-20] antibiotic resistance, [21-22] etc. A visual representation of QS can be seen in Figure 1.1, with common QS molecules for the bacterium studied in this dissertation, *Pseudomonas aeruginosa*, depicted in Figure 1.2.

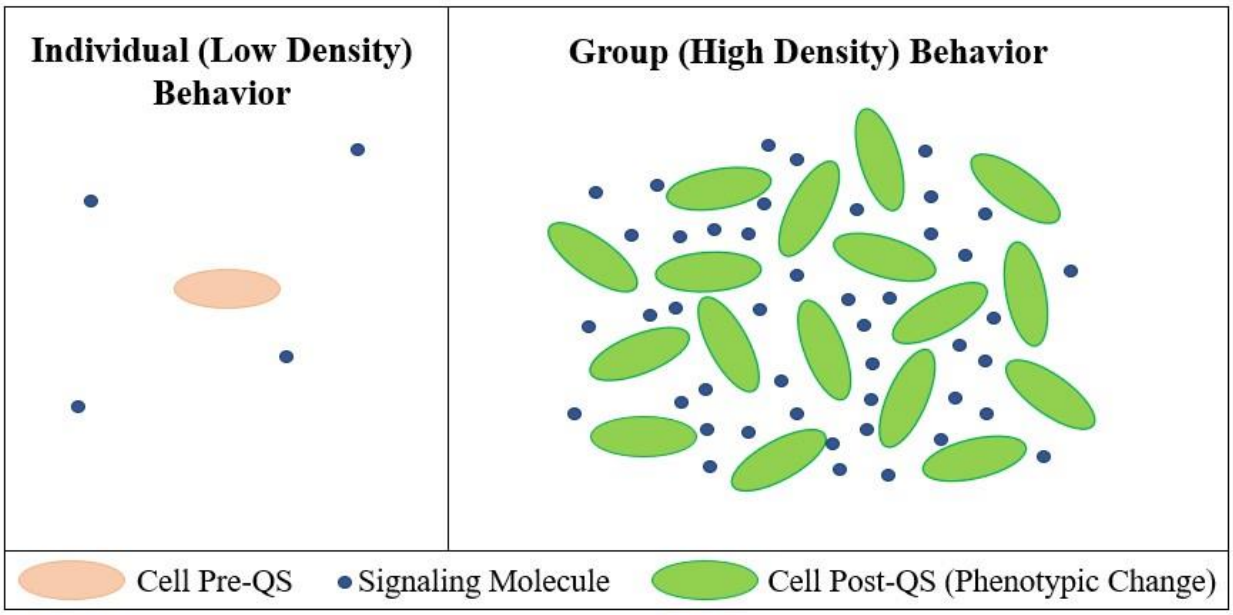

Figure 1.1: Illustrated Representation of Quorum Sensing

Quorum sensing is the process through which bacteria undergo intra- and interspecies communication. [17] Through the production, release, and uptake of various signaling molecules, bacteria can respond to population density of their own bacterial cluster, or that of a neighboring colony. When a bacterial colony has reached a high enough density, the colony as a whole undergoes phenotypic changes. This is represented schematically with the single peach-colored bacterium becoming green as a result of differential gene regulation when integrated into a high-density population. This allows a dense group of bacteria to act as a whole, rather than many individual cells.

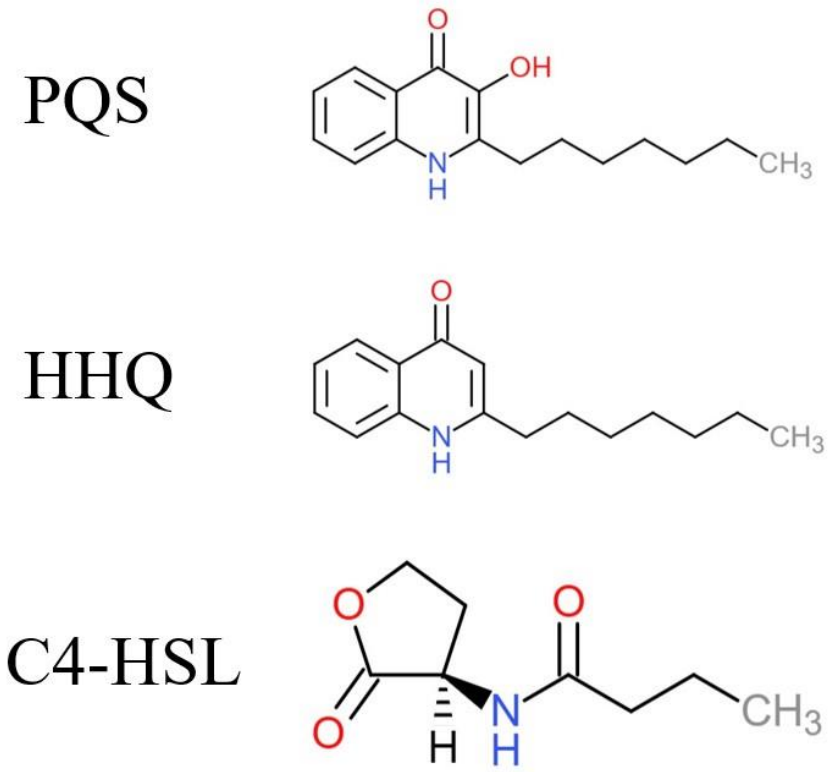

Figure 1.2: Common *P. aeruginosa* QS Molecules

Common QS molecules for the opportunistic pathogen *P. aeruginosa*. Pseudomonas Quinolone Signal (PQS) and its precursor 2-heptyl-4-quinolone (HHQ) have been implicated in the suppression of host immune systems, thus increasing the bacterium's pathogenicity. [23] N-butanoyl-L-homoserine lactone (C4-HSL) is implicated in biofilm formation. [24]

P. aeruginosa is an opportunistic pathogen commonly implicated in ailments such as cystic fibrosis, bacterial pneumonia, and hospital-acquired infections. [1, 3-8] QS pathways commonly used by *P. aeruginosa* have been well documented, [2] giving a basis of understanding for what small molecules are used in both intra- and interspecies communication. These factors, combined with the ease with which green fluorescence

protein (GFP) can be inserted into the cell's genetic code (allowing use of fluorescence microscopy), make it an ideal organism for the studies presented in this dissertation.

Understanding the mechanism by which signaling molecules mediate the onset and progression of QS requires new technologies for controlling the size, shape, and organization of microscopic cellular communities in vitro. Traditional culturing techniques, such as macro-scale plate and batch-liquid methods, remain the standard methods used in microbiology labs. However, due to their macroscopic scales, these methods lack the ability to precisely control the organization of bacterial colonies. Consequently, this limits their clinical relevance in characterizing the onset of bacterial infections, which are often initiated by clusters of bacteria organized in small, highly dense ($>10^8$ cells/mL) aggregates. [11] Additionally, these traditional cell culturing methods are unable to precisely control the distance between two discrete colonies, a parameter that may play key roles in the propagation of cellular group behaviors. [12]

Bacteria are known to engage in both synergistic and adversarial behaviors when located in close proximity to other bacterial species and/or eukaryotic, host cells. [3-5, 11-12, 25-29] To examine this, the Shear lab previously studied and reported that small aggregates of *Staphylococcus aureus*, a gram-positive bacterium known for its high responsivity to ampicillin, derives large protective advantages when embedded in dense populations of gram-negative, ampicillin-resistant *P. aeruginosa*. [28] However, these same species quickly engage in competition when grown together in planktonic culture, with *P. aeruginosa* rapidly killing off *S. aureus*. [29] *P. aeruginosa* engages in chemical

warfare against species competing for the same resources, lysing competing cells through production and release of various bacterial toxins, including pyocyanin. [30-33] While the importance of such interactions is well known, key questions still exist regarding the relationships between both the composition and spatial organization of complex bacterial communities and the importance of different types of social interactions.

A number of technological advantages in bacterial culture have been used to investigate polymicrobial interactions on a systematic and physiologically relevant level. Microfluidic strategies have been used to evaluate signaling capabilities between bacterial aggregates, as well as investigate the action of chemotactic factors towards microbial environments. For example, a microfluidic platform to study spatial organization within a bacterial monoculture was created using flow cells of different geometries. [34] While these studies provide valuable information regarding the self-organization capabilities of bacteria, they are limited with regards to closely representing real biological environments. Chemical interactions between multiple microbial species have also been examined, including studies in which colonies of different species were physically isolated in adjacent flow cells in an arrangement that permitted chemical communication between cells. [35-37] By allowing cells to communicate while maintaining physical isolation of each species, interspecies competition over nutrients and resources can be avoided, which creates a more realistic representation of how bacteria interact in non-artificial environments.

Although such platforms have enabled more detailed studies of some key variables influencing bacterial interactions on microscopic scales, these systems do not provide

capabilities for systematically characterizing bacterial social behaviors. Flow cells of varying geometry can be constructed, but do not provide the precise, spatiotemporal control needed to understand the response dynamics of defined, ultralow volume bacterial populations. Additionally, most microfluidic and hydrogel platforms employ materials of low physiological relevance, such as PDMS. While these materials are generally biocompatible, in that they do not cause visible cellular damage, they lack key chemical and physical properties of many natural environments. [35-37] To address these limitations, the Shear lab has reported a strategy for investigating bacterial interactions based on a micro-3D printing technique that enables fabrication of microscale structures around bacteria of interest using a photocrosslinkable protein matrix. These structures are biocompatible and porous in nature, allowing for the diffusion of solutes such as nutrients, waste products, and signaling molecules. Therefore, this technology can be used to create *in vitro* microbial models that more closely mimic physiological conditions. [38]

1.2 MULTIPHOTON LITHOGRAPHY

1.2.1 Multiphoton Excitation

The micro-3D printing technique mentioned previously utilizes mask directed multiphoton lithography. [38] Multiphoton lithography (MPL) is dependent on non-linear multiphoton excitation, or the nearly simultaneous excitation of two or more low-energy photons, as depicted in Figure 1.3.

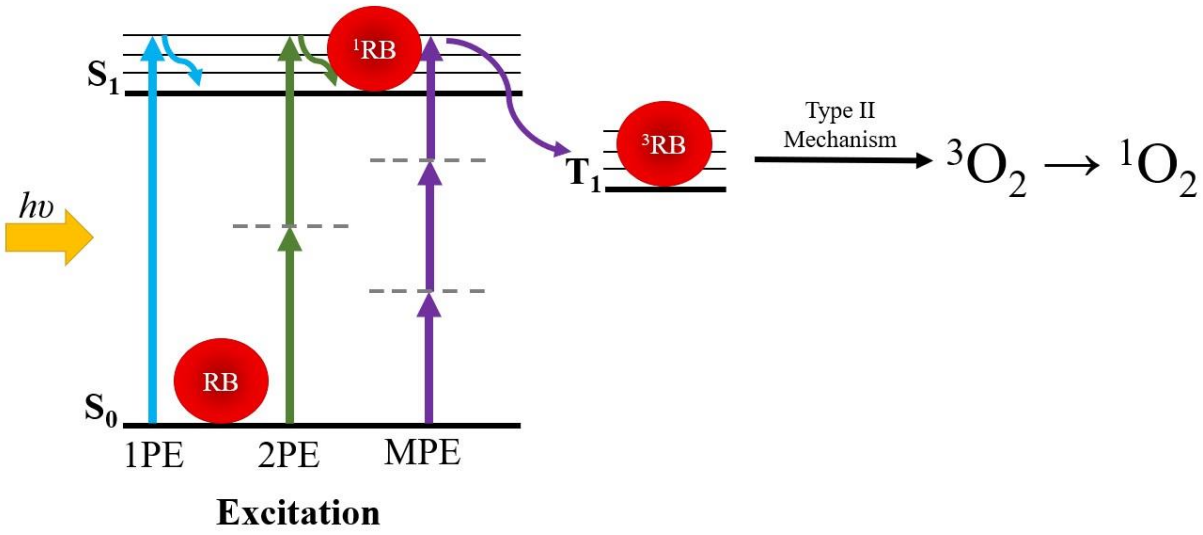

Figure 1.3: Jablonski Diagram Showing Progression of Single to Multiphoton Excitation and Relation to Rose Bengal's Excitation and Production of Singlet Oxygen

Multiphoton excitation occurs upon the near-simultaneous absorption of two or more photons. Compared to single photon excitation (1PE), in which a single photon bridges the entire energy gap between S_0 and S_1, two photon excitation (2PE) and, more generally, multiphoton excitation (MPE; involves two or more photons) traverse the energy gap in an additive manner. For example, absorption of two photons can traverse the energy gap provided that each photon has half the required energy and satisfies relevant two-photon selection rules. Commonly, this process is represented as a photon passing through a "virtual" state, as depicted by gray dotted lines, which exist for periods of time on the femtosecond scale. Through this process the photosensitizer Rose Bengal is also excited from S_0 to S_1, indicated by the progression of RB to ^{1}RB. Then, ^{1}RB undergoes intersystem crossing to the T_1 level, after which ^{3}RB catalyzes a Type II mechanism required to generate the singlet oxygen necessary to facilitate protein photocrosslinking.

For multiphoton absorption to occur, two or more photons must interact with a chromophore within femtosecond time frames, making the phenomena extremely rare under normal conditions. [39] However, this probability can be significantly increased through the use of a pulsed, femtosecond laser and an objective of high numerical aperture

(NA), which in combination allow for spatiotemporal focusing of discrete, extremely high-intensity packets of photons within a three-dimensional volume (~1 μm^3) centered around the laser focal point. Due to the nature of this process, extremely high instantaneous intensities (~10^{11} W cm^{-2}) can be generated using a time-averaged laser power of tens of milliwatts.

Unlike single photon absorption, in which molecules are excited equally in each plane along the entire optical axis (assuming low optical densitites), multiphoton absorption results in localized excitation of molecules at the focal point, thus constraining the MPL process to take place in a highly localized 3D position. The photonic absorption mechanism can be described analogously to a chemical reaction using Equation 1.1, in which *M* and *M** represent the ground and excited states of the molecule, *hν* represents a photon, and *n* represents the number of photons absorbed to bridge the gap from ground to excited state.

$$M + n(h\nu) \leftrightharpoons M^* \qquad \text{(Eqn. 1.1)}$$

The rate of reaction for the formation M* is described using Equation 1.2, a derivation in which *k* represents the rate constant, *I* is instantaneous intensity of the excitation light (photons s^{-1} cm^{-2}), and δ is the excitation cross-section ($cm^{2n}(s/photon)^{n-1}$).

$$\frac{d[M^*]}{dt} = k[h\nu]^n[M] = \delta I^n[M] \qquad \text{(Eqn. 1.2)}$$

1.2.2 MPL of Biocompatible Substrates

Biocompatible hydrogel substrates have been utilized in a wide variety of multiphoton lithography applications. [40-42] For biological applications, proteins capable of undergoing natural and photosensitizer-mediated photocrosslinking reactions are natural candidates for MPL. Prior studies exploiting these properties have included proteins such as bovine serum albumin, [41-43] avidin, [44] and fibronectin [45]. Following excitation photosensitizers release energy and catalyze reactions via two mechanisms, Type I, in which the photosensitizer interacts with the substrate to produce free radicals, or Type II, where the photosensitizer produces singlet oxygen. Both mechanisms facilitate crosslinking of oxidizable protein residues. [46]

The Shear lab has developed a dynamic, mask-based lithography technique for 3D printing of these biocompatible protein hydrogel substrates. [38] A simplified schematic of this technique is depicted in Figure 1.4. A more detailed explanation and schematic of the micro-3D printing process can be found in Section 2.2.5 of this dissertation.

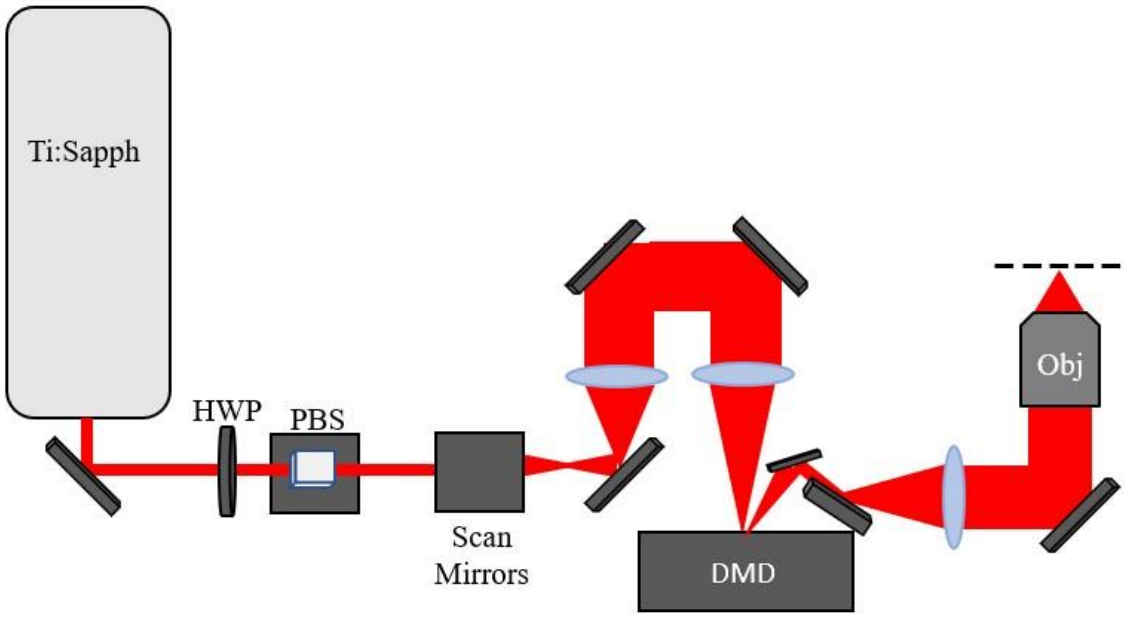

Figure 1.4: Simplified Schematic of Dynamic, Mask-Based MPL

The output of a 5W pump laser is directed into a titanium sapphire (Ti:Sapph) cavity, allowing the beam to be mode-locked and tuned to 740 nm. Upon exiting the Ti:Sapph cavity, the beam is attenuated using a half wave plate (HWP) and polarizing beam splitter (pBS) before being focused, collimated, and directed using a series of mirrors and lenses. Here, the beam is directed to a pair of scan mirrors, which is focused on and raster scanned across the face of a digital micromirror device (DMD) displaying a dynamic mask. As the beam exits the DMD, it passes through an additionally series of lenses and mirrors to expand and overfill the back aperture of a high numerical aperture (NA) objective. Fabrication occurs at the focal point of the objective, which is positioned in a plane conjugate to the DMD plane, identified by the dotted line. This configuration allows patterns displayed on the DMD to be transferred in a one-to-one correspondence as an exposure pattern at the objective focal plane.

Previous members of the Shear lab have utilized micro-3D printing to precisely organize polymicrobial communities within pico-liter sized containers that provide physiologically and clinically relevant chemical and physical growth conditions. [8] The platform has

provided new capabilities for examining the role of spatial factors on various bacterial responses, including the onset of QS, [13] antibiotic resistance, [14] polymicrobial interactions, [28] and creation of and response to oxygen limitation. [47]

1.3 Hydrogel Properties and Use in Fabrication

The term "hydrogel" describes a water-rich substrate, often composed of polymeric networks with strong hydrophilic properties. These hydrophilic properties commonly stem from hydrophilic functional groups located along a polymeric backbone, which allow for absorption of water into the substrate. [48] Hydrogels can be divided into two categories, natural and synthetic. Synthetic polymers are composed of materials such as polyethylene glycol (PEG), [49-51] while natural hydrogels are derived from biological substances including proteins and polysaccharides such as collagen, [52] alginate, [53] and BSA. [38, 43, 54] Many hydrogels also have highly tunable physical and chemical properties, allowing substrates to be manipulated via exposure to elements such as light [55] or heat. [14, 56]

In hydrogel studies incorporating living organisms, natural hydrogels are often employed to maintain strong biomimetic properties. Hydrogels can be fabricated from materials derived from both plants [57] and animals [54] and have been used to create substrates with high biocompatibility and functionality for a wide range of both mammalian [58-59] and bacterial cells. [8, 11, 14, 28] These properties also make them ideal candidates for tissue engineering applications. [60-62] As discussed in the previous section, it is possible to fabricate hydrogels using MPL via crosslinked mediated by a photosensitizer. In an early demonstration, Pitts *et al*. used multiphoton lithography to fabricate protein substrates into submicron, free-form structures such as pyramids and microchannels. These studies utilized a femtosecond Ti:Sapph cavity pumped by an argon ion laser, which was then directed into a laser scanning confocal microscope with an

average fabrication power of 120 mW. Structures were fabricated out of BSA and fibrinogen, with Rose Bengal acting as a photosensitizer. While structures were successfully fabricated using both protein substrates, Pitts *et al.* could only hypothesize as to what the protein's reactive species was, concluding that tryptophan, tyrosine, and histidine residues appeared most advantageous for cross-linking purposes. [63]

Within the past decade, the Shear lab has used MPL of hydrogels almost exclusively for cell-based studies. In 2008, Drs. Rex Nielson and Bryan Kaehr developed a dynamic-mask-based multiphoton lithography technology has formed the basis of this work. By integrating an automated, dynamic mask into the fabrication setup, lithography transitioned from being a time-intensive technique to a rapid process capable of building complex cellular scaffolds with submicron features within minutes. [38] This increase in fabrication speed is especially important in cellular studies, during which exposure to cytotoxic elements such as activated photosensitizers should be kept to a minimum. Since the creation of this technique, members of the Shear lab have used naturally-derived hydrogels in the fabrication of microfluidic devices, [64] scaffolding for mammalian cell guidance, [65] and traps for the study of bacterial communities. [8, 13-14, 28, 47]

1.4 Application of Optical Fibers in Fabrication and Sensing

One critical limitation of the current micro-3D printing platform is the need to affix structures to static substrates, such as coverslips. Many bacteria are highly social with the ability to self-regulate and form complex polymicrobial communities. These polymicrobial communities require distinct spatial awareness from all bacterial species, as slight changes in distance between two neighboring microbial clusters could result in a behavioral shift from synergistic to adversarial. For example, *Aggregatibacter actinomycetemcomitans* and *Streptococcus gordonii* are two bacteria commonly found in close proximity within the oral cavity. This occurs as a result of *S. gordonii* producing the preferred carbon source for *A. actinomycetemcomitans*, L-lactate. However, *S. gordonii* also produces high levels of hydrogen peroxide (H_2O_2), commonly used in microbial chemical warfare. To maximize exposure to L-lactate while minimizing exposure to H_2O_2, *A. actinomycetemcomitans* has been shown to precisely position itself at an optimal distance of ~4 μm. [66]

Restriction of MPL to static substrates prevents studies from being conducted that might examine the role of dynamic positioning regarding clinically relevant bacterial aggregates, such as those in chronic wounds or suspended within the CF lung matrix. Without understanding how bacteria spatially orient themselves to create synergistic polymicrobial communities, there will continue to be a lack of knowledge over factors increasing virulence of polymicrobial infections. Thus, key questions remain regarding dynamic interactions between distinct cellular populations, as well how to integrate these structures into both *in vitro* and *in vivo* environments.

This dissertation proposes a solution for these limitations by extending our current micro-3D printing technology to enable fabrication of structures directly onto fiber tips, thus allowing us to precisely tune where clusters are in relation to varying stimuli, including those in remote environments. This expansion of the currently used technology provides a means to study the spatiotemporal interactions between distinct cellular populations through dynamic positioning of the fiber tip with regards to bacterial microclusters of interest.

Microfabrication on an optical fiber is not a new phenomenon, as techniques based on e-beam lithography, [67] etching, [68], and patterned photoresist [69] have been previously reported. The first published studies using two-photon lithography to fabricate materials on an optical fiber was reported in 2009 by Cojoc *et al*, [70] who reported fabrication of micro-optic structures (such as a convergent and axicon lens) using a piezo-stage and commercial UV curing adhesive. Advancements since this initial study in the use of MPL on optical fiber tips have included the use of mode field expansion for centering of fabricated structures on the fiber core, [71] as well as fabrication of antireflection gratings [72] and near-field probes [73] via nanoimprint lithography. In terms of multiphoton fabrication, most experimental techniques rely on photoresist for the polymerization of various 3D architectures. [74, 77] Although the fabrication of 3D structures on fiber tips has been demonstrated, this dissertation reports the first fabrication of biocompatible bacterial enclosures on the core of an optical fiber.

Optical fibers have also been used extensively in the field of biosensors, utilizing phenomena such as nanoplasmonics, photonic crystals, and SERS. [74] Sensors integrated onto the tip of the fiber have been of particular interest due to optical fibers' inherent ability to couple light and transmit information across long distances. Data transmission through an optical fiber is achievable through exploitation of total internal reflection. Total internal reflection is a phenomenon that occurs when light is travelling through one medium and approaches a medium of lesser refractive index. Instead of refracting through the interface into the neighboring medium, the light reflects internally. [75] With regards to optical fibers, this internal reflection allows data (transmitted as light) to remain within the fiber core for long distances with minimal signal attenuation, as depicted in Figure 1.5.

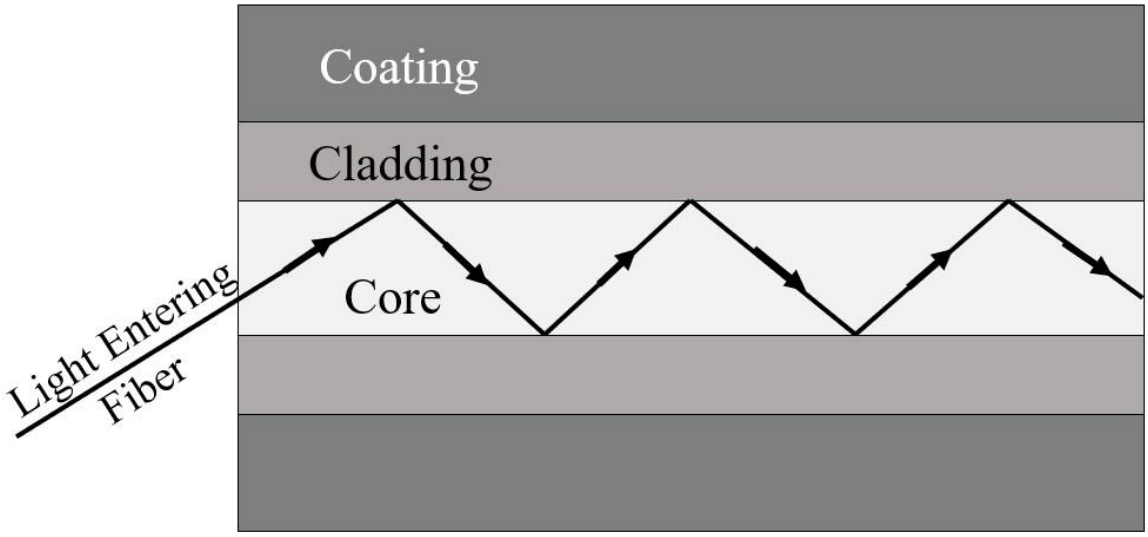

Figure 1.5: Simplified Schematic of Total Internal Reflection in Optical Fiber

An optical fiber is composed of three distinct layers, the core, cladding, and coating. The core is traditionally composed of silica, while the cladding is composed of silica doped with a low-loss dopant like germanium (GeO_2). [76] This doping results in the cladding possessing a lower refractive index than the core, facilitating total internal reflection of all light modes entering the core. Additionally, the low-loss characteristic of the dopant results in minimal attenuation of the light travelling down the core. To protect the two glass layers a protective coating is added, usually composed of a polymer such as acrylate.

Regarding the integration of fiber optics into biological sensing, most cell-based sensors have relied on complete cellular immobilization on the fiber tip. [78-80] While these advancements have successfully collected data in the form of transmitted cellular fluorescence, the process of immobilizing cells can result in significant changes in metabolic activity, potentially halting cell growth. Additionally, the matrices currently being used, such as calcium alginate, are susceptible to degradation and dissolution into the environment being studied. This is undesirable for many reasons, including

introduction of potentially pathogenic bacteria to *in vivo* or *in vitro* settings, as well as the need to repeatedly reinforce the sensing matrix. [78]

Thus far, these immobilization techniques have had little to no control over the density or distribution of sensing cells on the fiber tip. This creates inconsistencies from one sensor to the next, and limits how well sensors can mimic the small, highly dense bacterial aggregates required for QS. [13] This limits the ability to study how dynamic changes between two bacterial clusters of physiologically relevant size impact factors such as virulence and antibiotic resistance. Precise capture (rather than immobilization) of cells on a fiber tip will allow for *in vivo* and *in vitro* studies to occur without the threat of cross-contamination from the fiber to the system being studied. These studies may include, but are not limited to, dynamic distance studies within polymicrobial communities, perturbation of local environments without further infection, and real-time fluorescence and/or luminescence sensing using the data transmission capabilities inherent of optical fibers.

1.5 Overview of Chapters

This dissertation describes the characterization of hydrogels composed of varying concentrations of BSA, gelatin, and Rose Bengal (RB), and how these hydrogels can be customized for cell-based experiments. In Chapter 2, the relationship between gelatin concentration and melting temperature is determined, as well as cytotoxic effects of increasing amounts of RB towards a model organism, *Pseudomonas aeruginosa*. These studies allow hydrogels to be optimized for any cell-based experiment with regards to a cell's optimal growth temperature and susceptibility to photosensitizers. In Chapter 3, information from Chapter 2 is utilized to create hydrogels with markedly different melting temperatures, which are then layered and utilized for the controlled release of fabricated structures. Hydrogels are also optimized for fabrication on the core of an optical fiber in Chapter 4, allowing for reproducible fabrication of structures of different size and shape while maintaining biocompatibility with regards to the organism being studied, *P. aeruginosa*. This chapter details the transition from fabricating on a static coverslip to a deployable fiber tip, greatly expanding our ability to study bacterial interactions in remote environments. Lastly, Chapter 5 details future work that can build upon the research presented in this dissertation, including controlled release of recaptured of bacteria-containing structures to remote environments, spatiotemporal studies of polymicrobial interactions, and real-time sensing through the optical fiber of bacterial activity via fluorescence detection.

1.6 REFERENCES

1. Lopes, S.P., Azevedo, N.F., and Pereira, M.O. *Developing a model for cystic fibrosis sociomicrobiology based on antibiotic and environmental stress*. Int. J. Med. Microbio., 2017. **307**(8): p. 460-470.
2. Bjarnsholt, T., *et al. Quorum sensing and virulence of Pseudomonas aeruginosa during lung infection of cystic fibrosis patients*. PLoS One, 2010. **5**(4): p. 1-11.
3. Sancho, S., *et al*. *Impact of nosocomial polymicrobial bloodstream infections on the outcome in critically ill patients*. Euro. J. Clin. Microbio. Infec. Disease, 2012. **31**(8): p. 1791-1796.
4. Pittet, D., Li, N., and Wenzel, R.P. *Association of secondary and polymicrobial nosocomial bloodstream infections with higher mortality*. Euro. J. Clin. Microbio. Infec. Disease, 1993. **12**(11): p. 813-819.
5. Marra, A.R., Bearman. G.M.L., Wenzel, R.P., and Edmond, M.B. *Comparison of the systemic inflammatory response syndrome between monomicrobial and polymicrobial Pseudomonas aeruginosa nosocomial bloodstream infections*. BMC Infect. Diseases, 2005. **5**:94, p. 1-7.
6. Parsek, M.R. and Greenberg, E.P. *Sociomicrobiology; the connections between quorum sensing and biofilms.* Trends Microbiol., 2005. **13**: p. 27-33.
7. Lax, S. and Gilbert, J.A. *Hospital-associated microbiota and implications for nosocomial infections.* Trends in Molec. Med., 2015. **21**: p. 427-432.
8. Connell, J.L., Whiteley, M., and Shear, J.B. *Sociomicrobiology in engineered landscapes*. Nature Chem. Bio., 2012. **8**(1): p. 10-13.
9. Xavier, J.B. *Sociomicrobiology and pathogenic bacteria*. Microbiol. Spectrum, 2016. **4**(3): p. 89-101.
10. Mellbye, B. and Schuster, M. *The sociomicrobiology of antivirulence drug resistance: a proof of concept.* mBio, 2011. **2**(5): p. 1-4.
11. Wessel, A.K., Hmelo, L., Parsek, M.R., and Whiteley, M. *Going local: technologies for exploring bacterial microenvironments*. Nature Rev. Microbio., 2013. **11**(5): 337-348.
12. Stacy, A., Mcnally, L., Darch, S.E., Brown, S.P. and Whiteley, M. *The biogeography of polymicrobial infection.* Nature Rev. Microbio. Nature Rev., 2016. **14**: p. 93-105.
13. Connell, J.L., Kim, J., Shear, J.B., Bard, A.J., and Whiteley, M. *Real-time monitoring of quorum sensing in 3D-printed bacterial aggregates using scanning electrochemical microscopy.* PNAS, 2014. **111**(51): p. 18255-18260.

14. Connell, J.L., *et al. Probing prokaryotic social behaviors with bacterial "lobster traps."* mBio, 2010. **4**: p. 202-210.

15. Miller, M.B. and Bassler, B.L. *Quorum sensing in bacteria*. Ann. Rev. Microbio., 2001. **55**: p. 165-199.

16. Antunes, L.C.M., Ferreira, R.B.R., Buckner, M.M.C., and Finlay, B.B. *Quorum sensing in bacterial virulence*. Microbio., 2010. **156**: p. 2271-2282.

17. Khmel, I.A. *Quorum-sensing regulation of gene expression: fundamental and applied aspects and the role in bacteria communication*. Microbiol., 2006. **75**(4): p. 390-397.

18. Kariminik, A., Baseri-Salehi, M., and Kheirkhah, B. *Pseudomonas aeruginosa quorum sensing modulates immune responses: an updated review article*. Immun. Lett., 2017. **190**: p. 1-6.

19. Pritchard, D.I. *Immune modulation by Pseudomonas aeruginosa quorum-sensing signal molecules*. Int. J. Med. Microbio., 2006. **296**(2): p. 111-116.

20. Kim, K., *et al. HHQ and PQS, two Pseudomonas aeruginosa quorum-sensing molecules, down regulate the innate immune responses through the nuclear factor-κB pathway.* Immunology, 2010. **129**(4): p. 578-588.

21. Wang, H., Tu, F., Gui, Z., Lu, X., and Chu, W. *Antibiotic resistance profiles and quorum sensing-dependent virulence factors in clinical isolates of Pseudomonas aeruginosa*. Indian J. Microbio., 2013. **53**(2): 163-167.

22. Skindersoe, M.E., *et al. Effects of antibiotics on quorum sensing in Pseudomonas aeruginosa.* Antimicrobial Agents and Chemotherapy, 2008. **52**(10): p. 3648-3663.

23. Kim, K., *et al. HHQ and PQS, two Pseudomonas aeruginosa quorum-sensing molecules, down-regulate the innate immune responses through the nuclear factor-κB pathway.* Immunology, 2010. **129**(4): p. 578-588.

24. Favre-Bonte, S., Kohler, T., and Van Delden, C. *Biofilm formation by Pseudomonas aeruginosa: role of the C4-HSL cell-to-cell signal and inhibition by azithromycin.* J. Antimicrobial Chemotherapy, 2003. **52**(4): p. 598-604.

25. Ramsey, M.M. and Whiteley, M. *Polymicrobial interactions stiumulate resistance to host innate immunity through metabolite perception*. PNAS, 2009. **106**(5): p. 1578-1583.

26. Wong, M.J.Q., *et al. Microbial herd protection mediated by antagonistic interaction in polymicrobial communities.* Microb. Ecology, 2016. **82**(23): p. 6881-6888.

27. Pidwill, G.R., Rego, S., Jenkinson, H.F., Lamont, R.J. and Nobbs, A.H. *Coassociation between group B Streptococcus and Candida albicans promotes interactions with vaginal epithelium*. Infection and Immunity, 2018. **86**(4): p. 1-18.

28. Connell, J.L., Ritschdorff, E.T., Whiteley, M., and Shear, J.B. *3D printing of microscopic bacterial communities*. PNAS, 2013. **110**(46): p. 18380-18385.

29. DeLeon, S., *et al. Synergistic interactions of Pseudomonas aeruginosa and Staphylococcus aureus in an in vitro would model*. Infection and Immunity, 2014. **82**: p. 4718-4728.

30. Michie, K.L., Cornforth, D.M., and Whiteley, M. *Bacterial tweets and podcasts #signaling#eavesdropping#microbialfightclub.* Molec. Biochem. Parasit., **2016**. 208: p. 41-48.

31. Jayaseelan, S., Ramaswamy, D., Dharmaraj, S. *Pyocyanin: production, applications, challenges and new insights*. World J. Microbiol. Biotech., 2014. **30**(4): p. 1159-1168.

32. Castaneda-Tamez, P., *et al. Pyocyanin restricts social cheating in Pseudomonas aeruginosa.* Front. Microbiol., 2018. **9**: p. 1-10.

33. Elliott, J., Simoska, O., Karasik, S., Shear, J.B., and Stevenson, K.J. *Transparent carbon ultramicroelectrode arrays for the electrochemical detection of a bacterial warfare toxin, pyocyanin.* Anal. Chem., 2017. **89**(12): p. 6285-6289.

34. Cho, H., *et al. Self-organization in high density bacterial colonies: efficient crowd control*. PLoS Biology, 2007. **5**: p. 2614-2623.

35. Wright, E., Neethirajan, S., and Weng, X. *Microfluidic would model for studying the behaviors of Pseudomonas aeruginosa in polymicrobial biofilms*. Biotechnol. Bioeng., 2015. **112**: p. 2351-2359.

36. Mohan, R., *et al. A microfluidic approach to study the effect of bacterial interactions on antimicrobial susceptibility in polymicrobial cultures.* RSC Adv., 2015. **5**: p. 35211-35223.

37. Kim, H.J., Boedicker, J.Q., Choi, J.W., and Ismagilov, R.F. *Defined spatial structure stabilizes a synthetic multispecies bacterial community.* PNAS, 2008. **105**: p. 18188-18193.

38. Nielson, R., Kaehr, B., and Shear, J.B. *Microreplication and design of biological architectures using dynamic-mask-based multiphoton lithography*. Small, 2009. **5**: p. 120-125.

39. Shear, J.B. *Multiphoton-excited fluorescence in bioanalytical chemistry*. Anal. Chem., 1999. **71**: p. 598A-605A.

40. LaFratta, C.N., Fourkas, J.T., Baldacchini, T., and Farrer, R.A. *Multiphoton fabrication*. Angew. Chem. Int. Ed., 2007. **46**: p. 6238-6258.

41. Cho, K., *et al. Enhanced two-photon excited fluorescence in three-dimensinally crosslinked bovine serum albumin microstructures.* Optics Express, 2011. **19**(12): p. 11732-11739.

42. Lin, C., *et al. Investigation of two-photon excited fluorescence increment via crosslinked bovine serum albumin.* Optics Express, 2012. **20**(13): p. 13669-13676.

43. Kaehr, B. and Shear, J.B. *Multiphoton fabrication of chemically responsive protein hydrogels for microactuation*. PNAS, 2008. **105**(26): p. 8850-8854.

44. Turunen, S., *et al. Pico- and femtosecond laser-induced crosslinking of protein microstructures: evaluation of processability and bioactivity.* Biofabrication, 2011. **3**(4): p. 1-14.

45. Ma, J., *et al. Multiphoton fabrication of fibronectin-functionalized protein micropatterns: stiffness-induced maturation of cell-matrix adhesions in human mesenchymal stem cells.* ACS Appl. Mater. Interfaces, 2017. **9**(35): p. 29469-29480.

46. Foote, C.S. *Definition of type I and type II photosensitized oxidation.* Photochem. and Photobio., 1991. **54**: p. 659.

47. Wessel, A.K., *et al. Oxygen limitation within a bacterial aggregate*. mBio, 2014. **5**: p. 1-9.

48. Ahmed, E.M. *Hydrogel: preparation, characterization, and applications: a review*. J. Adv. Research, 2015. **6**(2): p. 105-121.

49. Lutolf, M.P., Raeber, G.P., Zisch, A.H., Tirelli, N., and Hubbell, J.A. *Cell-responsive synthetic hydrogels.* Adv. Mat., 2003. **15**: p. 888-892.

50. Guvendiren, M., and Burdick, J.A. *Engineering sythentic hydrogel microenvironments to instruct stem cells*. Curr. Opin. Biotech., 2013. **24**(5): p. 841-846.

51. Mendez, U., Zhou, H., and Shikanov, A. *Synthetic PEG hydrogel for engineering the environment of ovarian follicles*. Biomat. Tissue Eng., 2018. **1758**: p. 115-128.

52. Helary, C., *et al. Concentrated collagen hydrogels as dermal substitutes.* Biomat., 2010. **31**(3): p. 481-490.

53. Jeon, O., Bouhadir, K.H., Mansour, J.M., and Alsberg, E. *Photocrosslinked alginate hydrogels with tunable biodegradation rates and mechanical properties.* Biomat., 2009. **30**(14): p. 2724-2734.

54. Upadhyay, A., Kandi, R., and Rao, C.P. *Injectable, self-healing, and stress sustainable hydrogel of BSA as a functional biocompatible material for controlled*

drug delivery in cancer cells. ACS Sustainable Chem. Eng., 2018. **6**(3): p. 3321-3330.

55. Sugiura, S., *et al. On-demand microfluidic control by micropatterned light irradiation of a photoresponsive hydrogel sheet.* Lab on a Chip, 2009. **9**(2): p. 196-198.
56. Kiyonaka, S., Sugiyasu, K., Shinkai, S., and Hamachi, I. *First thermally responsive supramolecular polymer based on glycosylated amino acid.* J. Amer. Chem. Soc., 2012. **124**(37): p. 10964-10955.
57. Wang, Q., *et al. 3D printing with cellulose materials.* Cellulose, 2018. **25**: p. 4275-4301.
58. Ziv, K., *et al. A tunable silk-alginate hydrogel scaffold for stem cell culture and transplantation*. Biomat., 2014. **35**(12): p. 3736-3743.
59. Barry III, R.A., *et al. Direct-write assembly of 3D hydrogel scaffolds for guided cell growth*. Adv. Mat., 2009. **21**(23): p. 2407-2410.
60. Lee, K.Y. and Mooney, D.J. *Hydrogels for tissue engineering*. Chemical Reviews, 2001. **101**(7): p. 1869-1880.
61. Nguyen, K.T. and West, J.L. *Photopolymerizable hydrogels for tissue engineering applications*. Biomat., 2002. **23**(22): p. 4307-4314.
62. Khademohosseini, A. and Langer, R. *Microengineered hydrogels for tissue engineering.* Biomat., 2007. **28**(34): p. 5087-5092.
63. Pitts, J.D., Campagnola, P.J., Epling, G.A., and Goodman, S.L. *Submicron multiphoton free-form fabrication of proteins and polymers: studies of reaction efficiencies and applications in sustained release*. Macromolecules, 2000. **33**: p. 1514-1523.
64. Kaehr, B. and Shear, J.B. *High-throughput design of microfluidics based on directed bacterial motility.* Lab on a Chip, 2009. **18**: p. 2632-2637.
65. Seidlits, S.K., Schmidt, C.E., and Shear, J.B. *High-resolution patterning of hydrogels in three dimensions using direct-write photofabrication for cell guidance.* Adv. Func. Mat., 2009. **19**: p. 3543-3551.
66. Stacy, A., *et al. Bacterial fight-and-flight responses enhance virulence in a polymicrobial infection*. PNAS, 2014. **111**(21): p. 7819-7824.
67. Lin, Y., Zou, Y., Mo, Y., Guo, J., and Lindquist, R.G. *E-beam patterned gold nanodot arrays on optical fiber tips for localized surface plasmon resonance biochemical sensing.* Snesors, 2010. **10**(10): p. 9397-9406.

68. Chenari, Z., Latifi, H., Ghamari, S., Hashemi, R.S., and Doroodmand, F. *Adiabatic tapered optical fiber fabrication in two step etching.* Optics Laser Tech., 2016. **76**: p. 91-95.

69. Williams, H.E., Freppon, D.J., Kuebler, S.M., Rumpf, R.C., and Melino, M.A. *Fabrication of three-dimensional micro-photonic structures on the tip of optical fibers using SU-8.* Optics Express, 2011. **19**(23): p. 22910-22922.

70. Cojoc, G., *et al. Optical micro-structures fabricated on top of optical fibers by means of two-photon photopolymerization*. Microelectronic Eng., 2010. **87**: p. 876-879.

71. Zukauskas, A., Melissinaki, V., Kaskelyte, D., Farsari, M., and Malinauskas, M. *Improvement of the fabrication accuracy of fiber tip microoptical components via mode field.* J. Laser Micro Nanoeng., 2014. **9**(1): p. 68-72.

72. Kanamori, Y., Okochi, M., and Hane, K. *Fabrication of antireflection subwavelength gratings at the tips of optical fibers using UV nanoimprint lithography*. Optics Express, 2013. **21**(1): p. 322-328.

73. Calafiore, G., *et al. Campanile Near-field probes fabricated by nanoimprint lithography on the facet of an optical fiber*. Sci. Rep., 2017. **7**: p. 1-7

74. Morales-Delgado, E.E., *et al. Three-dimensional microfabrication through a multimode optical fiber.* Optics Express, 2017. **25**(6): p. 1-19.

75. Huygens, C. *Traite de la Lumiere*. 1690.

76. Keck, D.B., Maurer, R.D., and Shultz, P.C. *On the ultimate lower limit of attenuation in glass optical waveguids.* Appl. Phys. Lett., 1973. **22**(7): p. 307-309.

77. Vaiano, P., *et al. Lab on fiber technology for biological sensing applications*. Laser Photonics Rev., 2016. **10**(6): p. 922-961.

78. Polyak, B., Bassis, E., Novodvorets, A., Belkin, S., and Marks, R.S. *Optical fiber bioluminescent whole-cell microbial biosensors to genotoxicants.* Water Sci. Technol., 2000. **42**(1): p. 305-311.

79. Kumar, J., Jha, S.K., and D'Souza, S.F. *Optical microbial biosensor for detection of methyl parathion pesticide using Flavobacterium sp. whole cells adsorbed on glass fiber filters as disposable biocomponent.* Biosensors and Bioelectronics, 2006. **21**(11): p. 2100-2105.

80. Eltzov, E., and Marks, R.S. *Whole-cell aquatic biosensors.* Anal. Bioanal. Chem., 2011. **400**(4): p. 895-913.

Chapter 2: Characterization of Hydrogels for Micro-3D Printing of Biological Environments.

2.1 INTRODUCTION

Hydrogel technology has emerged over the past two decades as a leader in the creation and engineering of biocompatible tissues. [1-5] Due to their relatively high water content, [6] responsivity to various environmental stimuli, [6-12] and ability to be derived and/or synthesized from natural materials, [11-19] hydrogel materials have highly desirable characteristics for incorporation into physiological studies. Often referred to as "functional materials" due to their highly tunable nature, hydrogels allow researchers to gain dynamic control over properties such as material stiffness, swelling, and electroaddressability. [20-23] These properties can be "tuned" through changing environmental factors like temperature, [10-12] ionic strength, [8] and pH. [7-9] Such hydrogels can be used in a wide variety of applications, including drug delivery [16, 24-26] as well as the creation of 3D cell scaffolding. [17, 18, 27-30]

Hydrogels have also been used in a variety of ways to investigate sociomicrobial interactions. One such study utilized alginate/Ɛ-poly-L-lysine microcapsules to investigate how spatial distribution of *Vibrio harveyi* impacted QS, discovering that larger aggregates of cells exhibited enhanced QS when compared to smaller aggregates or planktonic cells. [31] Additionally, supramolecular-polysaccharides, [32] functionalized alginate, [33] and alginate/chitosan complexes [34] represent just a few of the many other hydrogels types that have been used in studies of microbial behavior.

To successfully perform cell-based studies, physiological conditions such as temperature must be maintained to promote cell growth and normal cell behavior. Depending on the cell type being studied (either mammalian or bacterial), the optimal growth temperature varies. While marine bacteria from temperate waters have optimal growth at temperatures between 10-20 ºC, [35] bacteria that act as human pathogens, such as *Pseudomonas aeruginosa*, have an ideal growth temperature that more closely matches human physiological temperature, ~37 ºC. [36-37] Similarly, mammalian cells are grown at 37 ºC in 5% CO_2 to closely mimic the physiological conditions of human blood, as well as serve as a buffer to maintain pH. [38] Using these growth parameters as a guide, hydrogels being used in cellular studies must have a melting temperature below the ideal growth temperature of the cells being studied.

Maintaining hydrogels with relatively low melting temperatures when compared to ideal cellular growth temperatures is particularly important with regards to bacterial studies in the Shear lab. In both past and present micro-3D printing experiments, bacterial cells are introduced into a hydrogel matrix via deposition of small volumes of liquid cell culture into larger volumes of hydrogel. [53, 58] As the inclusion of gelatin in the hydrogel matrix results in thermal setting upon cooling to room temperature, hydrogels require pre-heating to ensure homogeneous dispersal of bacteria throughout the hydrogel solution. Then, upon setting, bacteria become temporarily immobilized, assisting in capture of bacteria during fabrication. Following fabrication, the hydrogel must be heated again to allow for melting, rinsing, and removal of uncrosslinked hydrogel. If the heat required for melting and rinsing

away excess hydrogel exceeds the ideal growth temperature of the bacteria being studied, this process could cause cells to enter heat shock, potentially resulting in cell death. [38-41]

Photosensitizers are commonly used to initiate covalent crosslinking of oxidizable protein residues during multiphoton lithography. While photosensitizers are a key component of these studies, they also exhibit cytotoxicity towards cells once certain concentration levels are surpassed. [42-43] A common photosensitizer, and the one used in all studies presented in this dissertation, is Rose Bengal. Rose Bengal is capable of undergoing two reaction mechanisms, one that produces radical products like hydroxyl (Type I) and one that creates reactive singlet oxygen species (Type II). [44] These studies utilize the Type II reaction, which promotes crosslinking of amino acid residues, particularly His-His. [45] This photosensitizer is commonly used to induce phototoxicity against both mammalian and bacterial cells, and has proven to be successful on both counts. [43-44, 46-47] However, when used to photocrosslink protein hydrogels in the presence of cells (such as studies conducted by the Shear lab), attempts must be made to minimize the cytotoxic effects of this photosensitizer to favorably create a biocompatible platform in which bacterial and mammalian cells can maintain high cell viability.

In the Shear lab, multiphoton lithography has been used to fabricate hydrogels based on intermolecular crosslinking of BSA for a variety of applications, including (a) the creation of complex, unconstrained 3D microstructures, [48] (b) directing mammalian cell growth and migration, [49-51] and most recently, (c) the capture and study of bacterial

microclusters. [52-58] In addition to creating thermally set reagents, the incorporation of gelatin into the hydrogel matrix creates a more versatile platform in which fabricated structures exhibit better adherence to coverslip substrates onto which they are fabricated, thus allowing greater complexity and elasticity with regards to structural design. [54, 58] Additionally, varying gelatin concentration allows for tunability of uncrosslinked hydrogel melting temperatures, where an increase in gelatin concentration corresponds to a subsequent increase in melting temperature. [59] As the research presented in this dissertation expands upon prior work surrounding growth and behavior of the opportunistic pathogen *P. aeruginosa*, hydrogels were optimized and characterized in detail in order to maintain maximum compatibility with Pa01, the strain used in all studies detailed hereafter.

2.2 Materials and Methods

2.2.1 Materials

Tryptic soy agar (TSA, R455002) and tryptic soy broth (TSB, 8053765) were purchased from Remel and EMD Millipore, respectively. Gelatin type A from porcine skin, 60 Bloom (160304) and Gelatin type A from porcine skin, 300 Bloom (9000-70-8) were purchased from EMS and Sigma, respectively. Bovine serum albumin (BSA, 9048-46-8) was obtained from Equitech Bio. Rose Bengal (RB, 632-69-9), carbenicillin disodium salt (BP2648-1), BupH phosphate buffer saline (PBS) packs (28372), microscope coverslips (#1 borosilicate, 22x22, Lab-Tek), and eight-well chambered coverslips (#1 borosilicate, 25x57, Lab-Tek) were purchased from Thermo Fisher Scientific. All reagents were stored and used according to supplier specifications.

2.2.2 Bacteria Strain and Culture

Wild-type *P. aeruginosa* strain Pa01, constitutively expressing green fluorescent protein (GFP) from plasmid pMRP9-1, was used in all toxicity studies. The plasmid was maintained using TSA plates containing 100 µg/mL carbenicillin. Planktonic cultures were grown aerobically overnight at 37 °C on a shaker set to 250 rpm, using the original culture plate to seed cells into a culture tube filled with 4 mL TSB. Following overnight culture, cells were diluted 1:50 into a fresh culture tube and allowed to grow on the shaker for an additional 2 h. in order to reach the desired experimental cell density of ~0.3 at OD600 (absorbance at 600 nm).

2.2.3 Hydrogel Preparation

Hydrogels were prepared using TSB, gelatin, BSA, and RB. All solutions used for melting temperature studies were composed of 250 µL TSB, 5 mM RB, 40 mg/mL BSA, and one of six different gelatin concentrations (75, 100, 125, 150, 175, or 200 mg/mL). Solutions used for toxicity studies were composed of 440 µL TSB, 40 mg/mL BSA, 200 mg/mL gelatin, and one of six different RB concentrations (5.5, 6.5, 7.5, 8.5, or 9.5 mM).

To begin hydrogel preparation for melting temperature studies, 10 mg RB were added to 2 mL of TSB and placed in a heated sonicator set to 60 ºC for 1 h. to facilitate complete dissolution of the photosensitizer. Upon completion in the sonicator, 250 µL aliquots of photosensitizer/TSB solution were added to six 1.5 mL Eppendorf tubes, followed by the addition of 10 mg BSA to each tube. Then, the appropriate amount of gelatin was added to each tube to reach the desired concentrations listed previously. Hydrogels were vortexed for 30 s before being placed in an oven set to 60ºC to facilitate complete dissolution of BSA and gelatin. Lastly, all tubes were placed on a heated shaker set to 37ºC for at least 45 min to encourage complete mixing and homogeneity of the final hydrogel solutions.

Hydrogel preparation procedures for toxicity studies were essentially identical, differing only in initial solution volume (from 250 µL to 440 µL) and variation of RB concentration as opposed to gelatin concentration, which was held constant at 200 mg/mL for all solutions.

2.2.4 Melting Temperature Protocol

Melting temperatures were determined using a custom-built setup consisting of a Corning PC 420 stirrer/hotplate, Fluke 179 True RMS multimeter and thermocouple, small glass petri dish, and 1 cm stir bar, shown in Figure 2.1.

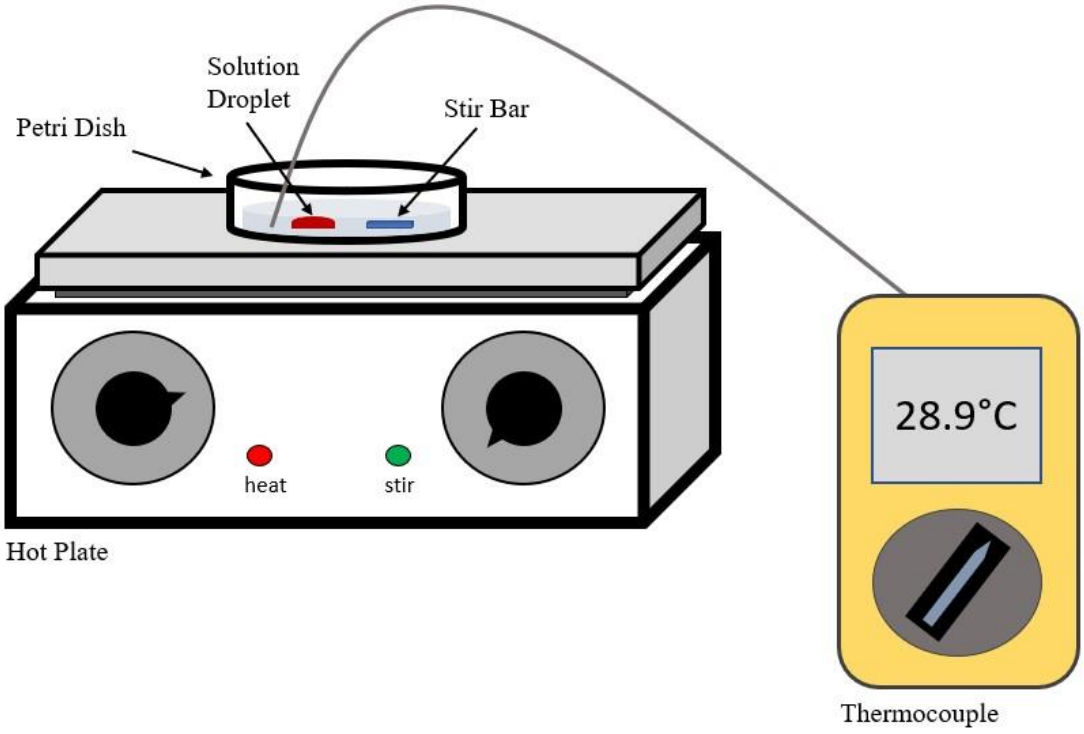

Figure 2.1: Melting Temperature Determination Setup

A droplet of solution is placed just off center of a small glass petri dish and allowed to cool for 10 min under ambient conditions to ensure full gelation occurs. The petri dish is then filled with enough buffer to fully submerse the gelled droplet, and the petri dish is placed on the hot plate. A small stir bar is added and the dish is manually adjusted so the stir bar does not impact the droplet while stirring. The stir strength was set to an intermediate value, and the heat was adjusted to a low setting, allowing the buffer solution to increase in temperature ~0.1 °C every 30 seconds. A final melting temperature is recorded when strands of droplet detach from the main droplet and begin to flow away with the current of the stir bar.

A small droplet (~30 µL) of solution was pipetted into the center of a small glass petri dish and allowed to cool for 10 min to reach full gelation. Then, the petri dish was filled with enough PBS to fully submerge the droplet and the dish was placed on a hotplate. A stir bar was added and positioned so it was close to, but not touching, any part of the droplet, and set to a medium stir speed. A thermocouple was introduced on the side of the droplet opposite the stir bar and placed in such a way that it was fully submersed in the buffer, but did not touch the bottom of the hotplate. The heating element was turned on to a low enough setting that the temperature of the PBS solution increased ~0.1 ºC every 30 seconds. The droplet was observed over time until it began to dissolve, which exhibited as trails of pink solution detaching from the original droplet. Once the first of these trails appeared, the temperature displayed on the thermocouple was recorded as the melting temperature of the solution. The hotplate and glass petri dishes were allowed to return to ambient temperature before testing a new solution droplet. Data for 300 Bloom solutions were collected and provided courtesy of Mignon Fitzpatrick.

2.2.5 Fabrication Setup

Microstructures for toxicity studies were fabricated on the untreated surface of an eight-well chambered coverslip. In order to fabricate the photo-crosslinked protein structures, a dynamic mask-based multiphoton lithography technique was used. [23] This technique employs a focused, femtosecond, mode-locked titanium:sapphire (Ti:Sapph) laser (Tsunami, Spectra Physics) tuned to 740 nm, where the output beam is directed onto a pair of galvanometer-driven scan mirrors (GVS002, Thor Labs), which raster scan the

laser beam onto the surface of a digital micromirror device (DMD, BenQ SVGA) modified by Tim Hooper. The DMD acts as a dynamic mask and displays intensity masks representing sequential slices along the z-axis of the structure being built over the course of fabrication, allowing for the creation of 3D structures in a layer-by-layer fashion. The reflected beam is then expanded and collimated to overfill the back aperture of an oil-immersion objective (Olympus UPlanApo 100X 1.35 NA) secured to an inverted microscope (Zeiss Axiovert 135). A schematic of the optical table setup is depicted in Figure 2.2.

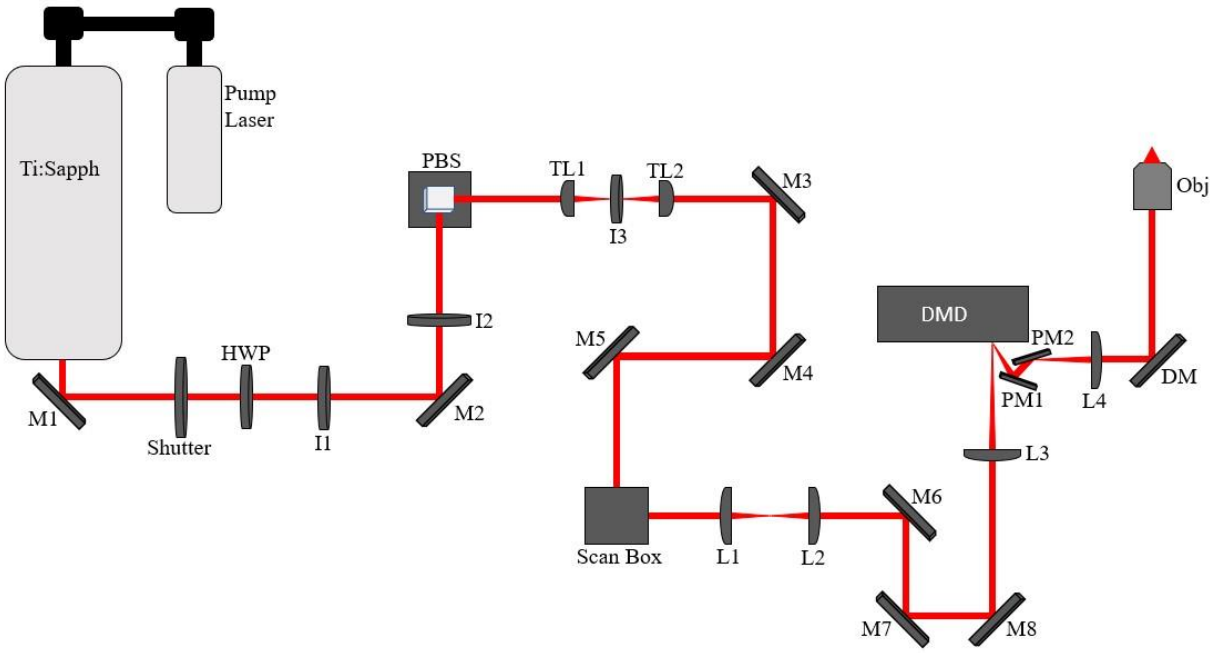

Figure 2.2: Optical Setup for Dynamic Mask-Based Multiphoton Lithography

The output of a 532-nm Nd:YVO_4 laser is used to optically pump a titanium sapphire (Ti:Sapph) oscillator, producing a mode-locked and femtosecond pulsed beam tuned to the desired near-IR wavelength, 740 nm. The Ti:Sapph, the beam is attenuated using a half wave plate (HWP) and polarizing beam splitter (pBS) before being collimated using two telescopic lenses (TL1 and TL2). The beam is then directed at a pair of galvo-driven scan mirrors (located in the scan box) which raster scan the beam as it is focused on the face of a digital micromirror device (DMD). Between the scan box and the DMD, the beam is expanded using a set of lenses (L1 and L2), focused on the surface of the DMD using L3, and expanded to overfill the back aperture of the microscope objective using L4. Periscopic mirrors PM1 and PM2 allow the beam to be raised to the height of the microscope input and dichroic mirror (DM). The beam is directed and aligned through these elements using a combination of mirrors (M1-M8) and irises (I1-I3). The focal lengths of each lens are as follows: TL1 and TL2: F = 2”, L1 and L2: F = 4”, L3: F = 15 cm, L4: F = 20 cm.

A binary mask sequence generating a square-to-dome shaped structure (Figure 2.3) was used in conjunction with the DMD to create 3D cellular enclosures.

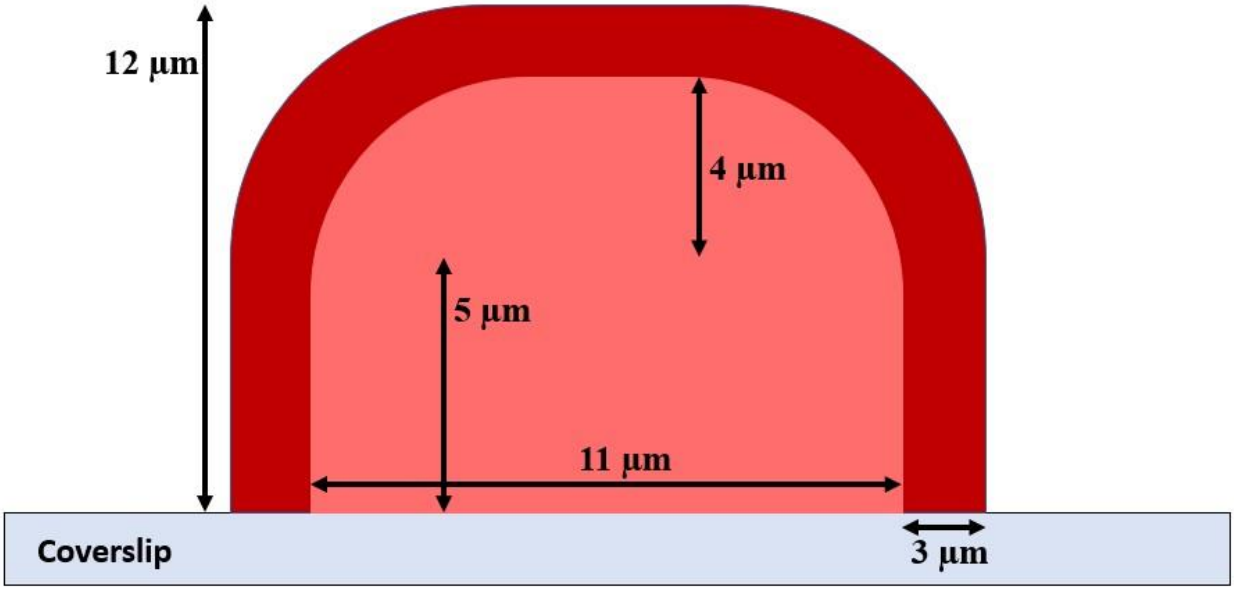

Figure 2.3: Schematic of Square-to-Dome Structure

Side view of trap used for all bacterial toxicity studies. Base of trap is square before gradually merging into a domed, flat-top roof. Traps were centered around a single or dividing bacteria, giving an initial population of ≤ 2 bacteria/trap. Approximate volume of inner cavity is ~1 pL.

Each mask was created using the ImageJ macro language. Structures were fabricated in a layer-by-layer fashion in which each sequential binary mask represents one layer of the final structure. Structures were printed at a rate of 5 seconds per plane, where display of sequential masks were synchronized with a motorized focus driver (H122, Prior Scientific) to raise the stage by 0.5 µm optical axis steps per plane. An average laser power of 40 mW (measured at the back aperture of the objective) was used during fabrication.

Each structure was composed of 24 binary masks and took approximately two minutes to fabricate.

2.2.6 Toxicity Study Protocol

Prior to fabrication, each hydrogel solution was diluted with 60 µL of bacteria suspended in TSB and mixed thoroughly at 37 °C on the heated shaker. A small droplet of each solution was placed in its own individual well of an eight-well chambered coverslip. The chambered coverslip was secured utilizing masking tape to the microscope stage insert and solution droplets were allowed to cool for 5-10 minutes prior to fabrication. Upon location of either a single or dividing cell, the first slice of the square-to-dome mask was centered over the cell, the microscope focused at the surface of the coverslip (to ensure anchoring of the structure to the glass), and fabrication was initiated via customized LabView software. Five structures were fabricated per well. If needed, a small volume of TSB was introduced into each well to maintain hydration during the fabrication procedure.

Following fabrication, ~500 µL of room temperature TSB was added to each well before placing the chambered coverslip in an incubator set to 37ºC for at least 45 minutes allowing the un-crosslinked hydrogel to melt. Then, the melted hydrogel was rinsed out of each well using multiple aliquots of fresh TSB warmed to 37°C. All crosslinked structures remained adhered to the coverglass. The trapped cells were counted immediately following rinsing to obtain a 0-hr population, then placed back in the incubator. Cell counts were taken at the 1, 2, and 4-hour time points for each structure, during which cell motility was

observed as an indicator of overall cell health. Cell counts were averaged and used to calculate the estimated generation time for each population using Equation 2.1

$$N = N_o e^{kt} \quad \text{(Eqn 2.1)}$$

where N represents bacteria population at the end time-point, N_o represents the initial population of bacteria, and k represents the exponential growth rate, and t represents the time elapsed.

2.3 Results and Discussion

2.3.1 Hydrogel Characterization for Micro-3D Printing

Since 2010, most micro-3D printing studies conducted by the Shear lab have utilized a hydrogel solution composed of varying concentrations of gelatin, BSA, and RB. [52-58] These studies have encompassed a wide range of applications with regards to bacterial interactions, ranging from determining the minimum cell population required to initiate antibiotic resistance [52] to studying the onset of quorum sensing via scanning electrochemical microscopy (SECM). [56-57] These experiments require biocompatible conditions for the bacteria being studied. Therefore, they must take into account hydrogel characteristics such as melting temperature and cytotoxicity, which could potentially impact cell viability to a significant degree.

The pathogenic bacterium used in these studies, *P. aeruginosa*, has an optimal growth temperature of 37 ºC, which aligns with the typical human body temperature. [36-37] Thus, an ideal fabrication solution for these studies would have a markedly lower melting temperature than 37 ºC, as this allows the bacteria to grow at their desired temperature while the un-crosslinked gelatin melts and is rinsed away. As the melting/rinsing process usually takes 45-60 minutes, it is vital to keep the cells at or below their ideal growth conditions in order to avoid heat shock over this extended period of time.

The cytotoxicity of photosensitizers towards both mammalian and bacterial cells is well documented and has been repeatedly demonstrated as an effective means to inactivate mutated or highly resistant cells. [43-44, 46-47] While this distinctive feature presents

exciting opportunities in the treatment of disease and infection, it poses a significant problem for studies in which minimal impact on cell viability is desired. Methods such as cell conditioning [54] and using the lowest possible RB concentration while maintaining high fabrication integrity have been used, but no formal study on how bacterial cell health is impacted by RB concentration when used as a photosensitizer in multiphoton lithographic reagents, and in the lithographic process itself, has been undertaken.

With every hydrogel component possessing unique physical properties, the ability to characterize each individually and gain greater control over factors such as toxicity and melting temperature is greatly advantageous for cell-based experiments. For the current studies, all hydrogels used TSB as the bacterial, liquid-growth medium, which assists in maintaining cell viability when bacteria are introduced and mixed into the solution immediately prior to fabrication. However, it should be noted that depending on what the hydrogel is being used for, a variety of different liquids could be used as a liquid medium, including phosphate-buffered saline (PBS), LB (Lysogeny broth), and HEPES buffers.

2.3.2 Melting Temperature Trends

The range of gelatin concentrations chosen for this study were selected based on previous studies, where hydrogels containing below 75 mg/mL of gelatin (across all bloom strengths) showed poor structural integrity post fabrication, and those containing above 200 mg/mL of gelatin (across all bloom strengths) exhibited poor solubility during initial mixing of the solution. Initial test experiments were performed to determine what setup would work most reliably for determining melting temperature. To maximize

reproducibility of melting temperature measurements, a single hotplate was used in all studies. In addition, droplets deposited on glass petri dishes were found to provide greater consistency than plastic surfaces, and therefore were used to acquire melting point data.

Upon introduction of ~5 mL PBS to the dish (enough to fully submerse the gelled droplet), a small amount of Rose Bengal leached out of the hydrogel, causing a color change of the surrounding PBS to faint shade of pink. As the PBS heated, this pink hue gradually became more pronounced as increasing levels of Rose Bengal transferred from the hydrogel to the solution. However, this was not considered an indicator of melting, as the integrity and viscosity of the droplet appeared unchanged to the naked eye. Upon approaching the melting temperature, the droplet became visibly less viscous and began to move in conjunction with the stir bar, with pieces and strands of hydrogel eventually detaching from the droplet completely when the melting temperature was reached.

As can be seen in Figures 2.4 and 2.5, a nearly linear trend for both 60 and 300 Bloom is present when comparing gelatin concentration and average melting temperature. Error bars, represented as the standard deviation of the mean, are likely attributes of minor discrepancies in the measured amounts of gelatin added to solution. Additional sources of error could be the hydrogel not fully setting prior to heating, as well as the hot plate not cooling sufficiently between trials. The small sample size for all gelatin concentrations tested (n=3) may also lead to larger error bars. As the largest error bars are present on both the lower and higher end of the melting range, it can be stated that the error is likely not a

function of gelatin concentration. Data for 300 bloom solutions were collected and provided courtesy of Mignon Fitzpatrick.

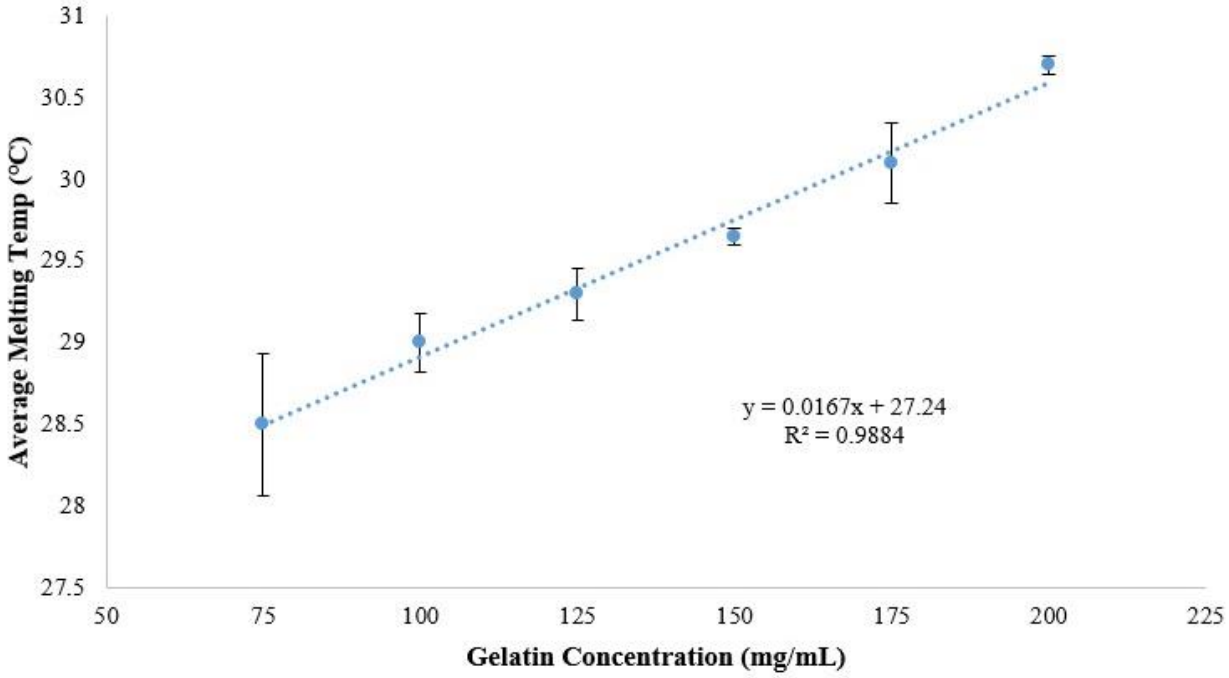

Figure 2.4: Melting Temperature Trends Based on 60 Bloom Gelatin Concentration

Melting temperature data for hydrogels containing 5 mM Rose Bengal, 40 mg/mL BSA, and varying concentrations of 60 bloom gelatin type A from porcine skin. Six concentrations of gelatin were tested, ranging from 75 mg/mL to 200 mg/mL with increasing increments of 25 mg/mL. A linear trend can be seen for average melting temperature as a function of time. Error bars represent standard deviation of the mean. For all concentrations, n=3.

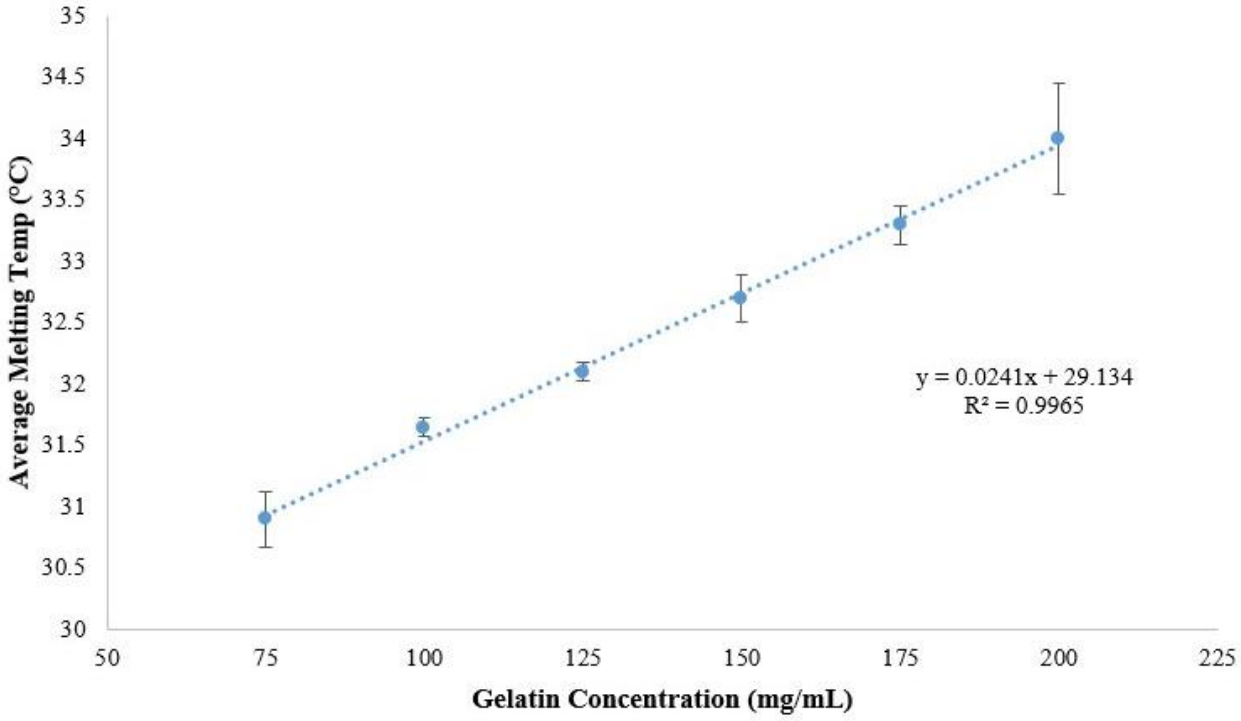

Figure 2.5: Melting Temperature Trends Based on 300 Bloom Gelatin Concentration

Melting temperature data for hydrogels containing 5 mM Rose Bengal, 40 mg/mL BSA, and varying concentrations of 300 bloom gelatin type A from porcine skin. Six concentrations of gelatin were tested, ranging from 75 mg/mL to 200 mg/mL with increasing increments of 25 mg/mL. A linear trend can be seen for average melting temperature as a function of time. Error bars represent standard deviation of the mean. For all concentrations, n=3. Data provided as courtesy of Mignon Fitzpatrick.

Gelatin bloom number is determined by measuring gel strength, a characteristic that is dependent on temperature, pH, and gelatin fragment length (higher bloom number equals longer fragment lengths). [59-62] Temperature conditions were kept consistent when generating hydrogels, and all hydrogels were created in TSB, which has a pH of 7.35

according to manufacturer specifications. Additionally, the pH of PBS (pH 7.4) was kept consistent during all melting studies. Therefore, it can be stated with a high level of confidence that any changes in melting temperature are a result of the varying bloom numbers and gelatin concentrations in each solution. The data presented here is consistent with prior studies stating that an increase in gelatin concentration results in an increase in melting temperature. [59]

Bloom number is positively correlated with triple-helix concentration within the gelatin, with a higher number of triple-helices producing gelatins of higher structural stability and thermal reversibility. [62] These higher triple-helix concentrations are a result of increased partial regeneration of the collagen triple-helix structure from which gelatin is derived, requiring a greater amount of energy to break the regenerated coiled structure. [63] This is consistent with the data presented here, as hydrogels made with 300 bloom gelatin possess a notably higher melting temperature than those made with 60 bloom gelatin. This is representative of a greater amount of energy needed to disrupt the hydrogel matrix and induce dissolution of the gelled hydrogel into the surrounding PBS solution.

That data plotted in Figures 2.4 and 2.5 allow future research to use the calculated trendlines as a guide when making solutions of a desired melting temperature, allowing customizable solutions to be made that are dependent on the ideal growth temperature of the organism being studied. Additionally, information obtained from these experiments can be utilized in studies where hydrogels of different melting temperatures are layered for

controlled release purposes. Studies such as these are further explained in detail in Chapter 3, where layered hydrogels are used in conjunction with multiphoton lithography.

2.3.3 Cytotoxicity Trends Based on Rose Bengal Concentration

Similar to selection of gelatin concentrations in Section 2.2.2, RB concentrations used for these studies were based on prior work from the Shear lab, with 5 mM RB having exhibited low cytotoxicity (normal growth rate, high cell motility) and 10 mM RB showing very high cytotoxicity (no cell division after ≥ 2 h. at 37 ºC, little to no cell motility). Therefore, in order to maximize RB concentration in fabrication reagents (thus improving fabrication quality) while maintaining low toxicity, five RB concentrations were examined in these studies ranging from 5.5 mM to 9.5 mM in 1 mM increments. To ensure consistency in all other aspects of experimental preparation, all hydrogels contained 1 mL TSB, 40 mg/mL BSA, and 200 mg/mL gelatin (60 bloom), a reagent mixture demonstrated previously to have high biocompatibility. [54] To maintain consistency regarding initial cell viability, experiments for each RB concentration were performed on cells from a single culture tube on the given experiment day. All culture tubes were in mid-logarithmic phase and were grown to a density of ~0.3 at OD600.

The first cell count, delineated as the “0 minute” mark, was taken following the melting and rinsing away of excess fabrication solution. As the melting and rinsing process takes approximately an hour to complete, a number of captured cells had already undergone one division. This means that while only one or two cells were captured at the time of

fabrication, initial cell counts could vary between one and four cells. This is consistent with previously determined doubling rates for *P. aeruginosa* grown at 37°C. [52]

When averaging the cell counts for all RB concentrations, a clear correlation can be seen between RB concentration and cell survival over time. While cell counts at the 0-minute mark were consistently either 2 or 4 cells, cell viability dropped dramatically over the course of 4 hours with each increase in RB concentration. This data is represented in Figure 2.6 with corresponding cell doubling times for each RB concentration outlined in Table 2.1.

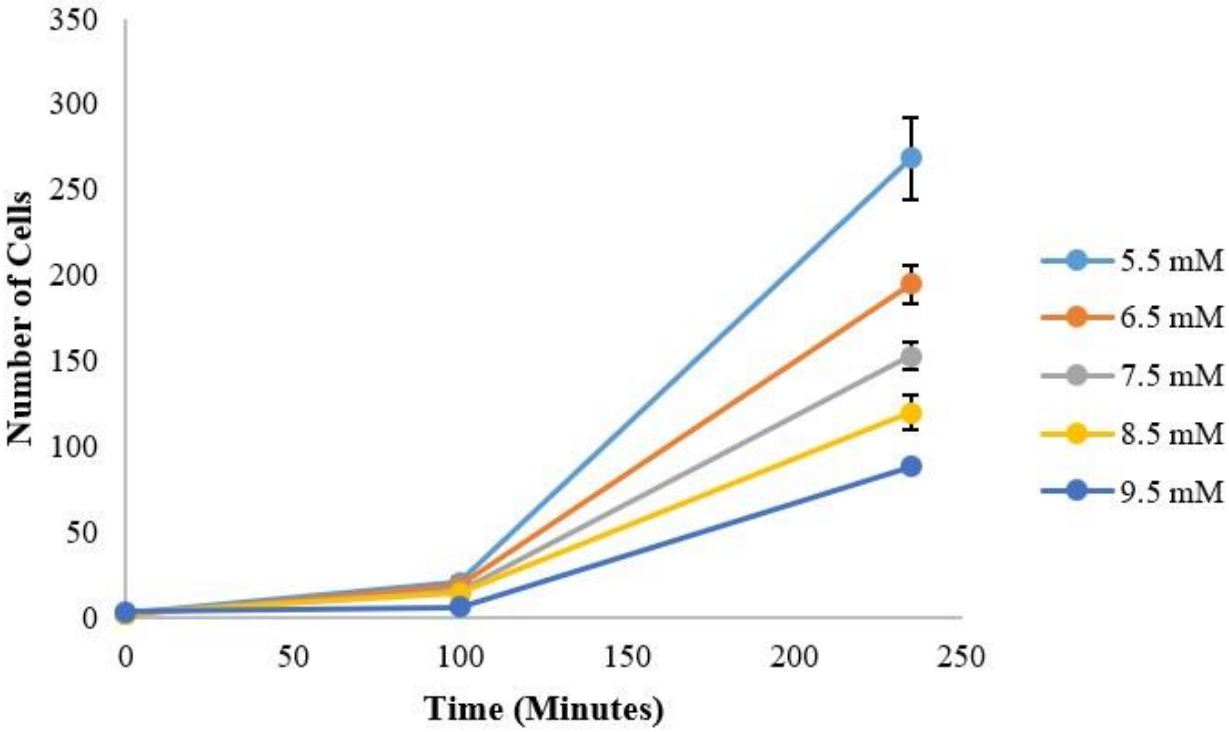

Figure 2.6: Cell Growth as a Function of Rose Bengal Concentration

Cytotoxicity data for hydrogels containing 40 mg/mL BSA, 200 mg/mL gelatin (60 bloom), and varying concentrations of Rose Bengal. Six concentrations of RB were tested, ranging from 5.5 mM to 9.5 mM with increasing increments of 1 mM RB. A negative correlation can be seen between RB concentration and cell viability, with increasing RB concentration resulting in a significant decrease in cell growth. For all concentrations and time points, n=3. Error bars represent standard deviation of the mean.

Table 2.1: P. aeruginosa Doubling Time as a Function of RB Concentration

Doubling times for Pa01 strain of *P. aeruginosa* trapped in structures fabricated using hydrogels with varying concentrations of Rose Bengal. An increase in RB can be seen to cause a gradual increase in doubling time. This is indicative of a decrease in cell viability, further supporting the conclusion that an increase in RB concentration results in a corresponding increase in hydrogel cytotoxicity. Error represents standard deviation of the mean.

RB Conc (mM)	5.5	6.5	7.5	8.5	9.5
Doubling Time (Min)	36 ± 1	37 ± 2	40 ± 2	43 ± 2	51 ± 2

When promoted to an excited state, Rose Bengal undergoes a Type II photochemical reaction, thereby producing singlet oxygen species. This singlet oxygen production has been determined to be the primary mechanism responsible for Rose Bengal's cytotoxic effect on bacterial cells, having a greater impact on gram positive over gram negative cells. [43] This explains why former studies in the Shear lab have had to condition gram positive *S. aureus* to grow in the presence of a photosensitizer [54] but have never had the need to do so with gram negative *P. aeruginosa*, due to the extra protection afforded by the peptidoglycan cell wall and lipopolysaccharide layers. However, high enough concentrations of photosensitizers such as Rose Bengal have been documented as successfully passing through these barriers to inactivate a variety of bacterial strains. [42-43]

Such studies are consistent with the data presented here, in which the gradual increase of photosensitizer concentration directly correlates to a decrease in cell survival. As Rose Bengal concentration becomes higher, an increase in the concentration of singlet

oxygen species is produced, increasing toxicity to bacterial cells. Therefore, it is of utmost importance to understand the concentration threshold of Rose Bengal at which the photosensitizer transitions from having minimal effect on bacteria to a marked effect on cell viability.

2.4 CONCLUSIONS

This chapter discussed the characterization of protein-based hydrogels commonly used in bacterial studies conducted by the Shear lab. Expanding upon the knowledge that changes in gelatin concentration directly correspond to a change in melting temperature, linear fit curves were generated using data points gathered during the melting of 60 and 300 Bloom gelatins. Both curves displayed a linear relationship between gelatin concentration and melting temperature, which will allow future research to use the trend line generated from these curves as a guide when customizing hydrogels for maximum compatibility with a cell's optimal growth temperature, all while maintaining cellular biocompatibility. As all studies conducted here utilized gelatin derived from porcine skin, it remains unknown how melting temperature would change with gelatins derived from other sources, such as bovine skin.

In addition to melting temperature, cytotoxicity of Rose Bengal was also evaluated in this chapter. For the bacterial strain being studied, *P. aeruginosa*, a marked increase in doubling time was seen at concentrations greater than 7.5 mM, indicative of a decrease in cell health. This indicates that in order to maintain maximum cell viability during fabrication, rose Bengal concentration must be kept less than or equal to 7.5 mM. It should be noted that gram-negative cells such as *P. aeruginosa* have a lower susceptibility to photosensitizers compared to gram-positive cells. [43] Thus, the maximum photosensitizer concentration allowable to maintain cell viability in gram-positive cells is likely much lower than those presented in this chapter, which should be of focus in future studies.

The ability to customize hydrogels to the desired melting temperature while maintaining low cytotoxicity provides valuable information for cell-based studies. In addition to future experiments completed under physiological conditions, this information can be used to capture and grow cells from more diverse environmental climates. The data collected and presented in this chapter provided the fundamental information needed to successfully complete experimental studies presented in Chapters 3 and 4 of this dissertation.

2.5 REFERENCES

1. Lee, K.Y. and Mooney, D.J. *Hydrogels for tissue engineering*. Chemical Reviews, 2001. **101**(7): p. 1869-1880.
2. Nguyen, K.T. and West, J.L. *Photopolymerizable hydrogels for tissue engineering applications*. Biomaterials, 2002. **23**(22): p. 4307-4314.
3. Basu, S. and Campagnola, P.J. *Properties of crosslinked protein matrices for tissue engineering applications synthesized by multiphoton excitation*. J. of Biomed. Mat. Research, 2004. **71A**(2): p 359-368.
4. Khademohosseini, A. and Langer, R. *Microengineered hydrogels for tissue engineering*. Biomaterials, 2007. **28**(34): p. 5087-5092.
5. Chia, H.N. and Wu, B.W., *Recent advances in 3D printing of biomaterials*. J. or Biological Eng., 2015. **9**(4): p. 1-14.
6. Zhou, C., *et al*., *High water content hydrogel with super high refractive index*. Macromolecular Bioscience, 2013. **13**(11): p. 1485-1491.
7. Ruan, W., Lian, Y., Zhen, T., Huang, L., and Qiao, J. *pH-response superabsorbent hydrogel synthesized by ultraviolet photopolymerization*. J. of App. Polymer Sci., 2006. **103**(3)1847-1852.
8. Peng, X., Ren, J., Zhong, L., Peng, F., and Sun, R. *Xylan-rich hemicelluloses-graft-acrylic acid ionic hydrogels with rapid responses to pH, salt, and organic solvents*. J. of Agricultural and Food Chemistry, 2011. **59**(15): p. 8208-8215.
9. Zhou, X., *et al*. *A pH and magnetic dual-response hydrogel for synergistic chemo-magnetic hyperthermia tumor therapy*. RSC Advances, 2018. **8**: p. 9812-9821.
10. Klouda, L., and Mikos, A.G. *Thermoresponsive hydrogels in biomedical applications*. Euro. J. of Pharm. And Biopharm., 2008. **68**(1): p. 34-45.
11. Schuetz, Y.B., Gurny, R., and Jordan, O. *A novel thermoresponsive hydrogel based on chitosan*. Euro. J. of Pharm. And Biopharm., 2008. **68**(1): p. 19-25.
12. Wang, K., Buschle-Diller, G., and Wu, Y. *Thermoresponsive hydrogels from BSA esterified with low molecular weight PEG.* J. of App. Polymer Sci., 2014. **131**(20): p. 1-8.
13. Lieleg, O. and Ribbeck, K. *Biological hydrogels as selective diffusion barriers*. Trends in Cell Biology, 2011. **21**(9): p. 543-551.
14. Hu, X., Li, D., Zhou, F., and Gao, C. *Biological hydrogel synthesized from hyaluronic acid, gelatin and chondroitin sulfate by click chemistry*. Acta Biomaterialia, 2011. **7**(4): p. 1618-1626.
15. Helary, C., *et al. Concentrated collagen hydrogels as dermal substitutes*. Biomaterials, 2010. **31**(3): 481-490.

16. Upadhyay, A., Kandi, R., and Rao, C.P. *Injectable, self-healing, and stress sustainable hydrogel of BSA as a functional biocompatible material for controlled drug delivery in cancer cells*. ACS Sustainable Chem. And Eng., 2018. **6**(3): p. 3321-3330.

17. McCain, M.L., Agarwal, A., Nesmith, H.W., Nesmith, A.P., and Parker, K.K. *Micromolded gelatin hydrogels for extended culture of engineered cardiac tissues.* Biomaterials, 2014. **35**(21): p. 5462-5471.

18. Duan, B., Hockaday, L.A., Kang, K.H., and Butcher, J.T. *3D bioprinting of heterogeneous aortic valve conduits with alginate/gelatin hydrogels.* J. of Biomed. Mat. Res. Part A, 2013. **101A**: p. 1255-1264.

19. Xu, J., Liu, Z., and Erhan, S.Z. *Viscoelastic properties of a biological hydrogel produced from soybean oil*. J. of American Oil Chemists Society, 2008. **85**(3): 285-290.

20. Tong, M.H., *et al*. *Multiphoton photochemical crosslinking-based fabrication of protein micropatterns with controllable mechanical properties for single cell traction force measurements*. Scientific Reports, 2016. **6**(1): 1-12.

21. Wust, S., Godla, M.E., Muller, R., and Hofmann, S. *Tunable hydrogel composite with two-step processing in combination with innovative hardware upgrade for cell-based three-dimensional bioprinting*. Acta Biomaterialia, 2014. **10**(2): 630-640.

22. Skardal, A., *et al*. *A tunable hydrogel system for long-term release of cell-secreted cytokines and bioprinted in situ wound cell delivery*. J. of Biomed. Mat. Res. Part B: App. Biomat., 2016. **105**(7): p. 1986-2000.

23. Kaehr, B. and Shear, J.B. *Multiphoton fabrication of chemically responsive protein hydrogels for microactuation*. PNAS, 2008. **105**(26): p. 8850-8854.

24. Hoare, T.R. and Kohane, D.S. *Hydrogels in drug delivery: progress and challenges*. Polymer, 2008. **49**(8): p. 1993-2007.

25. Ashley, G.W., Henise, J., Reid, R., Santi, D.V. *Hydrogel drug delivery system with predictable and tunable drug release and degradation rates*. PNAS, 2013. **110**(6): p. 2318-2323.

26. Qiu, Y. and Park, K. *Environment-sensitive hydrogels for drug delivery*. Adv. Drug Delivery Rev., 2012. **64**: p. 49-60.

27. Yan, H., Saiani, A., Gough, J.E., and Miller, A.F. *Thermoreversible protein hydrogel as cell scaffold*. Biomacromolecules, 2006. **7**(10): p. 2776-2782.

28. Tan, H., Xiao, C., Sun, J., Xiong, D., and Hu, X. *Biological self-assembly of injectable hydrogel as cell scaffold via specific nucleobase pairing*. Chem. Comm., 2012. **48**: p. 10289-10291.

29. Ziv, K., *et al. A tunable silk-alginate hydrogel scaffold for stem cell culture and transplantation.* Biomaterials, 2014. **35**(12): p. 3736-3743.

30. Barry III, R.A., *et al. Direct-write assembly of 3D hydrogel scaffolds for guided cell growth*. Adv. Mat., 2009. **21**(23): p. 2407-2410.

31. Gao, M., *et al*. *A crucial role for spatial distribution in bacterial quorum sensing*. Scientific Reports, 2016. **6**: p. 1-10.

32. Li, P. *et al. Autoinducer sensing microarrays by reporter bacteria encapsulated in hybrid supramolecular-polysaccharide hydrogels*. Macromolec. Biosci., 2017. **17**(1700176): p. 1-13.

33. Yi, C., *et al*. *Electroaddressing functionalized polysaccharides as model biofilms for interrogating cell signaling*. Adv. Func. Mat., 2012. **22**: 519-528.

34. Rhoads, M.K., *et al*. *Incorporating LsrK AI-2 quorum quenching capability in a functionalized biopolymer capsule*. Biotech. Bioeng., 2018. **115**: 278-289.

35. Pomeroy, L.R. and Wiebe, W.J. *Temperature and substrates as interactive limiting factors for marine heterotrophic bacteria*. Aquat. Microb. Ecol., 2001. **23**: p. 187-204.

36. Wang, X., *et al*. *Modeling growth of Pseudomonas aeruginosa single cells with temperature shifts.* J. Food Safety, 2016. **36**(2016): 442-449.

37. Van Derlinden, E., Bernaerts, K., and Van Impe, J.F. *Accurate estimation of cardinal growth temperatures of Escherichia coli from optimal dynamic experiments*. Int. J. Food Microbio., 2008. **128**(1): 89-100.

38. Wang, J., Yun, W., Zhao, S., Zhou, Y., and He, W. *The analysis of viability for mammalian cells treated at different temperatuers and its application in cell shipment*. PLoS One, 2017. **12**(4): p. 1-16.

39. Roncarati, D. and Scarlato, V. *Regulation of heat-shock genes in bacteria: from signal sensing to gene expression output*. FEMS Microbio. Rev., 2017. **41**(4): p. 549-574.

40. Sollich, M., *et al. Heat stress dictates microbial lipid composition along a thermal gradien in marine sediments*. Front. Microbiol., 2017. **8**: p. 1-19.

41. Hindmarsh, J.P., Prasad, J., Gopal, P., and Singh, H. *NMR measurement of bacteria death kinetics during heat stress*. LWT Food Sci. Tech., 2015. **60**(2): p. 876-880.

42. Luksiene, Z. *New approach to inactivation of harmful and pathogenic microorganisms by photosensitization*. Food Technol. Biotechnol., 2005. **43**(4): p. 411-418

43. Ergaieg, K. and Seux, R. *A comparative study of the photoinactivation of bacteria by meso-substituted cationic porphyrin, rose bengal, and methylene blue*. Desalination, 2009. **246**: p. 353-362.

44. Ochsner, M. *Photophysical and photobiological processes in the photodynamic therapy of tumors*. J. Photochem. and Photobiol., 1997. **39**: p. 1-18.

45. Shen, H.R., Spikes, J.D., Smith, C.J., and Kopecek, J. *Photodynamic cross-linking of proteins IV. Nature of the His-His bond (s) formed in the rose bengal-photosensitized cross-linking of N-benzoyl-L-histidine.* J. Photochem. Photobiol., A: Chem., 2000. **130**: p. 1-6.

46. Mousavi, S.H., Tavakkol-Afshari, J., Brook, A., and Jafari-Anarkooli, I. *Direct toxicity of rose bengal in MCF-7 cell line: role of apoptosis.* Food Chem. Toxic., 2009. **47**: p. 855-859.

47. Srivastav, A.K., *et al*. *Photosensitized rose bengal-induced phototoxicity on human melanoma cell line under natural sunlight exposure*. J. Photochem. Photobio. B: Biology, 2016. **156**: p. 87-99.

48. Spivey, E.C., *et al. Multiphoton lithography of unconstrained three-dimensional protein microstructures.* Adv. Func. Mat., 2013. **23**: p. 333-339.

49. Seidlits, S.K., Schmidt, C.E., and Shear, J.B. *High-resolution patterning of hydrogels in three dimensions using direct-write photofabrication for cell guidance*. Adv. Func. Mat., 2009. **19**: p. 3543-3551.

50. Seidlits, S.K., *et al. Fibronectin-hyaluronic acid composite hydrogels for three-dimensional endothelial cell culture*. Acta Biomaterialia, 2011. **7**(6): p. 2401-2409.

51. Hardy, J.G., *et al*. *Multiphoton microfabrication of conducting polymer-based biomaterials*. J. Mat. Chem. B, 2015. **3**(25): p. 5001-5004.

52. Connell, J.L. *et al. Probing prokaryotic social behaviors with bacterial "lobster traps."* mBio, 2010. **1**(4): p. 1-8.

53. Connell, J.L., Whiteley, M. and Shear, J.B. *Sociomicrobiology in engineered landscapes*. Nature Chem. Bio., 2012. **8**(1): p. 10-13.

54. Connell, J.L., Ritschdorff, E.T., Whiteley, M., and Shear, J.B. *3D printing of microscopic bacterial communities*. PNAS, 2013. **110**(46): p. 18380-18385.

55. Wessel, A.K., *et al*. *Oxygen limitation within a bacterial aggregate*. mBio, 2014. **5**(2): p. 1-9.

56. Connell, J.L., Kim, J., Shear, J.B., Bard, A.J., and Whiteley, M. *Real-time monitoring of quorum sensing in 3D-printed bacterial aggregates using scanning electrochemical microscopy.* PNAS, 2014. **111**(51): p. 18255-18260.

57. Kim, J., Connell, J.L., Whiteley, M., and Bard, A.J. *Development of a versatile in vitro platform for studying biological systems using micro-3D printing and scanning electrochemical microscopy*. Anal. Chem., 2014. **86**(24): p. 12327-12333.

58. Connell, J.L., Ritschdorff, E.T., and Shear, J.B. *Three-dimensional printing of photoresponsive biomaterials for control of bacterial microenvironments*. Anal. Chem., 2016. **88**: p. 12264-12271.

59. Osorio, F.A., Bilbao, E., Bustos, R., and Alvarez, F. *Effects of concentration, bloom degree, and pH on gelatin melting and gelling temperatures using small amplitude oscillatory rheology*. Int. J. Food Properties, 2007. **10**: p. 841-851.

60. Lai, J. *The role of bloom index of gelatin on the interaction with retinal pigment epithelial cells*. Int. J. Molec. Sci., 2009. **10**: p. 3442-3456.

61. Lai, J., *et al*. *Low bloom strength gelatin as a carrier for potential use in retinal sheet encapsulation and transplantation*. Biomacromolecules, 2009. **10**: p. 310-319.

62. Chou, S., Luo, L., Lai, J., and Ma, D.H. *On the importance of bloom number of gelatin to the development of biodegradable in situ gelling copolymers for intracameral drug delivery*. Int. J. Pharmaceutics, 2016. **511**: p. 30-43.

63. Bigi, A., Panzavolta, S., and Rubini, K. *Relationship between triple-helix content and mechanical properties of gelatin films.* Biomaterials, 2004. **25**(25): p. 5675-5680.

Chapter 3: Layering of Hydrogels and Fabrication at the Hydrogel-Hydrogel Interface

3.1 INTRODUCTION

As discussed in Chapter 2 of this dissertation, hydrogels are commonly used in physiological studies today due to their desirable biocompatible properties. When specific characteristics about a hydrogel are known and able to be manipulated, such as viscosity or melting temperature, research possibilities broaden significantly. For example, attempts to layer hydrogels have been employed to mimic various biological interfaces, as the hydrogel's relatively high water content mimics that of naturally occurring lubrication materials such as mucin. [1] Often these layers are composed of substances with different viscoelastic profiles, such as silicone contact lenses and mucin that protects the ocular surface of the eye. [1-5]

The ability to generate model hydrogel layers allows for physiological scenarios such as biocompatibility of contact lens materials [6-7] and controlled drug release via contact lens-eye interaction [8-10] to be studied in depth prior to clinical trials. Additional applications include artificial organs, [11-12], wound management, [13-17], and artificial membranes. [17-20] In addition to hydrogel layering, these materials are also widely used for drug delivery through controlled release mechanisms, which include hydrogel diffusion, swelling and biodegradation. [21-28]

In order to create hydrogel layers of a desired shape and size, molds can be employed to secure each hydrogel as they transition from a viscous to a gelled product. A commonly used material in molding hydrogels is polydimethylsiloxane (PDMS). [29-31]

PDMS is non-toxic and largely biocompatible, [31-36] making it ideal for the study of biological systems such as those presented here. Since hydrogels being used in the experiments described in this chapter come in direct contact with the mold, it was of utmost importance to ensure the mold material would have minimal impact on bacterial cells dispersed throughout the hydrogel solution. Additionally, adhesion between hydrogel and mold needed to be minimal to allow for full removal of the mold with little to no structural impact on the set hydrogels. The highly hydrophobic nature of PDMS makes it ideal in preventing significant adhesion, [37-38] as hydrogels have hydrophilic qualities due to their high water content. The combination of these hydrophobic and hydrophilic properties results in weak interaction between PDMS and hydrogel, enabling smooth and non-destructive removal of the PDMS mold once the layered hydrogels fully set.

In former studies from the Shear lab, PDMS has been used in microfluidic platforms for the creation of non-toxic, biocompatible channels for bacteria to flow through. [39-40] The combination of PDMS with customizable hydrogel technology allows for an even greater breadth of experimental study, as PDMS can either be used as a platform for layered hydrogels or, in the studies presented here, as a mold to secure hydrogels when layering solutions of varying gelatin composition. Expanding upon the successful layering of hydrogels, micro-3D printing was integrated with fabrication of protein structures at the hydrogel-hydrogel interface.

Following layering of two hydrogels of markedly different melting temperature on the tip of a glass rod, structures were fabricated at the interface such that they captured

microbeads and/or bacteria (located in low-melting-temperature hydrogel) while simultaneously anchoring into the high-melting-temperature hydrogel (attached to a glass rod). This allowed for excess, uncaptured bacteria to be rinsed away with the low-melting-temperature hydrogel, while the captured bacteria remained in the fabricated structures attached to the high-melting-temperature hydrogel. The rod containing the bacterial structures can then be moved and introduced to any environment of interest (i.e. chronic wounds, CF lung sputum, etc), after which the high melting temp hydrogel can be slowly heated, allowing for controlled release of fabricated structures.

The ability to pre-fabricate these structures prior to release in biological systems is beneficial for many reasons. Biological environments, especially those involved in physiological processes (i.e. epithelial tissue, ocular surfaces, etc.) are quite delicate in nature, and would not be amenable to the capture of bacteria within micro-3D printed structures, as the addition of reagents, bacteria, and the laser scanning process itself would damage the native cells. Therefore, the ability to pre-fabricate these structures prior to release *in vitro* or *in vivo* allows us to deliver well-defined colonies of bacteria into environments where they cannot be readily printed. Additionally, as bacteria being released are contained within protein structures, the impact of captured bacteria on the environment of interest can be studied without introducing further infection.

3.2 Materials and Methods

3.2.1 Materials

Tryptic soy agar (TSA, R455002) and tryptic soy broth (TSB, 8053765) were obtained from Remel and EMD Millipore, respectively. Gelatin type A from porcine skin, 60 Bloom (160304) was purchased from EMS. Gelatin type A from porcine skin, 300 Bloom (9000-70-8) was purchased from Sigma. Bovine serum albumin (BSA, 9048-46-8) was obtained from Equitech Bio. Rose Bengal (RB, 632-69-9), carbenicillin disodium salt (4800-94-6), microscope coverslips (#1 borosilicate, 22x22, Lab-Tek), and eight-well chambered coverslips (#1 borosilicate, 25x57, Lab-Tek) were purchased from Thermo Fisher Scientific. 1-3 μm diameter microbeads (7732-8-5) were obtained from Polysci. PDMS base and crosslink kits were purchased from Sylgard. Ethanol was purchased from Pharm Co (64-17-5). HEPES (75277-39-3) was obtained from ACROS. Glass rods were cut and provided courtesy of the UT chemistry glass shop. All reagents were stored and used according to supplier specifications.

3.2.2 Bacteria Strain and Culture

Wild-type *Pseudomonas aeruginosa* strains Pa01 and Pa14, each constitutively expressing GFP from plasmid pMRP9-1, were used in all bacterial studies. The plasmid was maintained using TSA plates dosed with 100 μg/mL carbenicillin. Planktonic cultures were grown aerobically overnight at 37 °C on a shaker set to 250 rpm, using the TSA plate to seed cells into a culture tube filled with 4 mL TSB. Following overnight culture, cells

were diluted 1:50 into a fresh culture tube and allowed to grow on the shaker for an additional two hours to reach the desired experimental cell density of ~0.3 at OD600.

3.2.3 Hydrogel Preparation

Hydrogels were prepared using TSB, gelatin, BSA, and RB, as described in section 2.2.3. In studies without bacteria, solutions contained 1 mL TSB, 40 mg/mL BSA, and 10 mg/mL RB (giving a final photosensitizer concentration of 10 mM). In studies using bacteria, the initial volume of each solution was 880 µL, as the addition of 120 µL from the bacterial culture tube served to dilute each solution to the desired concentration. Two hydrogels were used during these studies, one that had a "low" melting temperature (LMT) and one that had a "high" melting temperature (HMT). The low temperature solution was prepared from 150 mg/mL Type A 60 bloom gelatin while the high temperature solution was made from 200 mg/mL Type A 300 bloom gelatin, compositions that resulted in average melting temperatures of 29.7 ºC and 34.0 ºC, respectively.

3.2.4 Preliminary Solution Molding

Initial molding studies utilized a flat PDMS sheet with shapes of customizable size excised from the center. Once the desired shape was obtained, the PDMS sheet was pressed to the surface of a glass coverslip to form as tight of a seal as possible. High melting temperature solution was then pipetted into the mold until all exposed glass was covered. To obtain a flat surface on both the top and bottom of the solution, the excised piece of PDMS was pressed back into the original PDMS sheet to apply gentle compression to the solution as it hardened, a schematic of which can be seen in Figure 3.1.

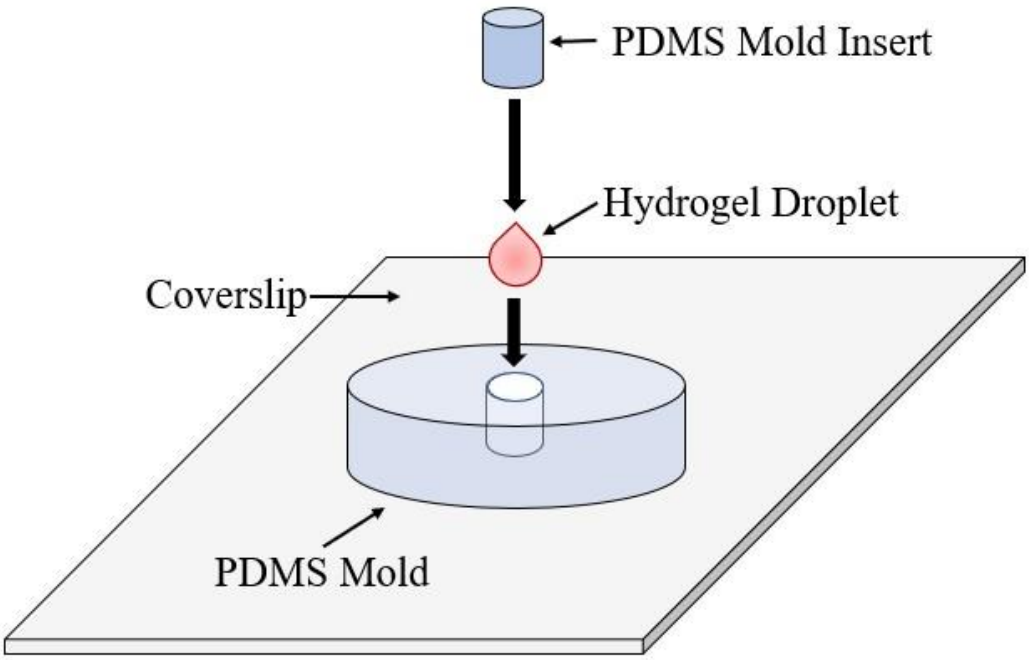

Figure 3.1: Initial Molding Schematic for Hydrogels

A solid, short cylinder made of PDMS was formed using base and crosslinker from a PDMS kit. A cylindrical piece was excised out of the center of the PDMS and stored for future use. The PDMS was pressed firmly against a borosilicate glass coverslip to form as tight of a seal as possible, then a small amount of hydrogel solution (~20 µL) was pipetted into the open central cavity. The excised piece of PDMS was then inserted back into the center of the cylinder and gently pressed against the top of the hardening hydrogel, creating a flat surface on the top and bottom of the molded solution. Upon insertion of the excised piece, the setup was stored at 4 ºC to promote further gelation before the PDMS cylinder was removed from the coverslip approximately 10-15 minutes later.

The solution was then placed in a fridge set to 4 ºC for 10-15 minutes to encourage complete gelation. Upon removal from the fridge, the PDMS was gently peeled away from the solution, leaving behind a molded hydrogel of the desired shape and size.

When molding the hydrogel on to a glass rod (diameter = 1.85 mm), a cylinder of slightly larger diameter was excised from the PDMS sheet, and the rod itself was used to compress the solution during cooling as opposed to the excised piece of PDMS. To ensure that the molded hydrogel preferentially attached to the rod over the coverslip, the coverslip was placed on an ice pack (frozen at 4 ºC) for 5 minutes prior to removing the PDMS and lifting the rod away from the glass.

3.2.5 Layering of Solutions on Glass Rod

To layer the hydrogels for fabrication, a small droplet (~10 µL) of LMT hydrogel was placed on a coverslip, after which the glass rod with attached molded HMT hydrogel was gently pressed into the low temperature droplet, thereby creating a coverslip, LMT hydrogel, HMT hydrogel, glass rod progression of layers. Mechanisms by which the glass rod was stabilized during this step can been seen in Figure 3.2.

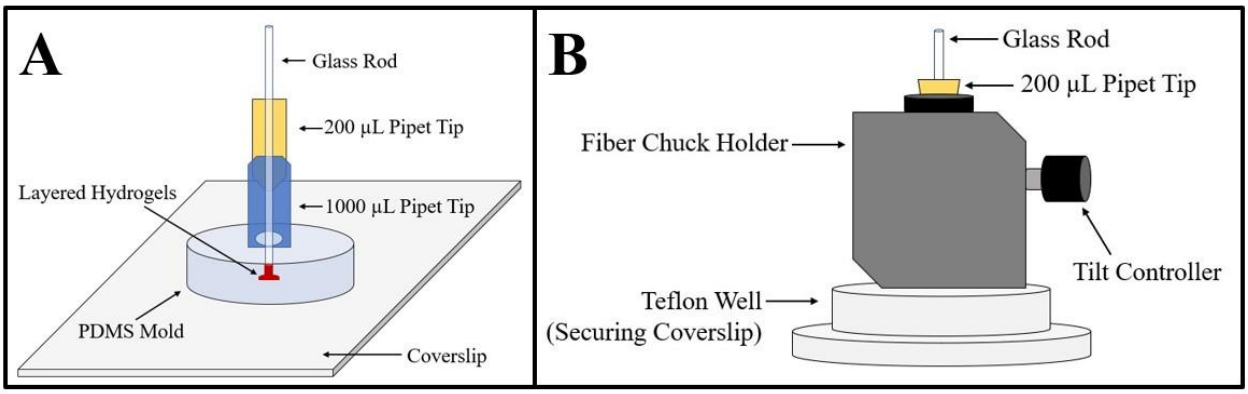

Figure 3.2: Glass Rod Stabilization Methods for Hydrogel Layering

Two methods were used to stabilize the glass rod during the hydrogel layering and setting process. (A). Two pipet tips of different sizes were cut and wedged together to create an apparatus that would hold the rod steady while having a large enough area at the base to balance on top of the PDMS mold. This was the initial hydrogel molding step before proceeding to fabrication. (B). A fiber chuck holder from ThorLabs was used in conjunction with a smaller cut pipet tip to stabilize the glass rod over a Teflon well, allowing the rod to be positioned and prepared for fabrication at the hydrogel interface.

3.2.6 Location of Solution Interface

The interface between the layered hydrogels can be extremely difficult to precisely identify using bright-field microscopy due to similar composition of the two hydrogels being used. To more accurately locate the solution interface, the molded HMT hydrogel was dipped into a suspension of 1-3 µm diameter microbeads in ethanol and allowed to stand for 10 minutes to allow the ethanol to fully evaporate from the hydrogel surface. The hydrogels were then layered in the same fashion as seen in Figure 3.2, and the interface was identified by locating and focusing on the microbeads using bright-field microscopy.

To create the microbead solution used, two drops of concentrated microbead suspension were added to a 1.5 mL Eppendorf tube, then diluted to 1 mL with DI water.

The tube was then centrifuged at level 10 for 5 minutes to separate the beads from the supernatant. After removal of the DI water, 1 mL of pure ethanol was added and the solution was vortexed for 15 seconds. For all experiments, 10 µL of the microbead solution was pipetted onto a clean coverslip for use in introducing the beads to the molded hydrogel layer on the glass rod.

3.2.7 Fabrication Setup and Procedure

Fabrication was conducted using the procedure detailed in Section 2.2.5, with a one major change regarding the stage setup. Due to the height of the rod-holding adapter, the traditional microscope lamp housing could not be used. To accommodate for this, a portable light source with a flexible head was employed as an illumination source. The light output was positioned directly above the rod and set to “medium” intensity, providing sufficient light through the glass rod to visualize microbeads when the hydrogel interface was positioned at the objective focal plane (Figure 3.3).

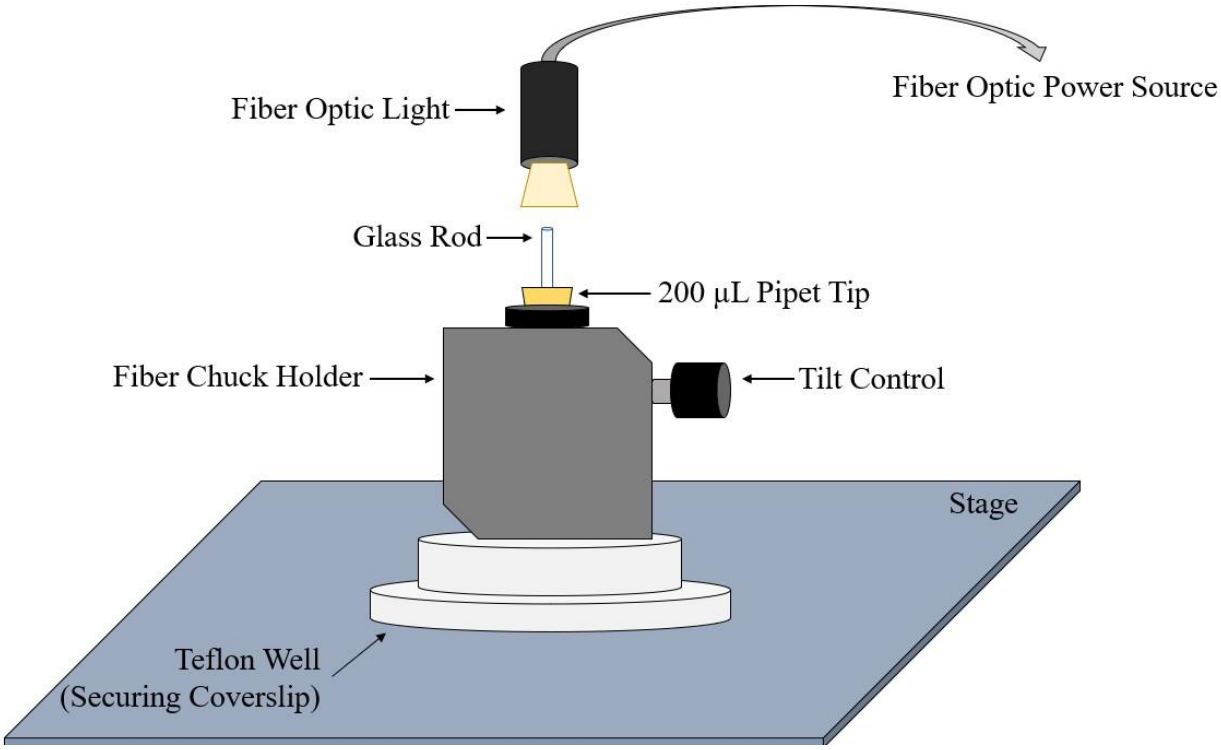

Figure 3.3: Schematic of Fabrication Setup

Following hydrogel molding and rod stabilization, the fiber chuck holder and Teflon well were moved to the microscope stage to prepare for fabrication. A fiber optic light was positioned directly over top of the glass rod and set to "medium" intensity, allowing the hydrogel interface to be illuminated and located. Due to the height of the fiber chuck holder, the traditional microscope lamp housing could not be used.

Protein boxes were fabricated around clusters of beads at the interface in such a way that the bulk of the structure was fabricated in the LMT hydrogel, while the far end was anchored into the HMT hydrogel. A schematic of the box along with its dimensions can be seen in Figure 3.4.

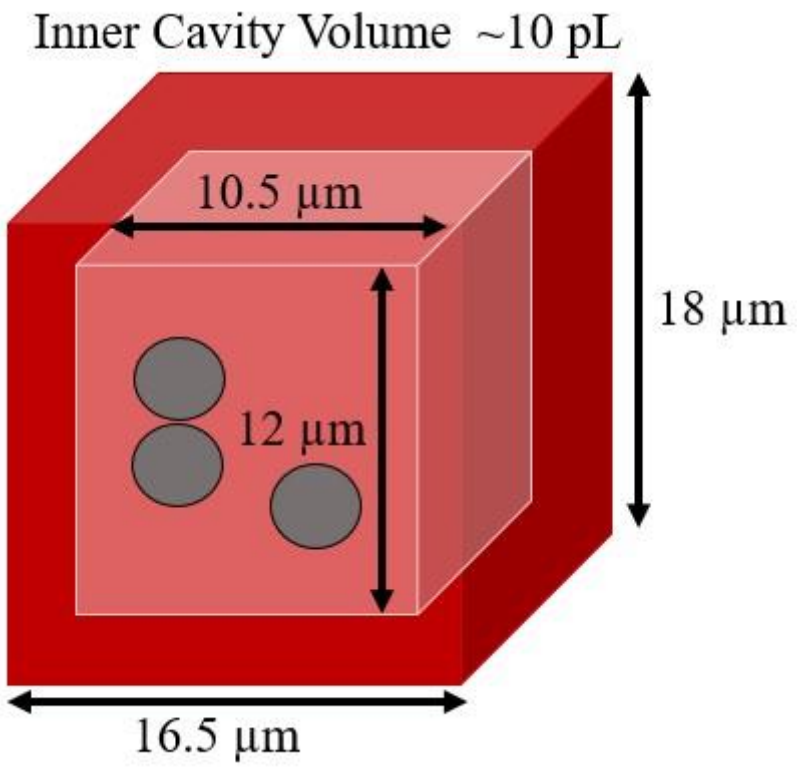

Figure 3.4: Structure Used for Fabrication Around Microbeads

A binary mask sequence was created using ImageJ to generate a hollow box for use in trapping microbeads at the interface of the layered hydrogels. Nominal outer dimensions were 18x16.5 µm and inner dimensions were 12x10.5 µm, creating a nominal inner cavity volume of ~10 pL. Each box was fabricated in such a way that one or more microbeads were captured (seen as grey circles above), with the top of the structure anchored in the high melting temperature hydrogel.

Upon completion of fabrication, the rod/adapter/well were placed on top of an 4 ºC ice pack for 5 minutes to encourage easier separation of the hydrogel from the coverslip (as a result of a thin layer of condensation forming between they coverslip and hydrogel).

3.2.8 Environmental Chamber Setup and Melting Procedure

A custom environmental chamber was used in all layered melting studies. The apparatus consisted of an arc lamp, heat gun, Hamamatsu camera, Prior Proscan stage capable of submicrometer resolution in the x-, y-, and z- dimensions, and a Zeiss 135 Axiovert inverted microscope, whose imaging procedures were controlled by MetaMorph software. A plexiglass box outfitted with attachments for the heat gun air ducts were connected to a stage insert and controlled by a set of attached drivers. For secondary confirmation of chamber temperature, a thermocouple was placed just inside the plexiglass box.

Upon securing a petri dish or fabrication well containing layered hydrogels on a coverslip, and HEPES buffer inside the chamber, the heat gun was adjusted to a set temperature of 40 °C. Change in chamber temperature were monitored via thermocouple until structures anchored in the HMT hydrogel were released. This release was indicative of complete dissolution of the LMT solution and partial dissolution of the HMT solution. Released structures were visualized via bright-field microscopy, with images captured and analyzed using MetaMorph and ImageJ, respectively.

Two additional methods for removing the LMT solution from the layered hydrogels attached to the glass rod were also examined, both of which required removal of the rod and attached hydrogel layers from the glass coverslip used during fabrication. This required contact between an ice pack and the base of the coverslip for ~5 minutes, thereby loosening the bond between the borosilicate glass and hydrogel.

The first method used HEPES buffer that was pre-heated to 60 ºC in an oven. The rod and hydrogels were secured over one well of an eight-well chambered coverslip in a manner such that the layered hydrogels were contained within the well without touching the bottom of the well. Multiple aliquots of heated buffer were pipetted into the well to agitate and gradually rinse away the hydrogels attached to the rod, with the LMT hydrogel being removed first. The tip of the glass rod was examined via microscopy following every rinse to keep track of when the boxes started to release from the HMT hydrogel. Boxes were fabricated at the interface of the two hydrogels, as mentioned in the previous section, with each box trapping one or more microbeads. No bacteria were used in these studies.

The second method secured the hydrogels in a glass petri dish containing room temperature (20 ºC) HEPES buffer and a small stir bar, all of which were placed on a hot plate. The HEPES was gradually heated until the hydrogels began to dissolve, using the stir bar to continuously agitate the solution, as can be seen in Figure 3.5.

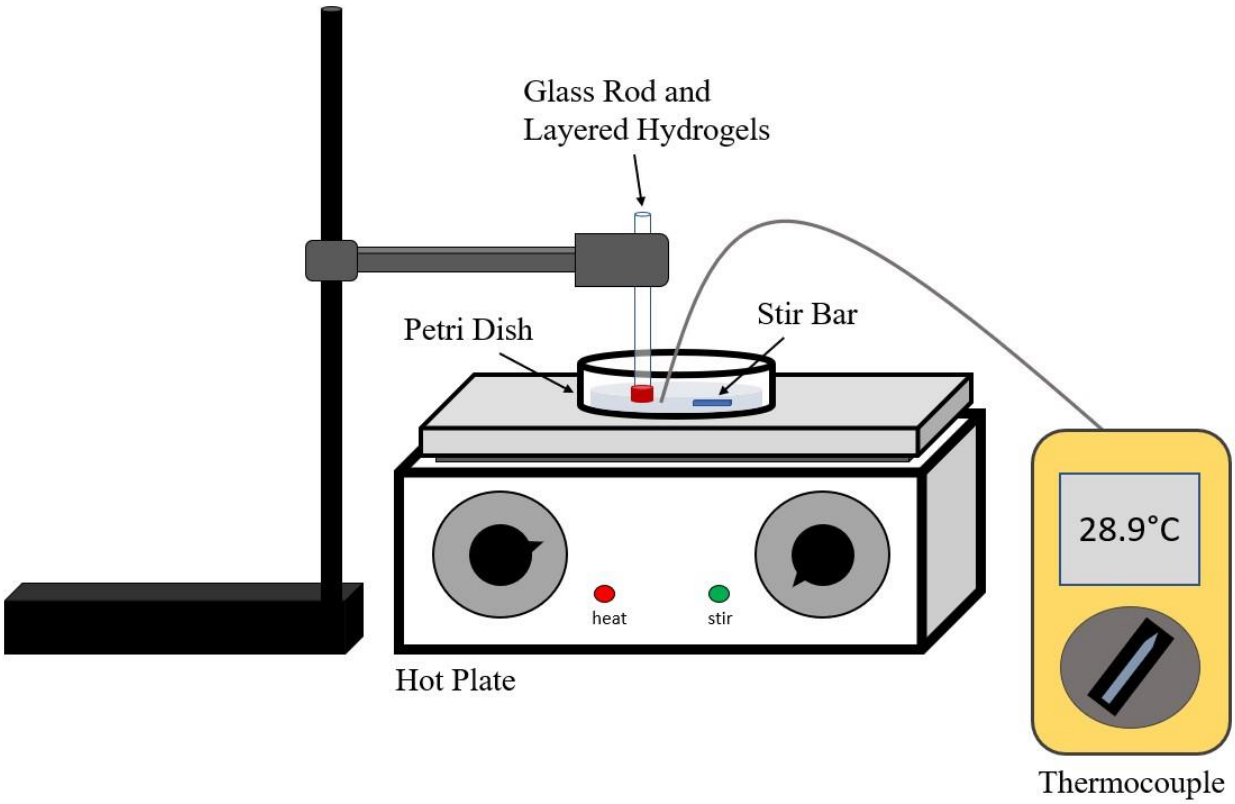

Figure 3.5: Setup for Melting of Layered Hydrogels and Release of Fabricated Structures

Following fabrication and removal from the coverslip, the rod to which the layered hydrogels are attached was secured to a ring stand via clamp and positioned over a petri dish filled with HEPES buffer. The rod was then lowered in such a way that the layered hydrogels were completely submersed in HEPES buffer. A stir bar was added to induce agitation, and the hot plate was turned on to a low setting, allowing the buffer to raise in temperature approximately 0.1 ºC every 30 seconds.

The temperature of the HEPES was monitored via thermocouple, while the tip of the rod was periodically checked via microscopy to gauge the level of dissolution that had taken place. Upon release of the boxes, the HEPES solution was pipetted out of the glass petri

dish and distributed amongst the wells of an eight-well chambered coverslip to locate and image each released box.

3.3 Results and Discussion

3.3.1 Efficacy of Layering Techniques and Molding Methods

Many different layering and molding techniques were attempted before finding the most efficient and reproducible methods, which are detailed in Sections 3.2.4 and 3.2.5. The first layering attempt was the most simplistic, in which two hydrogels of different melting temperatures were layered in an 'X' shape on a coverslip. The HMT hydrogel layer was pipetted onto the coverslip first and allowed to fully set before introducing the LMT layer, which was layered in an orthogonal manner. Almost immediately upon introduction, the LMT hydrogel began to slide off the high temperature hydrogel due to the low viscosity of the pre-heated LMT hydrogel. These results confirmed that in order to maintain the desired shape and position of layered hydrogels during the setting process, a mold would be necessary.

When deciding what material to make the mold out of, PDMS was the most obvious choice due to its elasticity and flexibility. As detailed in Section 3.2.4, a short cylindrical PDMS sheet was created, after which two small cylinders of different sizes were excised to create the holes that would act as molds for the hydrogel. During the first experiment using the PDMS mold, 200 µL of HMT solution was pipetted into the mold and placed in a 60 ºC oven for 5 minutes to assess whether the top of the hydrogel would settle into a flat surface. However, the PDMS mold did not form a tight seal with the coverslip, resulting in the hydrogel melting and leeching into the space between the mold and the coverslip. When a new trial was attempted in which the HMT hydrogel was allowed to set at room

temperature (~20 ºC) for 20 minutes, the result was an uneven surface containing small pockets from bubbles in the solution. These experiments indicated that an additional force would be needed to create the desired flat surface of the HMT hydrogel layer, which led to the excised piece of PDMS being pressed back into the mold (as seen in Figure 3.1). Once the HMT hydrogel was fully set, the excised piece of PDMS was removed and the LMT hydrogel was pipetted into the mold to create the final layered product.

Once the layering technique had been refined, the next hurdle was figuring out how to locate the interface between two hydrogels. As each layered hydrogel was made from the same components (gelatin, BSA, and RB), there were no distinct identifying features to assist with locating the interface between layers via bright-field microscopy. As a result, microbeads were utilized as a method to quickly and reproducibly locate where the HMT hydrogel ended and the LMT hydrogel began. A proof of concept experiment was done in which 10 µL of microbead solution was pipetted on top of the set HMT hydrogel prior to introducing the LMT hydrogel layer. It should be noted that allowing the ethanol from the microbead solution to evaporate was a crucial step with regards to the success of layering, as any liquid between the two hydrogels would only serve to weaken the bond between the two layers and cause fabrication difficulties in the future. A representative image of beads located at the hydrogel interface can be seen in Figure 3.6.

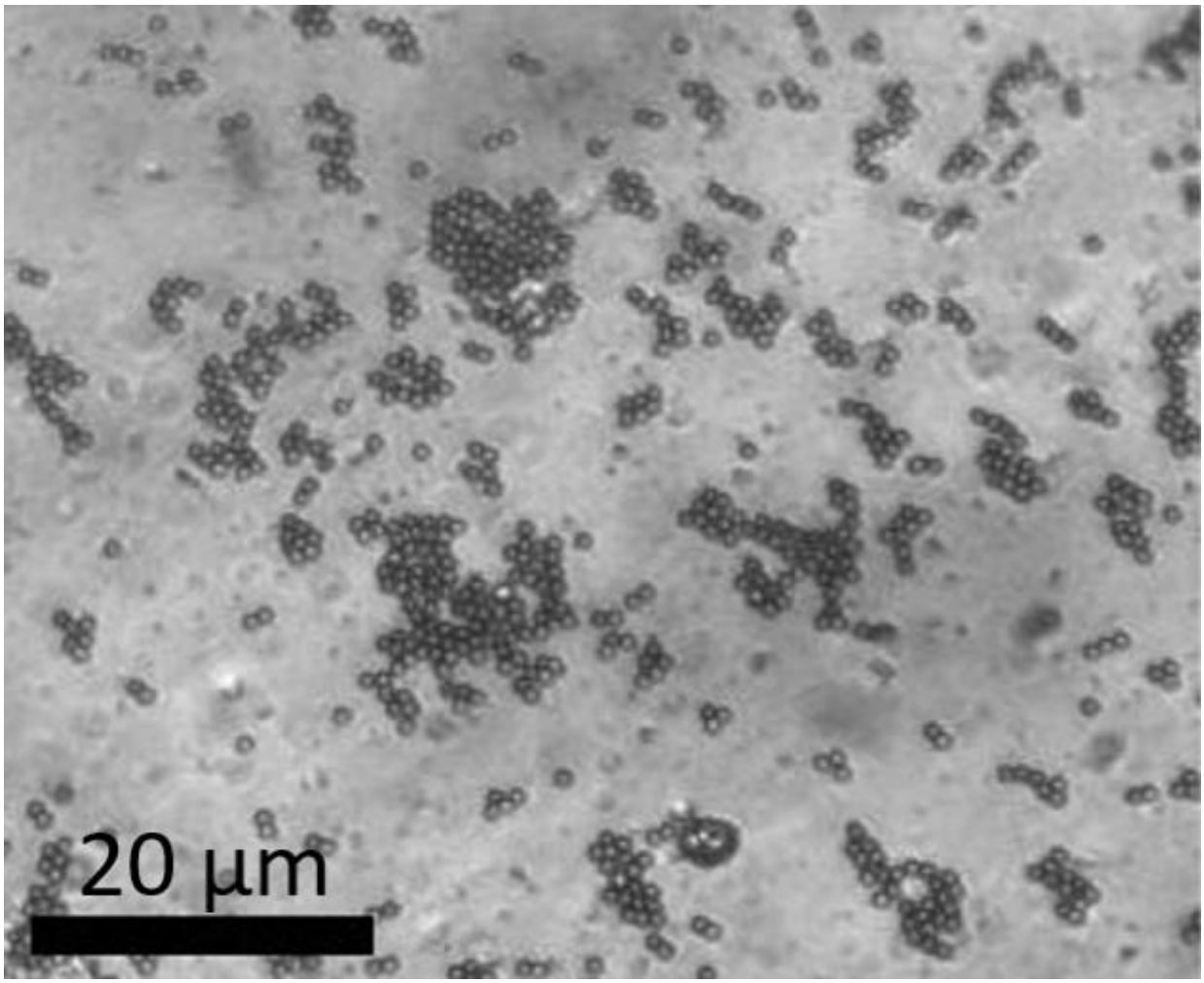

Figure 3.6: Microbeads Located at Hydrogel Interface

Microbeads were used to assist in locating the interface between the HMT and LMT hydrogels. Microbeads seen in this image are 1 µm in diameter.

3.3.2 Melting of Layered Hydrogels

Before attempting layering experiments on a moveable rod, we first evaluated our capacity to micro-3D print structures at, or near, the HMT/LMT interface of layered hydrogels on a borosilicate coverslip. Following reproducible location of the interface,

proof of concept experiments were completed in which solid rectangular structures were fabricated at the interface in such a way that structures were either entirely located in the LMT layer or anchored in the HMT layer. This allowed for a more thorough examination of how successfully and precisely the different hydrogel layers could be melted away.

The LMT and HMT hydrogels melted at 28.8 ºC and 33.8 ºC, respectively. Five solid rectangles were fabricated just above the hydrogel interface, meaning that they were all fully encased in the low temperature layer. Following fabrication, HEPES buffer was added to the fabrication well and the well was placed in the environmental chamber detailed in Section 3.2.8. Observations over the two-hour melting period can be seen in Table 3.1, with corresponding images in Figure 3.7.

Table 3.1: Dual-Layer Hydrogel Melting Observations with Fabricated Structures

Five rectangular structures were fabricated in the LMT hydrogel just above the LMT/HMT hydrogel interface. Gradual heating of the hydrogels in HEPES buffer occurred using a custom environmental chamber. After the HEPES buffer surpassed the recorded melting temperature of the LMT (28.8 ºC), the hydrogel began to melt, and structures were slowly released into solution, leaving only the HMT layer remaining.

Time Elapsed	Temperature	Structures Remaining/Observations
0 min	23.0 ºC	No structure movement, all five structures remain in field of vision
30 min	25.6 ºC	No structure movement, all five structures remain in field vision
60 min	27.4 ºC	No structure movement, all five structures remain in field of vision
80 min	29.0 ºC	No structure movement, buffer became light pink indicating melting of hydrogel
100 min	29.8 ºC	Three structures moved out of field of vision indicating melting of LMT hydrogel and release of structures
120 min	30.5 ºC	Only one structure remains in field of vision, can see edge of LMT hydrogel

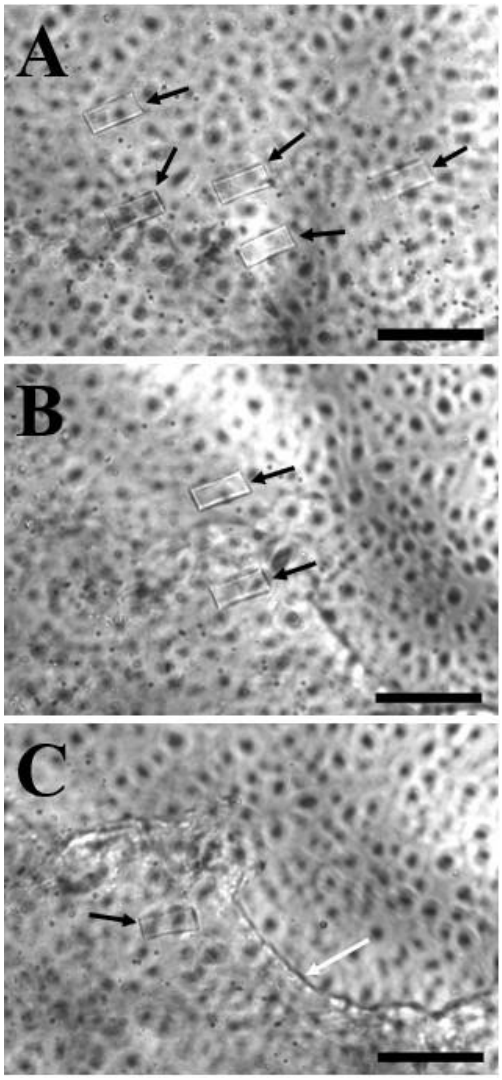

Figure 3.7: Dual-Layer Melting of Fabricated Structures at 60, 100, and 120 Minutes

All images were taken at 200x magnification while being heated in an environmental chamber. Scale bars represent 30 µm, black arrows identify structures. LMT and HMT hydrogels have melting temperatures of 28.8 ºC and 33.8 ºC, respectively. (A). 60-minute timepoint at 27.4 ºC, all five structures remain. (B). 100-minute timepoint at 29.8 ºC, two of five structures remain, indicating release of three structures due to melting of low temperature layer. (C). 120-minute timepoint at 30.5 ºC, only one structure remains. Edge of melted low temperature layer can be seen, as identified by white arrow.

3.3.3 Controlled Release of Structures Fabricated on Tip of Glass Rod

Expanding upon the work presented in Section 3.3.2 in which glass coverslips were used as the substrate of choice, a more versatile technology was developed that allowed for hydrogel layering and fabrication to occur on the tip of a 1.85 mm glass rod. By transitioning to a rod over a coverslip, greater mobility and versatility of the structures was obtained, as the rod could be placed in any environment and structures released accordingly. However, due to the size of the apparatus used to secure the rod prior to fabrication, the custom environmental chamber could not be used for melting purposes. Additionally, for controlled release of structures to take place, the rod and layered hydrogels had to be separated from the glass coverslip following fabrication.

Removing the rod and hydrogels from the glass coverslip proved to be a challenge, as the hydrogels preferentially adhered to the coverslip over the glass rod at room temperature. An example of this can be seen in Figure 3.8.

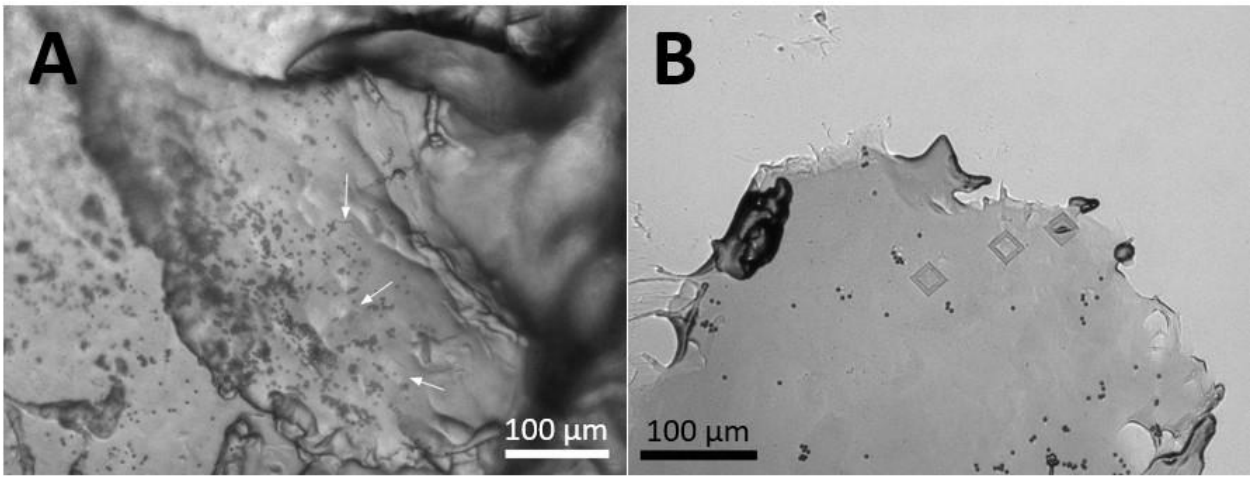

Figure 3.8: Ripped Hydrogel Comparison, Rod vs. Coverslip

Removal of glass rod and layered hydrogels from coverslip at room temperature. (A). Remaining hydrogel on tip of rod following removal at room temperature. White arrows identify fabricated structures. Rough and uneven surface texture is an artifact of hydrogel ripping during removal. (B). Hydrogel that remained adhered to glass coverslip following removal of layered hydrogels molded to glass rod. Half of fabricated structures, as well as scattered microbeads, remained in the hydrogel stuck to coverslip.

Warming the solution to loosen the bond between coverslip and hydrogel was not an option due to lack of precise control over melting, making the premature release of structures a recurring problem. By taking the opposite approach, placing the fabrication well on top of a 4ºC ice pack for at least one minute, a small amount of condensation formed between the coverslip and molded hydrogel. This allowed the rod and molded hydrogels to be gently slid and removed from the coverslip without any tearing of the hydrogel or loss of fabricated structures.

Out of the two melting procedures detailed in Section 3.2.8, the method using HEPES buffer pre-heated to 60 ºC proved to be more amenable to locating the released

(i.e. free-floating) structures. Representative images of captured structures can be seen in Figure 3.9.

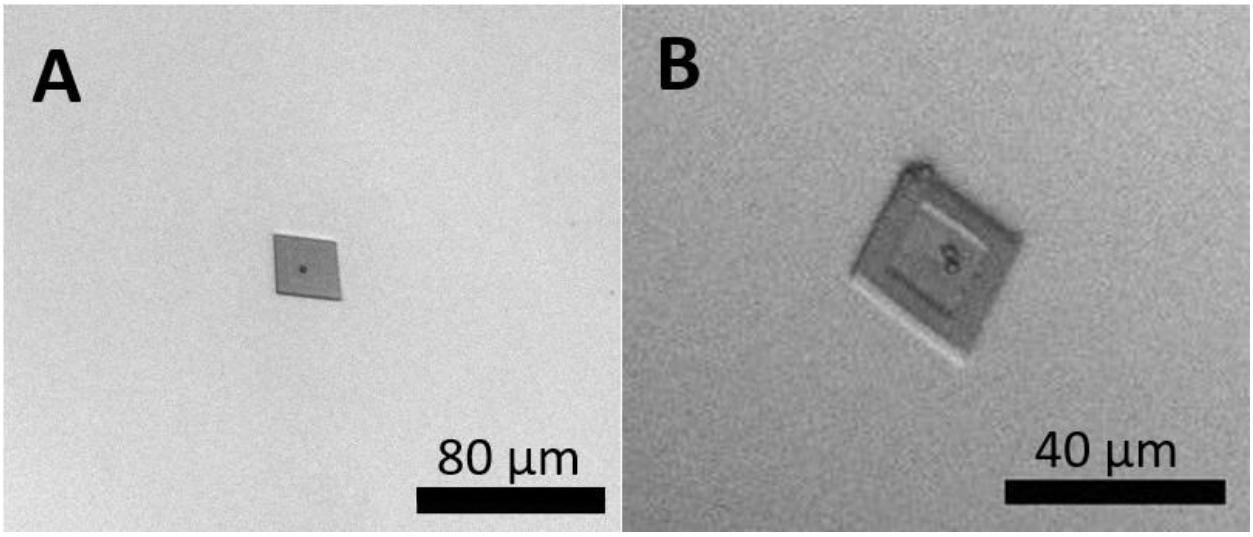

Figure 3.9: Structures Captured During Rinsing/Melting of Hydrogels on Tip of Glass Rod

Structures captured following melting and controlled release of layered hydrogels using preheated PDMS buffer in eight-well chambered coverslip. Captured beads are 3 µm in diameter. (A) Box containing one microbead. (B) Box containing two microbeads. One additional microbead can be seen in the top corner of the structure wall in panel B, indicating the wall was built surrounding it during fabrication.

This technique used an eight-well chambered coverslip, which proved to be a better receptacle than a petri dish with regards to locating and imaging structures following release. An attempt was made to centrifuge the solution from the petri dish as a method of isolating structures before re-immersing them in fresh HEPES, but no structures were recovered following this process, probably as a result of either remaining in the petri dish or adhering to the sides of the Eppendorf tube. There was also an attempt to filter the

structures out of solution, but once filtered they were unable to be removed from the filter itself without impacting the integrity of the structures.

Another component of the melting process that proved important was the strength with which the hydrogels were rinsed. Whether using buffer that was preheated or gradually heated on a hot plate, gentle rinsing was integral to maintaining homogenous melting of the layered hydrogels. When agitation became too vigorous, strips of hydrogel would detach before fully melting and releasing of fabricated structures. This phenomenon is illustrated in Figure 3.10.

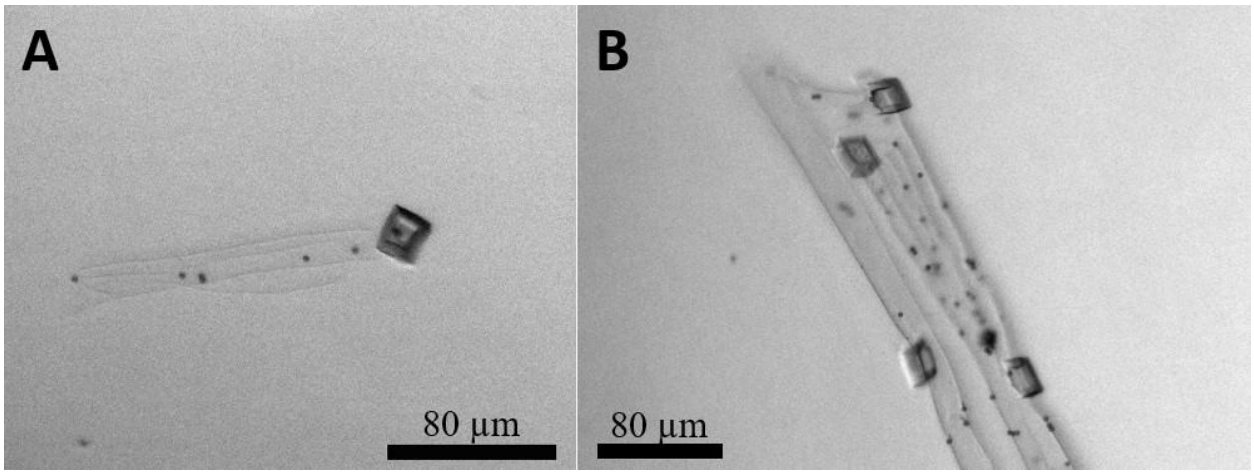

Figure 3.10: Structures Attached to Strips of Unmelted Hydrogel

Structures remaining partially adhered to strips of hydrogel that tore away during melting and rinsing of layered hydrogels. (A) Single fabricated box attached to thin strip of hydrogel, which can be seen extending to the left of the structure. (B) Four boxes adhered to a strip of hydrogel, allowing three-dimensional structure of boxes to be visualized.

This is not an ideal scenario, as the most successful controlled release studies would have minimal un-crosslinked hydrogel released. Additionally, an excess of hydrogel being

released into solution could also result in the release of excess bacterial cells that went uncaptured during the fabrication process, causing potential infection of the site being examined.

3.4 CONCLUSIONS

This chapter discussed layering hydrogels on the tip of a glass rod using a PDMS mold, as well as fabrication of structures at the hydrogel-hydrogel interface. Using the information gathered in Chapter 2 of this dissertation regarding customization of hydrogel melting temperatures, hydrogels of significantly different melting temperatures were created and used in all layering studies. To simplify location of the hydrogel-hydrogel interface, microbeads were incorporated between layers. However, in future studies it may be preferable to use an alternate method to identify the interface, as there were inconsistencies regarding successfully rinsing away all microbeads during melting and removal of the low-temperature hydrogel layer. If microbeads remain adhered to the high-temperature hydrogel, they will be released with fabricated structures into the environment being studied, which is not ideal.

The ability to fabricate structures at the hydrogel-hydrogel interface presents an exciting opportunity to combine multiphoton lithography with controlled release technologies. Traditionally, our lab has fabricated structures around bacteria on a coverslip, [41-46] an approach that is inherently static and provides no capabilities for manipulating, and potentially releasing, aggregates of defined size, shape, and sociomicrobiological state into remote environments. Layering hydrogels on a moveable surface (i.e. a glass rod tip) provides a means to capture bacteria, rinse away excess uncaptured bacteria (thus preventing further infection of the environment being studied), and release structures into any environment through controlled heating of the remaining hydrogel. Additionally, using the information presented in Chapter 2, hydrogels can be customized to maximize

compatibility with the cells or organisms being studied, as well as the environment captured cells are being released in. This chapter represents the first approach the Shear lab has taken at fabricating structures on a moveable surface, a technology that is expanded and advanced upon in studies presented in Chapter 4 of this dissertation.

3.5 REFERENCES

1. Dunn, A.C., *et al*. *Lubricity of surface hydrogel layers.* Tribol. Lett., 2013. **49**: p. 371-378.
2. Davidson, H.J. and Kuonen, V.J. *The tear film and ocular mucins*. Veterinary Ophtham., 2004. **7**(2): p. 71-77.
3. Peng, C. and Chauhan, A. *Ion transport in silicone hydrogel contact lenses*. J. Membrane Sci., 2012. **399**: p. 95-105.
4. Samsom, M., *et al. In vitro friction testing of contact lenses and human ocular tissues: effect of proteoglycan 4 (PRG4).* Tribology Int., 2015. **89**: p. 27-33.
5. Hori, Y., Argueso, P., Spurr-Michaud, S., and Gipson, I.K. *Mucins and contact lens wear*. Cornea, 2006. **25**(2): p. 176-181.
6. Qiao, H., Pham, C.M., Walther, H., Subbaraman, L.N., and Jones, L. *Depth profile assessment of the early phase deposition of lysozyme on soft contact lens materials using a novel in vitro eye model*. Eye Contact Lens, 2018. **44**: S11-S18.
7. Childs, A., *et al. Fabricating customized hydrogel contact lens*. Sci. Rep., 2016. **6**(1): p. 1-9.
8. Phan, C., *et al*. *Effects of antifungal soaked silicone hydrogel contact lenses on Candida albicans in an agar eye model*. Eye & Contact Lens: Science and Clinical Practice, 2016. **42**(5): p. 313-317.
9. Peng, C., and Chauhan, A. *Extended cyclosporine delivery by silicone-hydrogel contact lenses.* J. Controlled Release, 2011. **154**(3): p. 267-274.
10. Kim, J., Conway, A., and Chauhan, A. *Extended delivery of ophthalmic drugs by silicone hydrogel contact lenses*. Biomaterials, 2008. **29**(14): p. 2259-2269.
11. Wang, X., *et al*. *Gelatin-based hydrogels for organ 3D bioprinting.* Polymers, 2017. **9**(401): 1-24.
12. Verhulsel, M., *et al*. *A review of microfabrication and hydrogel engineering for micro-organs on chips.* Biomaterials, 2014. **35**(6): p. 1816-1832.
13. Anjum, S., Arora, A., Alam, M.S., and Gupta, B. *Development of antimicrobial and scar preventive chitosan hydrogel would dressings*. Int. J. Pharma. **508**(1): p. 92-101.
14. Singh, B., Sharma, S., and Dhiman, A. *Design of antibiotic containing hydrogel wound dressings: biomedical properties and histology study of wound healing*. Int. J. Pharma. **457**(1): p. 82-91.
15. Koehler, J., Brandl, F.P., and Goepferich, A.M. *Hydrogel wound dressings for bioactive treatment of acute and chronic wounds*. Euro. Polymer J., 2018. **100**: p. 1-11.

16. Balakrishnan, B., Mohanty, M., Umashankar, P.R., and Jayakrishnan, A. *Evaluation of an in situ forming hydrogel would dressing based on oxidized alginate and gelatin.* Biomaterials, 2005. **26**(32): p. 6335-6342.

17. Lacin, N.T. *Development of biodegradable antibacterial cellulose based hydrogel membranes for would healing*. Int. J. Bio. Macromol., 2014. **67**: p. 2-27.

18. Ye, Y.N., *et al. Tough and self-recoverable thin hydrogel membranes for biological applications.* Adv. Func. Mat., 2018. **28**(31): p. 1-11.

19. Kusters, I., *et al*. *Taming membranes: functional immobilization of biological membranes in hydrogels*. PLoS One, 2011. **6**(5): p. 1-9.

20. Ladet, S.G. Tahiri, K., Montembault, A.S., Domard, A.J. and Corvol, M.T.M. *Multi-membrane chitosan hydrogels as condrocytic cell bioreactors.* Biomaterials, 2011. **32**(23): p. 5354-5364.

21. Lin, C., and Metters, A.T. *Hydrogels in controlled release formulations: network design and mathematical modeling*. Adv. Drug Delivery Rev., 2006. **58**(12): p. 1379-1408.

22. Basu, S., Banerjee, D., Chowdhury, R. and Bhattacharya, P. *Controlled release of microencapsulated probiotics in food matrix*. J. Food Eng., 2018. **238**: p. 6169.

23. Wu, Z., Lin, X., Zou, X., Sun, J., and He, Q. *Biodegradable protein-based rockets for drug transportation and light-triggered release*. App. Mat. Interfaces, 2014. **7**: p. 250-255.

24. Nguyen, M.K. and Alsberg, E. *Bioactive factor delivery strategies from engineered polymer hydrogels for therapeutic medicine*. Progress in Polymer Sci., 2014. **39**: p. 1235-1265.

25. Gaowa, A., *et al*. *Combination of hybrid peptide with biodegradable gelatin hydrogel for controlled release and enhancement of anti-tumor activity in vivo*. J. Controlled Release, 2014. **176**: p. 1-7.

26. Zhang, Y., Tao, L., Li, S., and Wei, Y. *Synthesis of multiresponsive and dynamic chitosan-based hydrogels for controlled release of bioactive molecules*. Biomacromol., 2011. **12**: p. 2894-2901.

27. El-Ghaffar, M.A.A., Hashem, M.S., El-Awady, M.K. and Rabie, A.M. *pH-sensitive sodium alginate hydrogels for riboflavin controlled release.* Carbohydrate Polymers, 2012. **89**: p. 667-675.

28. Huynh, C.T., Nguyen, M.K., and Lee, D.S. *Biodegradable pH/temperature-sensitive oligo(β-amino ester urethane) hydrogels for controlled release of doxorubicin.* Acta Biomaterialia, 2011. **7**: p. 3123-3130.

29. Dang, T., Kim, Y.H., Choi, J.H., and Kim, G. *A novel simple preparation method of a hydrogel mold for PDMS micro-fluidic device fabrication*. J. Micromech. And Microeng., 2011. **22**: p. 1-8.

30. Rudy, A., *et al*. *Lubricous hydrogel surface coatings on polydimethylsiloxane (PDMS).* Tribiology Lett., 2017. **65**(3): 1-11.

31. Morales-Hurtado, M., Zeng, X., Gonzalez-Rodriguez, P., Ten Elshof, J.E., and van der Heide, E. *A new water absorbable mechanical epidermal skin equivalent: the combination of hydrophobic PDMS and hydrophilic PVA hydrogel*. J. Mech. Behav. Biomed. Mat., 2015. **46**: p. 305-317.

32. Yao, M. and Fang, J. *Hydrophilic PEO-PDMS for microfluidic applications*. J. Micromech. Microeng., 2012. **22**(2): p. 1-6.

33. Hwang, Y., Paydar, O.H., and Candler, R.N. *3D printed molds for non-planar PDMS microfluidic channels*. Sensors and Actuators A: Phys., 2015. **226**: p. 137-142.

34. Lin, Y., *et al. Preparation and evaluation of chitosan biocompatible electronic skin*. Computers in Industry, 2018. **100**: p. 1-6.

35. Hu, X., *et al. A novel method to prepare homogeneous biocompatible graphene-based PDMS composites with enhanced mechanical, thermal, and antibacterial properties.* Polymer Composites, 2018. **0**(0): p. 1-10.

36. Bosman, W.M.P.F., *et al*. *Treatment of types II-IV endoleaks by injecting biocompatible elastomer (PDMS) in the aneurysm sac: an in vitro study*. J. Endovasc. Therapy, 2011. **18**: p. 205-213.

37. Stanton, M.M., Ducker, R.E., MacDonald, J.C., Lambert, C.R., and McGimpsey, W.G. *Super-hydrophobic, highly adhesive, polydimethylsiloxane (PDMS) surfaces*. J. Colloid and Interface Sci., 2012. **367**(1): p. 502-508.

38. Jin, M., *et al*. *Super-hydrophobic PDMS surface with ultra-low adhesive force.* Macromol. Rapid Comm., 2005. **26**(22): p. 1805-1809.

39. Moorjani, S., Nielson, R., Chang, X.A., and Shear, J.B. *Dynamic remodeling of subcellular chemical gradients using a multi-directional flow device*. Lab on a Chip, 2010. **10**: p. 2139-2146.

40. Spivey, E.C., Xhemalce, B., Shear, J.B., and Finkelstein, I.J. *3D-printed microfluidic microdissector for high-throughput studies of cellular aging.* Anal. Chem., 2014. **86**(15): p. 7406-7412.

41. Connell, J.L., *et al*. *Probing prokaryotic social behaviors with bacterial "lobster traps."* mBio, 2010. **1**(4): p. 1-8.

42. Connell, J.L., Whiteley, M., and Shear, J.B. *Sociomicrobiology is engineered landscapes.* Nature Chem. Bio., 2012. **8**(1): p. 10-13.

43. Connell, J.L., Ritschdorff, E.T., Whiteley, M., and Shear, J.B. *3D printing of microscopic bacterial communities.* PNAS, 2013. **110**(46): p. 18380-18385.

44. Wessel, A.K., *et al. Oxygen limitation within a bacterial aggregate*. mBio, 2014. **5**(2): p. 1-9.

45. Connell, J.L., Kim, J., Shear, J.B., Bard, A.J., and Whiteley, M. *Real-time monitoring of quorum sensing in 3D-printing bacterial aggregates using scanning electrochemical microscopy*. PNAS, 2014. **111**(51): p. 18255-18260.

46. Connell, J.L., Ritschdorff, E.T., and Shear, J.B. *Three-dimensional printing of photoresponsive biomaterials for control of bacterial microenvironments.* Anal. Chem., 2016. **88**: p. 12664-12271.

Chapter 4: Fabrication on Optical Fiber Tip

4.1 Introduction

Fiber optic technology has been a force in the transmission of data since its first applications in the 1960-70s. [1] Upon development of the first low-loss (20 db/km) fiber in 1970, [2] glass fibers became a primary component in telecommunications systems, with multimode fibers being of particular interest due to their high numerical aperture and large diameter, allowing multiple wavelengths of light to be propagated simultaneously. [3-4] Fiber optic bundles were utilized in public telephone systems and submarine cables as early as 1978, allowing for long-distance communication to occur with ever-increasing speed. [5]

The guiding principle behind the propagation of light down an optical fiber is total internal reflection, which was introduced theoretically by Kepler in 1611 [6] and presented mathematically by Huygens in 1690. [7] Total internal reflection occurs when light encounters a medium of lesser refractive index, causing the light to reflect internally, thus preventing transmission or loss of light from the original medium. For optical fibers, this is achieved by coating the glass fiber with a low-loss dopant such as GeO_2 [8] or P_2O_5, [9-10] which forms an exterior layer with a lower refractive index than the SiO_2 core. This doped layer is referred to as the cladding, which can be further protected by a buffer coating.

Since these early discoveries, optical fibers have been used for a wide variety of applications, including communications, [11] manufacturing, [12] medicine, [13] and

sensing. [14] In particular, optical fiber sensing has become a popular technique with regards to biomedical applications. Optical fibers offer a multitude of advantages over conventional sensing techniques, as fibers are not susceptible to electromagnetic interference and possess a high tolerance for harsh environments such as high temperature and pressure. [14] Additionally, the small size of the fiber, generally with a diameter of 250 μm or less, makes it minimally invasive in experiments such as tissue heat-mapping [15] and cryo-ablation. [16] Biosensing techniques have advanced significantly in recent years, allowing for sensing and imaging to occur at the single-cell [17-18] and single-molecule levels. [19-20]

Within the past two decades, fiber optic cell sensing applications have begun immobilizing whole cells on the fiber surface to function as a light-producing, chemical-sensing element. [21-26] One of the first such applications came in 2000, when Polyak et al. immobilized bioluminescent *E. coli* around an optical fiber tip. [22] These bacteria were genetically modified to luminesce in the presence of genotoxicants (i.e. mitomycin C, which damages cellular DNA), thus creating a microbial-based optical biosensor. In this study, bacteria were immobilized on an optical fiber tip using a calcium alginate matrix. While calcium alginate is a biocompatible matrix, it is prone to degradation due to gradual leeching of calcium, resulting in the sodium alginate, and thus reporter cells, dissolving back into solution. Additionally, this method provides little to no control over location and density of the immobilized bacteria, causing inconsistencies in bacterial population from one probe to the next. [21-22] More recent studies have transitioned from alginate matrices

to silica gels for cellular immobilization. [27] While this solves the issue of matrix dissolution, the limitations regarding density and spatial control of bacterial populations remains.

Recent studies from the Shear lab have utilized dynamic, mask-based multiphoton lithography to 3D print micron-scale protein structures around bacteria of interest. [28-32] The biocompatible, porous nature of these structures allows bacteria to exchange nutrients, waste, and sensing molecules with the surrounding environment. These qualities help facilitate the growth of discrete, high-density low-volume (as small as ~1 pL) bacterial populations. [32] Previously, these microstructures have been restricted to static coverglass substrates, [28-32] limiting their applications with regards to remote sensing. However, by translating this 3D printing technology from glass coverslips to optical fiber tips, we can overcome these spatiotemporal limitations. The research presented in this chapter details this technological advancement, opening exciting and previously unforeseen possibilities regarding dynamic distance studies and microbial sensing using discretely designed bacterial microstructures on the tip of an optical fiber.

4.2 Materials and Methods

4.2.1 Materials

Tryptic soy agar (TSA, R455002) and tryptic soy broth (TSB, 8053765) were obtained from Remel and EMD Millipore, respectively. Gelatin type A from porcine skin, 60 Bloom (160304) was purchased from EMS. Bovine serum albumin (BSA, 9048-46-8) was obtained from Equitech Bio. Rose Bengal (RB, 632-69-9), carbenicillin disodium salt (4800-94-6), and microscope coverslips (#1 borosilicate, 22x22, Lab-Tek) were purchased from Thermo Fisher Scientific. PDMS base and crosslink kits were purchased from Sylgard. Ethanol was purchased from Pharm Co (64-17-5). PDMS base and crosslink kits were purchased from Sylgard. Fiber optic (FG105LCA, TS1472053) and a corresponding fiber chuck were purchased from ThorLabs. Copper tape (16074), colloidal graphite paste (16053), and SEM pin stub mounts (16111) were purchased from Ted Pella. All reagents were stored and used according to supplier specifications.

4.2.2 Optical Fiber Specifications

A multimode fiber with 105 µm diameter pure silica core was used in all experiments. The core was surrounded by 125 µm diameter cladding composed of fluorine-doped silica and 250 µm diameter acrylate coating. A numerical aperture (NA) of 0.22 and the presence of a low concentration of hydroxyl groups results in this fiber being best suited for visible to IR transmission, making it ideal for our purposes. For all experiments, fiber was cleaved using the SainSmart FC-6S Optical Fiber Cleaver.

4.2.3 Bacteria Strains and Culture

Wild-type *Pseudomonas aeruginosa* strains Pa01 and Pa14, each constitutively expressing GFP from plasmid pMRP9-1, were used in all bacterial studies. The plasmid

was maintained using TSA plates dosed with 100 μg/mL carbenicillin. Planktonic cultures were grown aerobically overnight at 37 °C on a shaker set to 250 rpm, using the TSA plate to seed cells into a culture tube filled with 4 mL TSB. Following overnight culture, cells were diluted 1:50 into a fresh culture tube and allowed to grow on the shaker for an additional two hours to reach the desired experimental cell density of ~0.3 at OD600.

4.2.4 Hydrogel Preparation

Hydrogels were prepared using TSB, gelatin, BSA, and RB, as described in Chapter 2 (Section 2.2.3) of this dissertation. Three hydrogel compositions were used during these studies in an effort to find the ideal combination of low cytotoxicity and high structural adhesion to the fiber core. The hydrogel with the lowest melting temperature (26 ºC) contained 40 mg/mL BSA, 150 mg/mL Type A 60 bloom gelatin, and 5.09 mg/mL RB, giving a final photosensitizer concentration of 5 mM. The final two hydrogels both had a melting temperature of 29ºC. Each contained 200 mg/mL Type A 60 bloom gelatin but differed in their respective concentrations of BSA and RB. One solution had 40 mg/mL BSA and 5 mM RB, while the second solution contained 80 mg/mL BSA and possessed a RB concentration of 7 mM (7 mg/mL). In studies without bacteria, solutions were mixed in 1 mL TSB. In studies using bacteria, the initial volume of each solution was 880 μL, as the addition of 120 μL from the bacterial culture tube served to dilute each solution to the desired concentration.

4.2.5 Use of PDMS Mold to Secure Fiber

A circular PDMS mold was created by mixing PDMS base and crosslinker and allowing the solution to set overnight in a small plastic petri dish. Upon removing the PDMS mold from the petri dish, a small cross-cut was made using a razor blade through which a 1-inch segment of optical fiber was threaded and secured. Upon securing a glass coverslip in a Teflon fabrication well, a small droplet of hydrogel was placed on the coverslip. The PDMS mold and fiber were then quickly placed on top of the well in such a way that the tip of the fiber was submerged in the hydrogel prior to the solution fully setting. A schematic of this setup can be seen in Figure 4.1.

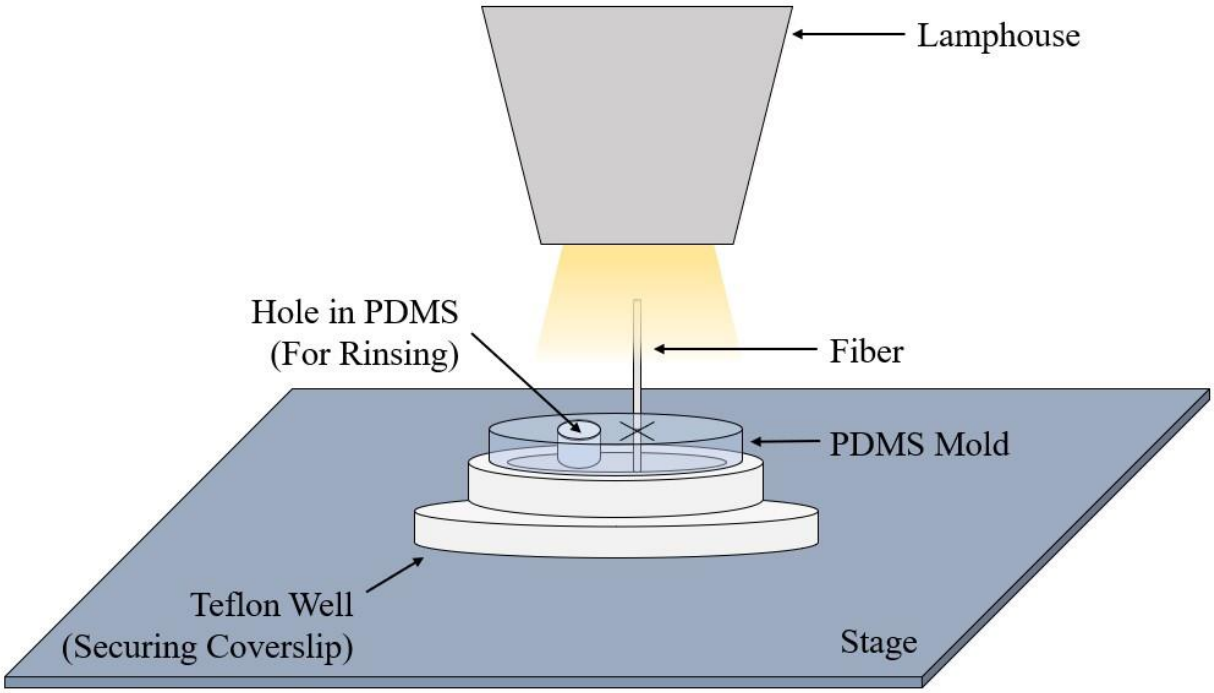

Figure 4.1: Fabrication Using PDMS Mold to Secure Fiber

A solid, short cylinder made of PDMS was formed using base and crosslinker from a PDMS kit. A crosscut transecting the mold was made using a razor blade, creating the opening through with the fiber was threaded. A small, cylindrical hole was excised from the PDMS to allow for rinsing and removal of excess hydrogel while not disturbing the PDMS or fiber location. Upon threading the fiber through the PDMS crosscut, the fiber was manually manipulated to the desired height above the coverslip. Then, a small amount of fabrication reagent solution (~20 µL) was pipetted onto the coverslip and the PDMS mold immediately placed on top of the well such that the tip of the fiber was submerged in reagent. The hydrogel was allowed to set for 5-10 minutes at ambient temperature before fabrication began.

4.2.6 Creation of Custom Stage

A custom fiber optic mount was created for fabrication purposes to improve upon the spatial accuracy and manipulation of the PDMS mold. The mount, secured on a microscope stage insert, consists of three individually addressable microactuators controlling the x, y, and z-axes. These manipulate an attached fiber chuck through which

the optical fiber was threaded and secured in place. A schematic of the stage can be seen in Figure 4.2.

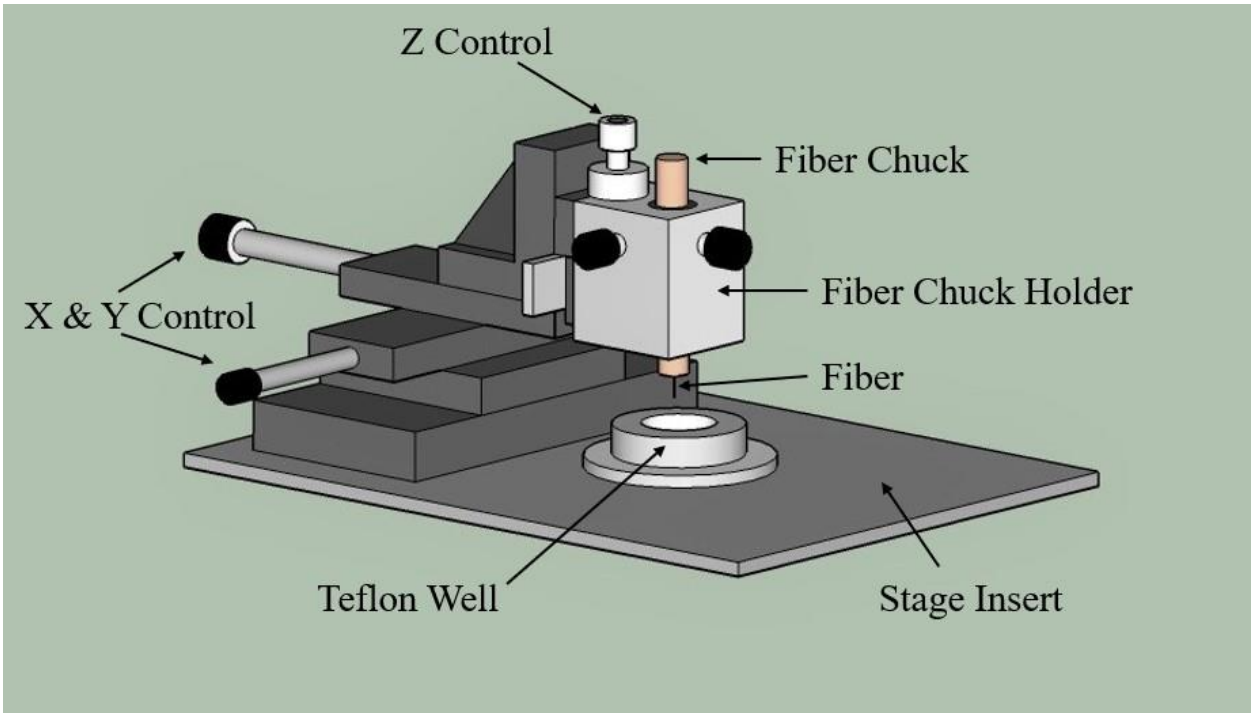

Figure 4.2: Custom Fiber Stage Schematic

Custom mount consists of three individually addressable microactuators controlling the x, y, and z-axes. These manipulate an attached fiber chuck through which an optical fiber is threaded and secured in place. The mount is attached to a microscope stage insert, which is slotted into an Axiovert 135 microscope stage. The Teflon well holding the hydrogel droplet (~15 µL) is placed below the fiber chuck and secured in place with tape, after which the fiber is quickly lowered and positioned ~30 µm above the coverslip. The hydrogel is then allowed to set around the fiber for 5-10 minutes before fabrication begins. The stage is counterbalanced during fabrication using a metal weight on the opposite side of the Teflon well from the fiber chuck holder.

To minimize movement of the mount during fabrication, a metal counterweight was placed on the side of the stage opposite of the fiber. To account for the increased height of the stage, any objective used during fabrication and/or imaging must be elevated using a

threaded adapter from ThorLabs. Additionally, the increased stage height removed the ability to use the existing microscope lamp housing. In its place, an independent fiber optic light source was used for illumination purposes during fabrication and imaging, as can be seen in Figure 4.3.

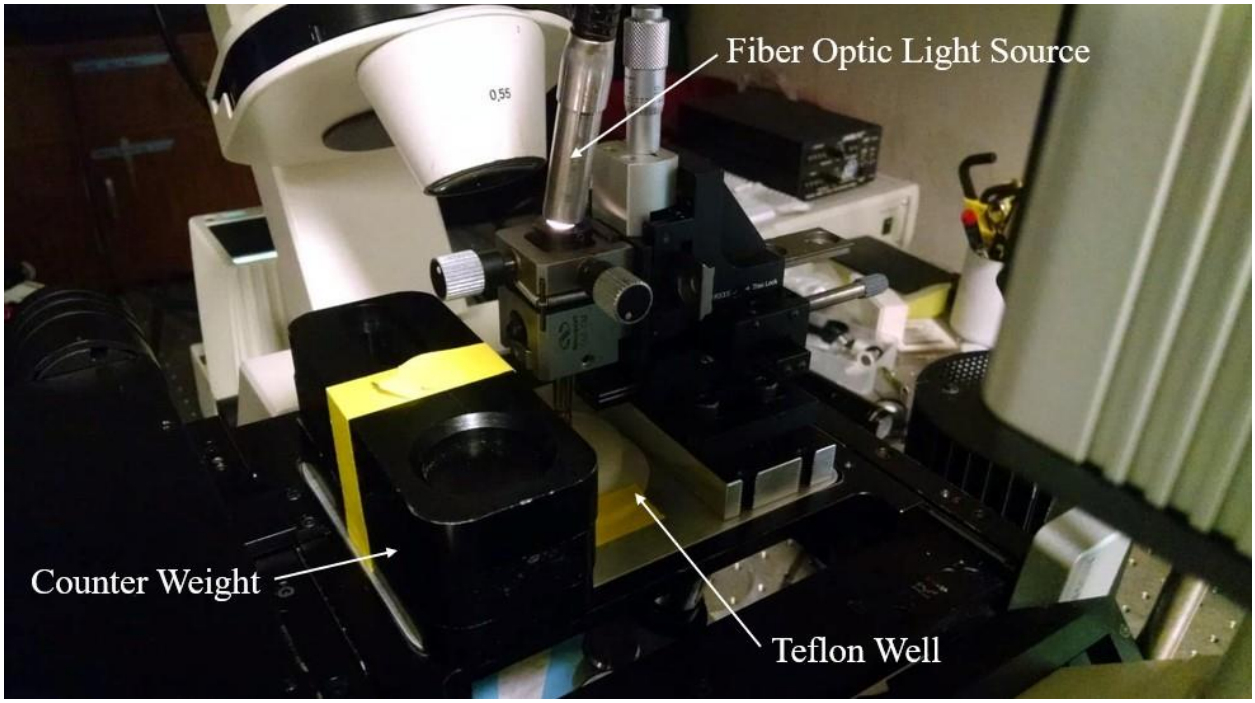

Figure 4.3: Experimental Setup Using Fiber Optic Light Source

Image showing use of fiber optic light source with a flexible neck in place of traditional microscope lamp housing. Due to the height of custom stage, the microscope's lamp housing cannot be utilized, requiring the use of an auxiliary light source. The stage counter-weight can be seen on the left side of the image, wrapped in yellow tape. To the right of the counter-weight is the Teflon fabrication well, followed by the fiber, fiber chuck, and custom mount, the schematic of which is seen in Figure 4.2.

4.2.7 Structure Specifications

Several different structures were fabricated on the untreated silica core of the fiber. To exhibit the flexibility of this technique, structures of varying size and shape were fabricated and imaged via both bright-field and SEM. The structures used in these experiments, all of which were solid (as opposed to having a hollow inner cavity), consisted of a cylinder, dome, pyramid, and rotating triangle. A schematic of each structure and their corresponding dimensions can be found in Figure 4.4.

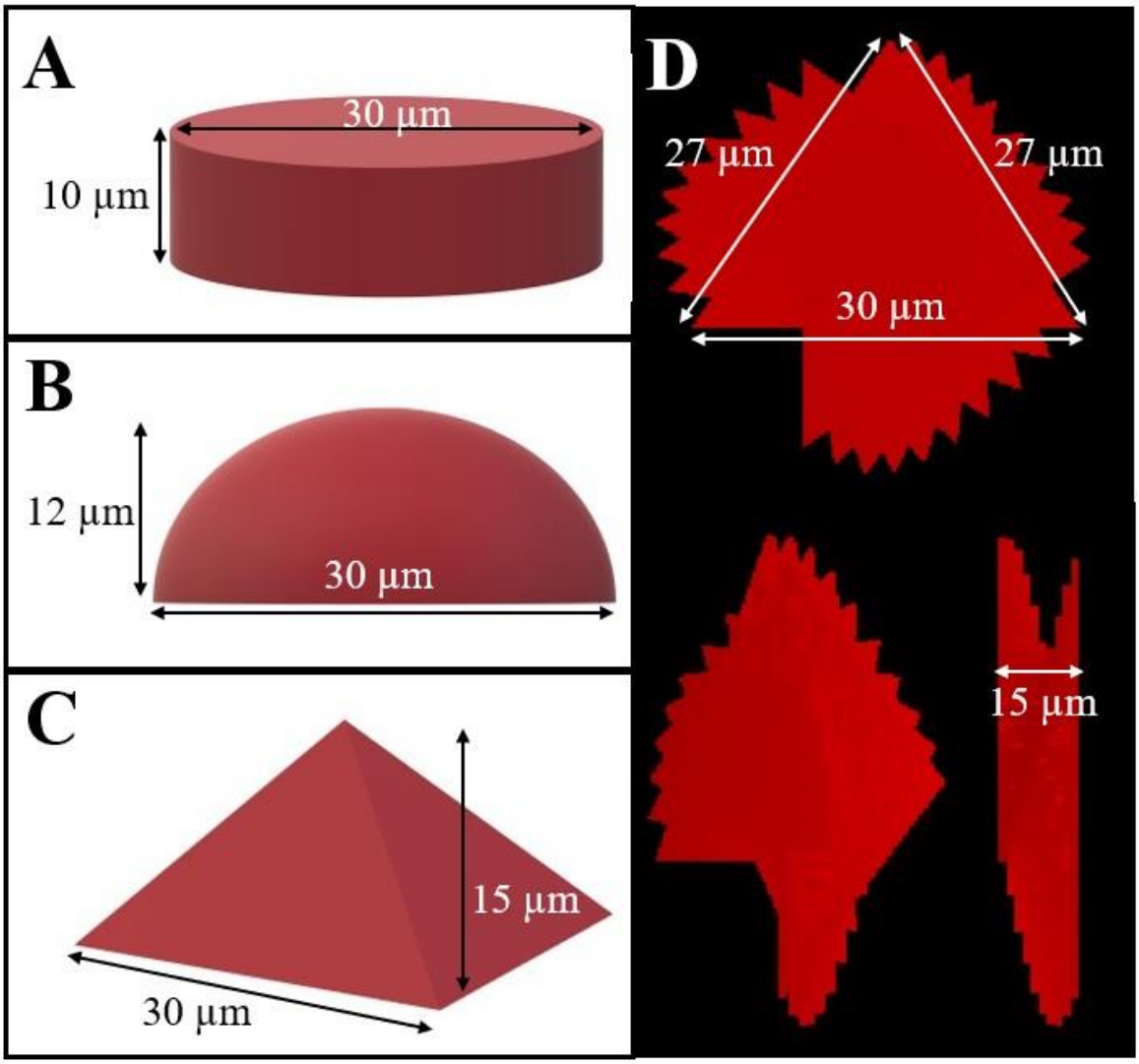

Figure 4.4: Structural Schematics for Fabrication on Fiber

Four structures of varying shape were used to display the flexibility present when fabricating on the tip of an optical fiber. (A) The most basic of the shapes was a solid cylinder, similar to the hollow cylinder used in bacterial studies. (B, C) The masks used to generate the dome and pyramid structures were inverted, resulting in each structure being rotated 180º during fabrication. This allowed for the base of each structure (i.e. – the side of the structure with the largest surface area) to be anchored directly to the fiber core. (D) The rotated triangle mask resulted in the most complex structure, with a triangular mask being rotated by 10º every 3 slices.

Bacterial studies utilized one of two structures, either a small cylinder or a larger, stitched cylinder. The small cylinder possessed an inner cavity volume of ~1.5 pL, 2 μm thick cap, and 3 μm thick walls and base, giving an overall structure height of 5 μm. The large cylinder possessed an inner cavity volume of ~19 pL, 5 μm thick walls, and 4 μm thick base and cap, giving an overall structure height of 11 μm. Due to the size of the large cylinder and limitation of mask area available on the DMD, this cylinder had to be split into four separate quadrants, which were individually stitched together to make the final structure. A schematic of each of these structures can be seen in Figure 4.5. Masks used for all structures were created using the ImageJ macro language.

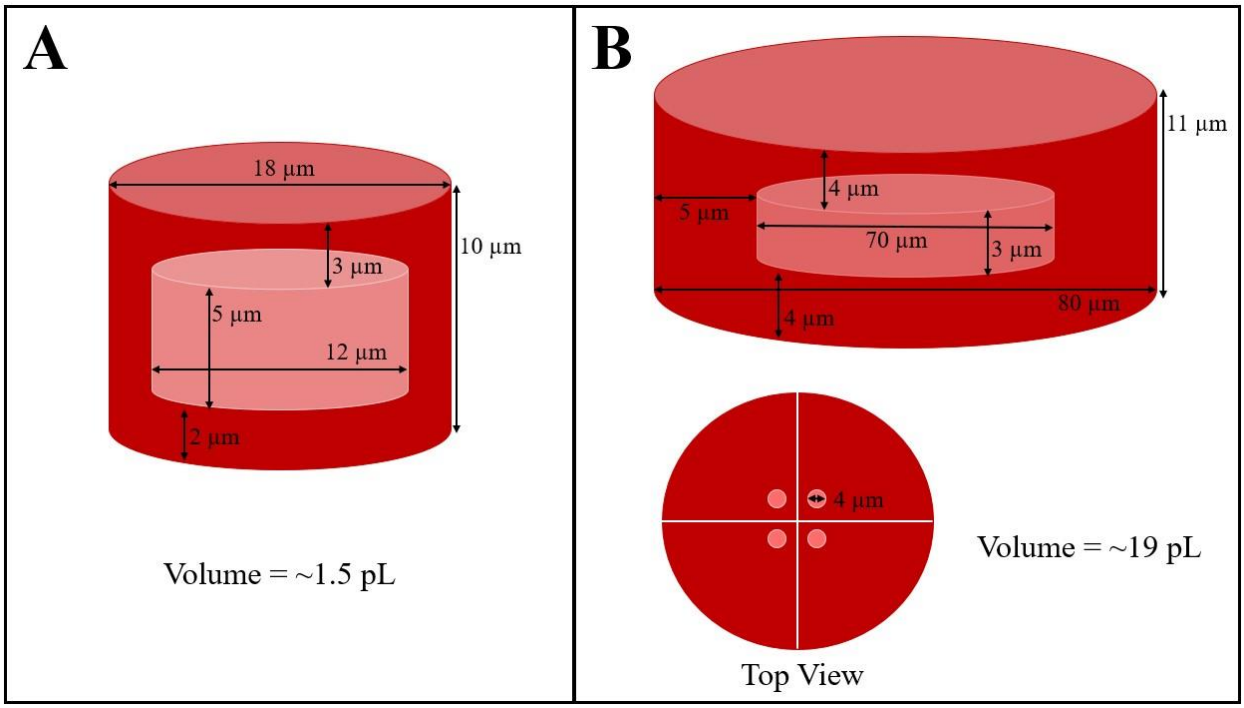

Figure 4.5: Structural Schematics for Bacterial Capture on Fiber Tip

Schematic of structures used for bacterial capture on tip of optical fiber. (A) A small cylinder was used to capture single or dividing bacterial cells, requiring the use of fluorescence microscopy to determine cell location prior to fabrication. This structure was used during single-day experiments, when the goal was to fill the trap within 3-4 hours. (B) A larger, stitched cylinder was used to increase the probability of capturing bacteria on the fiber tip. While the large schematic shows a complete, un-sectioned structure, the structure itself was too large to fabricate in one single piece. Therefore, the top view shows the sectioning of the main structure into four separate wedges, each with a 4 µm support post in the inner corner to provide support and prevent structural collapse. This structure was used when a single bacterial trap on the tip was desired, and required overnight bacterial growth to fill completely.

4.2.8 Fabrication Setup and Procedure

Prior to fabrication, fabrication solution was diluted with 60 µL of bacteria suspended in TSB and mixed thoroughly at 37 ºC. A small droplet (~15 µL) was placed on a glass coverslip, which was secured via an O-ring in a Teflon sample well. The sample

well was then placed below the fiber chuck and secured in place with tape. Prior to full gelation the tip of the optical fiber was lowered into solution and positioned ~30 μm above the coverslip using the fine focus knob and the 10x air and 60x oil-immersion objectives, after which the solution was left at room temperature for 10 minutes to allow the hydrogel to fully set around the fiber. The gelation temporarily immobilized the bacteria in solution, allowing structures to be fabricated around the cells *in situ* onto the core of the optical fiber.

The need to ascertain bacteria location prior to fabrication was dependent on the size of the structure being created. If fabricating a small cylinder (Figure 4.5A), cells needed to be located beforehand to allow the cylinder to be positioned correctly and centered over the cell being captured. To accomplish this, a fluorescence lamp was used to visualize any bacteria present on or close to the core of the fiber. The image of fluorescent cells was then used as a map to guide the positioning of the small cylinder mask prior to fabrication. If fabricating a large, stitched cylinder (Figure 4.5B), location of bacteria prior to fabrication was unnecessary, as the structure itself covered almost the entirety of the core area.

Immediately prior to fabrication, the focal point of the objective was positioned below the surface of the fiber at a distance ~2 μm less than the nominal (designed) height of the structure being fabricated, ensuring that the structure would successfully anchor to the fiber core. For example, if a structure were 20 μm tall, the focal point would be focused ~18 μm below the surface of the core, and laser scanning would terminate nominally ~2 μm within the fiber core. Upon final positioning, fabrication was initiated via custom

LabView software. An average laser power of 35 mW (measured at the back aperture of the objective) was used for all experiments.

4.2.9 Post-Fabrication Procedure

Immediately following fabrication, 1 mL room temperature TSB was added to the sample well, and the portion of the well surrounding the fiber chuck was covered with a petri dish. The fiber optic mount was then placed in an incubator set to 37 ºC for one hour. This allowed the un-crosslinked hydrogel to melt, which was then rinsed and removed from the sample well using multiple aliquots of TSB warmed to 37 ºC. To help maintain structural adherence to the fiber core, the fiber was fully lifted out of the fabrication well following two or more gentle rinses, thus allowing a more vigorous rinsing to take place in the well in an effort to remove any residual hydrogel or bacteria adhered to the coverslip. Alternatively, a separate fabrication well containing fresh TSB could be swapped out with the well that was used during fabrication, thus removing any possibility that bacteria adhered to the original coverslip could interact with bacteria growing within the structures. Bacteria were then left to grow to the desired cell density. This usually consisted of allowing bacteria in the small structures to grow for 2-4 hours at 37 ºC, or overnight at room temperature for the large structures.

4.2.10 Bright-Field and SEM Imaging

Bright-field images of each structure were taken using a Zeiss Axiovert 135 microscope coupled with a 10x air, 40x air, or 60x oil-immersion objective. Structures imaged via scanning electron microscopy (SEM) underwent SEM preparation following

previously determined protocol. [32] In brief, following fabrication, melting, and rinsing, the fiber tip was allowed to sit overnight in PBS buffer. The next day, the overnight buffer was removed, and the tip exposed to fresh buffer for 15 minutes. The fiber was then subjected to 2 mL each of the following solutions for 15-minute intervals: 5% glutaraldehyde in buffer, buffer, buffer, water, 50% ethanol, 50/50 ethanol/methanol, 100% methanol, 100% methanol. The fiber was then placed in the hood for an hour to dry, after which it was placed in a desiccator overnight to dry. Following dehydration and fixation, the fiber was attached to an SEM mount and sputter coated with a nominal 10 nm Pt/Pd layer using a Cressington Scientific 208HR sputter coater. The sample was then placed in a Zeiss Supra 40V SEM for imaging.

4.3 Results and Discussion

4.3.1 Transition from Glass Rod to Optical Fiber

As mentioned in Section 3.3.3, the process of transitioning fabrication from a stationary platform (glass coverslip) to a moveable tip required a number of adaptations to previously used protocols. [28-32] These adaptations became even more complex in nature upon advancing from layered hydrogels on a 1.85 mm diameter glass rod to fabricating directly on the surface of a 250 μm diameter optical fiber. Examples of experimental modifications required to make this new fabrication method successful include creation of a custom stage, employing an alternate illumination source, altering reagent properties, using fluorescence imaging for cell location prior to fabrication, and μ-3D printing a single, large cylinder using multiple, "stitched" portions that cover the majority of the fiber core.

The benefits of using an optical fiber over a glass rod are numerous. Whereas glass rods provide a larger surface area, they are also extremely prone to breaking or cracking. Additionally, the thicker and more brittle nature of the glass rod make it difficult to obtain a flat surface for fabrication in a reproducible manner. Optical fibers are widely known for their flexible and non-invasive nature, [11-16] both of which are desirable qualities for the research described below. Additionally, fibers can be quickly and reproducibly cut using a fiber cleaver containing grooves that match the diameter of the fiber being used. Lastly, while not presented in this work, optical fibers also provide the possibility for real-time detection through the fiber core, a capability that solid glass rods lack.

4.3.2 Initial Fabrication Method Using PDMS Mold

Upon first attempting to fabricate on the surface of an optical fiber, a similar method was used as detailed in Chapter 3 regarding stabilization of the glass rod using PDMS. As shown previously in Figure 4.1, a segment of optical fiber approximately 1-inch in length was threaded through a cross-hatch in a piece of PDMS and secured over a fabrication well. Locating bacterial cells prior to fabrication proved to be difficult, as using the traditional method of identifying cells via bright-field microscopy was ineffective due to low contrast and resulted in numerous empty traps fabricated on the fiber surface. The simplest solution to this problem, using fluorescence microscopy immediately prior to fabrication to create a "map" of cells on the fiber surface, proved to be the most effective. An example of this can be seen in Figure 4.6.

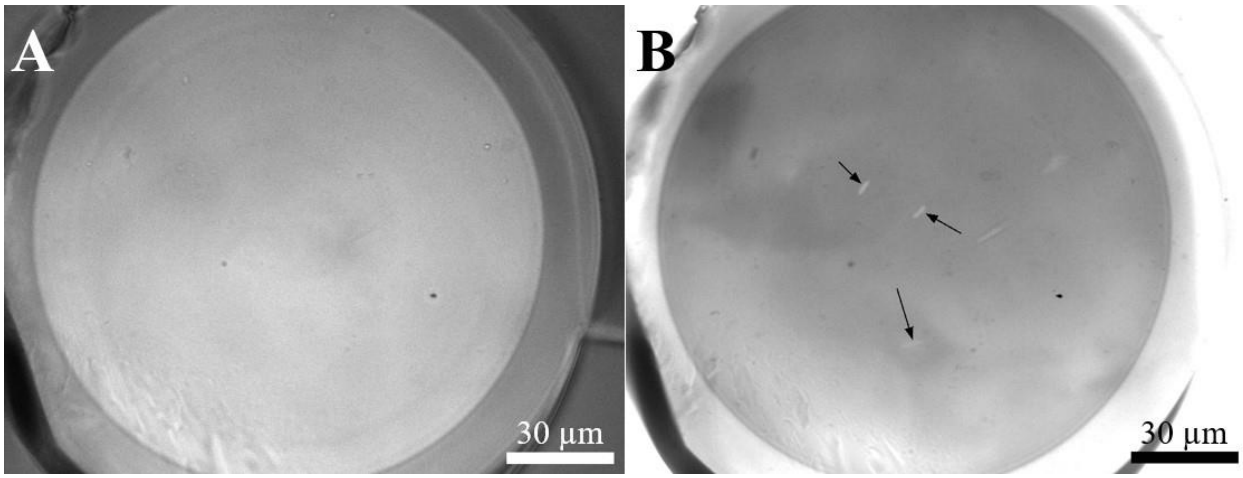

Figure 4.6: Location of Cells via Fluorescence Microscopy Prior to Fabrication

Transitioning from a coverslip to an optical fiber required a new method of locating cells prior to fabrication due to poor contrast between bacterial cells and hydrogel via bright-field microscopy. (A) Bright-field image showing the core of an optical fiber immersed in hydrogel containing *P. aeruginosa* cells, with no bacteria clearly visible. (B) Fluorescence image of same fiber core, clearly showing location of bacteria (marked with black arrows).

Once cells were located on the fiber core, the mask for the small cylinder structure shown in Figure 4.5A was centered over the area where the bacteria were detected, and fabrication was initiated. While this procedure resulted in a greater probability of cells being captured during fabrication, the reproducibility of cell capture was still below 50%, indicating that further improvements could be made, such as preconcentrating exponential phase cells prior to mixing them into fabrication solution, thus creating a more dense cell population in the reagent droplet while maintaining the desired phenotypic state. An example of successful fabrication using this method can be seen in Figure 4.7, in which a cell was captured in a small cylinder, which filled to capacity after incubation overnight at room temperature (~20 ºC).

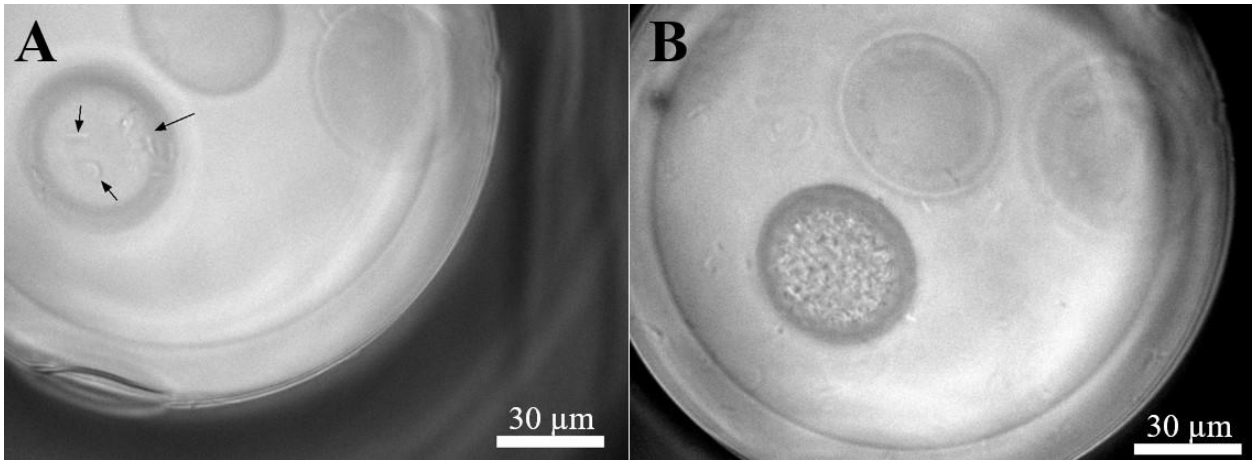

Figure 4.7: Cell Capture and Growth on Fiber Tip

Capture of *P. aeruginosa* cells in one of three fabricated cylinders on tip of fiber. (A) Image of fiber tip after 2 hours of incubation at 37 ºC. While the top two cylinders show no cell capture, the bottom cylinder contains 6 bacteria. The two left-most arrows identify single bacterial cells, while the right-most arrow identifies a cluster of 4 cells. Cells were left to grow at room temperature (~20 ºC) overnight for ~16 hours. (B) Captured cell population after overnight growth at room temperature. Bacteria remained highly motile but securely contained within the protein structure. Planktonic bacteria seen outside the structure are a result of cells dividing that were originally adhered to the coverslip following rinsing. Additional rinsing remedies this problem.

While structures were successfully fabricated on the fiber tip using this method, the reproducibility was very poor due to a lack of control over precise positioning of the fiber with relation to the hydrogel droplet and the coverslip secured in the Teflon well.

4.3.3 Transition to Custom Stage and Fiber Optic Illumination Source

A custom stage, seen in Figure 4.2, was created to address these issues. As the microscope lamp housing could no longer be used due to increased stage height, a portable light source with a flexible head was utilized for illumination during fabrication and bright field imaging. However, there was some trial and error in determining the best way to

illuminate the fiber tip using this light source. The first hurdle was locating the tip of the fiber pre-fabrication via bright-field microscopy. As seen in Figure 4.3, during fabrication and imaging the light is directed straight down the top of the fiber, illuminating only the fiber core. While this was a non-issue during and following fabrication, it presented a challenge when it came to locating the fiber tip and bringing it into focus prior to fabrication. Illuminating the fiber chuck and fabrication well from the side helped in locating the fiber but provided poor clarity of the fiber surface itself. Using both methods in a complementary fashion proved to be the most successful, i.e., locating the fiber and centering it over the objective via side illumination first, then focusing on the fiber surface and lowering the fiber to the desired distance from the coverslip via top illumination. Examples of each method can be seen in Figure 4.8.

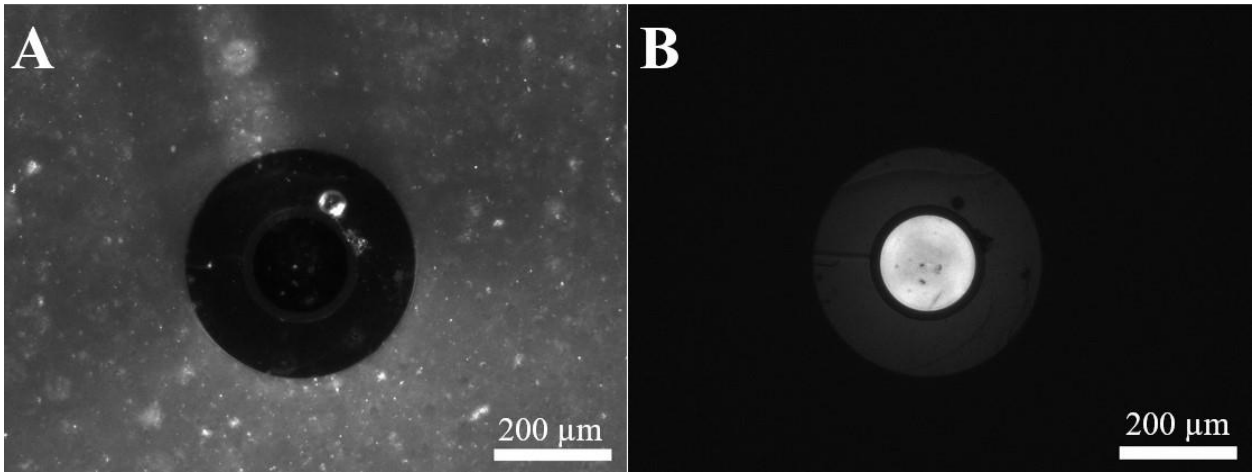

Figure 4.8: Different Illumination Methods Using Fiber Optic Light Source

Imaging of optical fiber tip using independent fiber optic light source. Both images are of same optical fiber immersed in hydrogel. (A) Fiber tip illuminated from side. This illumination method is most useful for locating and centering the optical fiber over the objective, as the core is not clearly discernible at this angle. Lighter gray matter around fiber is hydrogel. (B) Fiber tip illuminated from top. While surrounding hydrogel can no longer be seen, the core is clearly distinguishable and in focus, allowing for fabrication on the fiber surface.

To ensure the fiber core was sufficiently illuminated, the optical fiber had to be, at minimum, the length of the fiber chuck.

4.3.4 Fabrication Using Custom Stage

While the custom stage immediately made a significant difference in terms of precise positioning of the fiber tip, an immediate problem presented itself with regards to stage stability. Due to the flexibility and small size of the optical fiber, any minor disturbance of either the optical table directly, or caused by building vibrations (i.e., from a nearby jackhammer) would result in visible shaking/vibration of the fiber during fabrication. This resulted in poor anchoring of the structure to the fiber core, and overall

weak adherence both during and following rinsing. The first change was to add a counter weight to the custom stage, removing the unbalanced weight distribution of the stage itself. This counter weight can be seen in Figure 4.3. While creating a more equal weight distribution of the stage helped, it did not remove the shaking problem entirely. These problems were adequately resolved by using the counter weight in conjunction with floating the optical table. By floating the table, disturbances of both the table and building were minimized, allowing for vastly increased stability of the fiber during fabrication.

Another challenge involved melting the un-crosslinked hydrogel in a homogenous manner. Unlike traditional fabrication, in which the fabrication well can be removed from the stage, covered with parafilm, and placed in the incubator, the fiber could not be moved until all excess hydrogel had fully melted. This meant that while the stage could be removed from the microscope, no piece of the stage itself could be adjusted in any way, as any jostling or movement of the fiber would result in the fiber ripping away from the set hydrogel. If this occurs, the fiber also rips away from the fabricated structures, which remain securely embedded in the un-melted hydrogel. To prevent this from happening, the entire stage was placed in an incubator set to 37 ºC for 45-60 minutes. While melting did occur using this method, it was inconsistent and at times incomplete during the rinsing process, in some instances resulting in small strips of un-melted hydrogel ripping away, causing loss of fabricated structures.

4.3.5 Creation of Custom Hydrogel and Adhesion Statistics

To remedy this issue, the gelatin concentration in the hydrogel was decreased from 200 mg/mL to 150 mg/mL, thus decreasing the melting temperature from 29 ºC to 26 ºC. While this solved the inconsistent melting issue, adherence to the fiber surface was extremely poor, an example of which can be seen in Figure 4.9.

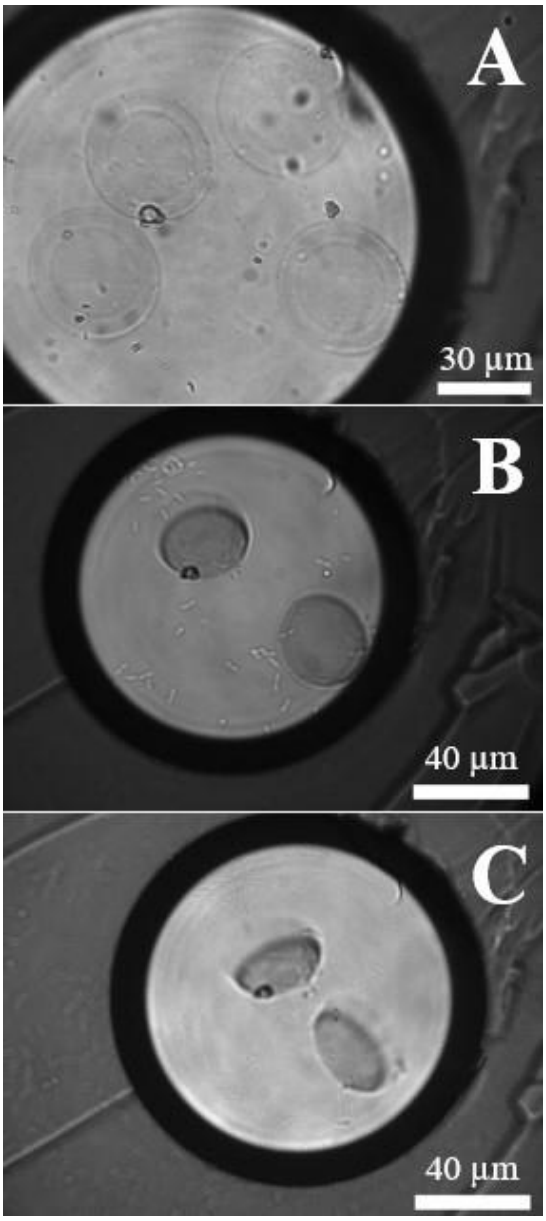

Figure 4.9: Structural Adherence Issues Following Rinsing

Decreased structural adherence at lower gelatin reagent concentrations. Structures presented here were fabricated with the 26 ºC melting temp hydrogel. (A) Four fabricated structures, imaged pre-melting and rinsing. (B) After 1 hour 40 minutes, only two of the four original structures remain, with one showing signs of partial detachment. (C) After 3 hours, both remaining structures show signs of detachment from the fiber core.

Consistently poor adherence of μ-3D printed structures using the 26 ºC melting temperature hydrogel indicated that an alternative solution to the melting and rinsing issues needed to be found. As a result, the higher gelatin concentration reagent was again adopted, and a modification was employed in which a rectangular slot was cut out from a petri dish and introduced such that the modified petri dish could slide over the majority of the fabrication well without disturbing the fiber or fiber chuck. This approach sufficiently addressed the difficulties with melting and rinsing; however, while adherence improved, it still afforded only an approximate 50% success rate.

Using the data presented in Chapter 2, a custom hydrogel was created in an attempt to improve overall structural adherence. To prevent further melting issues, the gelatin concentration was established at a constant value of 200 mg/mL to maintain an ~29 ºC melting temperature. However, both RB and BSA concentrations were increased to evaluate whether an increase in crosslink density would result in stronger adherence to the fiber core. To maintain cytotoxicity at what was assessed to be an acceptable level, the RB concentration was increased only up to 7 mM (from the original 5 mM), while the BSA concentration was doubled from 40 mg/mL to 80 mg/mL. A comparison of adherence data for all three reagent mixtures used can be seen in Table 4.1.

Table 4.1: Adherence Data for Three Different Hydrogel Compositions

Data was collected for three different hydrogels with regards to the reproducibility of structural adherence when used for fabrication on an optical fiber core. An increase in gelatin concentration resulted in just over a three-fold increase in adherence rate. However, further increase in gelatin concentration causes melting issues at 37 ºC, which is the optimal growth rate for cells being studied. By increasing both the RB and BSA concentrations, the percent adherence once again increased significantly. This increase is the max increase for RB before cytotoxicity becomes an increasingly present factor. The increase seen between Solution #2 and Solution #3 is likely due to an increase in BSA protein residues and RB singlet oxygen species, resulting in higher protein crosslink density and thus a stronger attachment to the fiber core.

	RB (mM)	**BSA (mg/mL)**	**Gelatin (mg/mL)**	**Fraction Adhered**	**Percent Adhered**
Solution #1	5	40	150	9/61	15%
Solution #2	5	40	200	27/53	51%
Solution #3	7	80	200	92/111	83%

As predicted, an increase in RB and BSA concentration improved structural adherence to the fiber core while minimizing cytotoxicity. This is likely a result of the higher protein crosslink density producing a stronger attachment to the silica optical fiber core. An example of this increase in structural adherence and integrity can be seen in Figure 4.10.

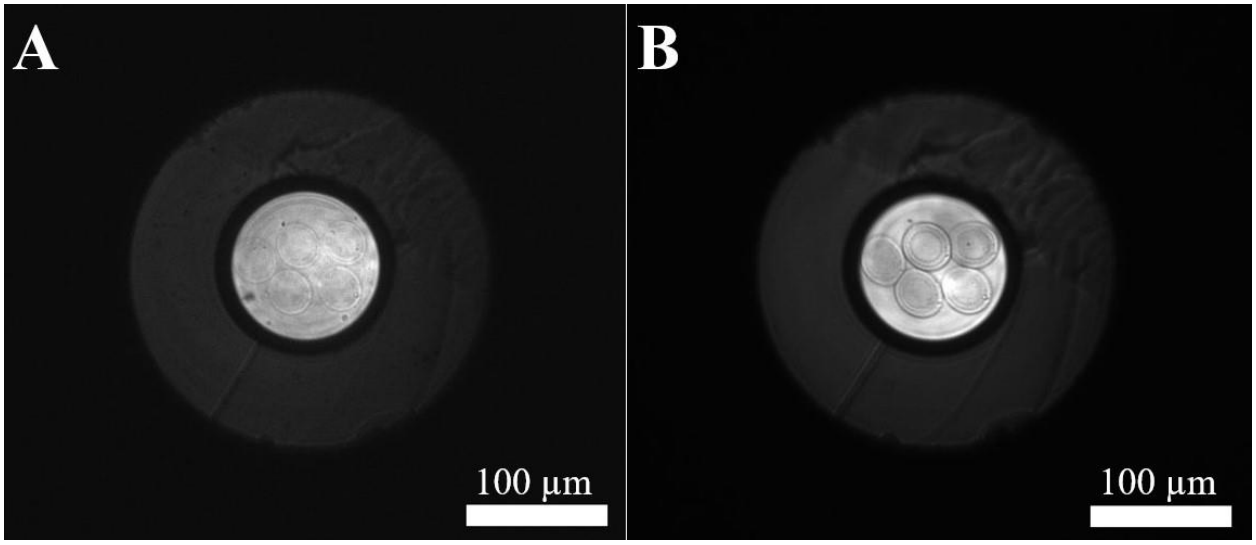

Figure 4.10: Improved Adherence of Structures to Fiber Core

Using hydrogel with higher RB and BSA concentrations greatly increased the rate of adherence to the fiber core. No bacteria were used in this experiment. (A) Fiber surface imaged immediately following fabrication, before melting or rinsing. Five small cylindrical structures can be seen on the core of the fiber. (B) Fiber surface following melting, rinsing, and 2 hours of heating at 37 ºC to mimic cell experiment conditions. All five structures remained securely adhered to fiber while maintaining strong structural integrity. Slight swelling of structures an artifact of irreversible hydrogel swelling at increased temperatures.

It should be noted that if cells are not involved in a fiber experiment, both RB and gelatin concentrations can be increased further to potentially achieve an even greater rate of structural adherence.

4.3.6 Fabrication of Solid Structures of Varying Shape

To showcase the flexibility of this technology, structures of varying shape and size (schematics of which can be seen in Figure 4.4) were fabricated on the fiber core. This shows that shapes more complex than the simple cylindrical geometry described thus far

can be successfully fabricated on the fiber tip and deployed to any desirable location. Bright-field and SEM images of these fabricated structures can be seen in Figure 4.11.

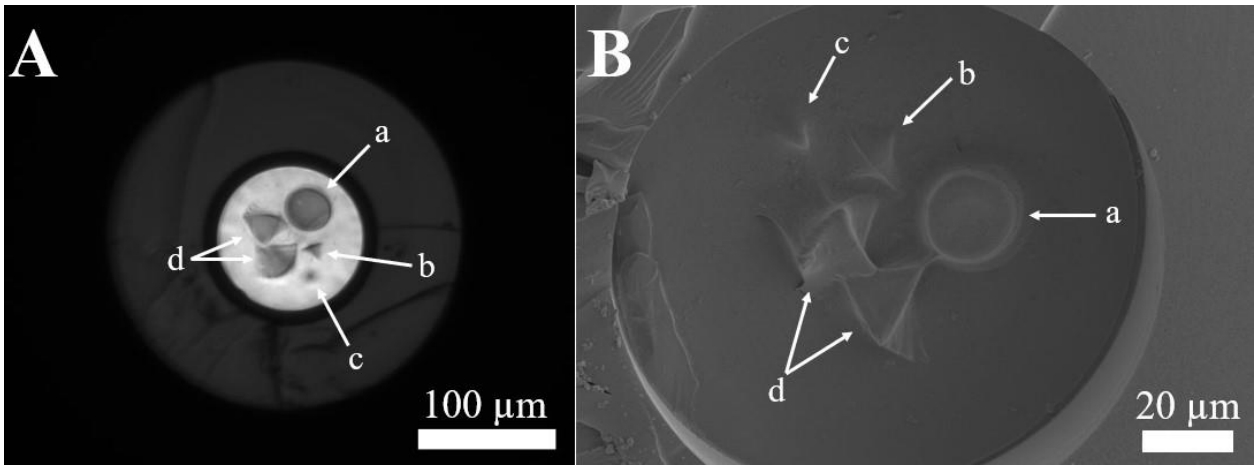

Figure 4.11: Varying Shapes Fabricated on Fiber Surface, Bright-Field and SEM

> Four different shapes were fabricated on the surface of the fiber. Each label is indicative of a specific shape, which are as follows: a – cylinder, b – pyramid, c – dome, d – rotated triangle. As can be seen, structures maintained strong adherence and high structural integrity following melting, rinsing, and SEM prep. (A) Bright-field image of structures immediately following fabrication. (B) SEM image of structures. Dome (c) is difficult to distinguish due to the thickness of the Pt/Pd coating compared to the size of the structure.

Recession of the fiber core in the SEM image is believed to be an artifact of the SEM prep process and did not impact the fabricated structures themselves.

While no bacteria were used in these studies, it should be noted that any of the structures seen here can be modified to have a hollow interior, thereby allowing them to capture cells. This may be of interest in determining if bacteria act differently in structures of varying shape and size, as well as present the possibility of creating more complex, nested structures in the future.

4.3.7 Transition from Small Cylinder to Large, Stitched Cylinder for Cell Capture

While the small cylinder detailed previously in this section has proven to be a successful method of capturing cells, it is highly dependent on chance when it comes to how many cells will be close enough to the core of the fiber to allow capture. If no cells are present on the core prior to fabrication, the experimental preparation must begin again with the cleaving of a new length of fiber to be lowered into a fresh droplet of hydrogel. This can be a time-consuming process, and at the same time is wasteful of materials. To simplify the experimental procedure and eliminate this problem, the small cylinder mask was replaced with a much larger, stitched cylindrical structure with an inner cavity volume of ~19 pL, a schematic of which can be seen in Figure 4.5B. This removed the need for fluorescence imaging to locate cells prior to fabrication, as the new structure possessed a large enough diameter to cover the majority of the fiber core. Additionally, fabrication solution was diluted with cells taken directly from an overnight culture tube, which had an optical density (OD) of ~2-3 at 600 nm (as opposed to an OD of ~0.3 at 600 nm following dilution of the overnight culture and 2 hours of growth in a fresh TSB).

An assumption was made that due to the high density of cells within the fabrication solution, there was a high probability that cells would be present within the ~19 pL cavity of the trap. However, limitations on available fabrication area due to workable DMD surface area required the mask to be partitioned into four equal sections. Due to the large size of the overall structure, a small support post (4 μm in diameter) was added to the inner corner of each section. The first section of the structure was fabricated to have the center

point align with the center of the fiber. Each subsequent section was then positioned in such a way that the walls of the structure slightly overlapped on all sides, effectively "stitching" the structure together upon completion.

Several modifications were made to the large cylinder mask before settling on the one presented in this chapter. For example, the original mask had 2 µm thick walls and an open base. However, it proved difficult to sequentially position four separate sections with the level of precision required to avoid any gaps from occurring between sections. This resulted in modifying the original mask to have the 5 µm walls presented here. Additionally, due to the size of the final structure, the outer walls themselves were not strong enough to keep the entire stitched structure adhered to the fiber core. Thus, a 4 µm base was added. This base had an added benefit of allowing the volume of the inner cavity of the structure to be known at all times, as without it the inner volume would undergo slight changes depending on how deeply each slice was fabricated (anchored) in to the fiber core. Lastly, the original structure had one central support post that was divided into four pieces upon sectioning of the mask. Due to the difficulty of lining these pieces up during fabrication, the central support post was replaced with four smaller support posts, one per section of the structure.

The increased density of bacteria in the hydrogel resulted in a greater number of cells adhering to the coverslip during fabrication. These cells remained adhered following melting and rinsing procedures and grew to high densities following overnight growth at room temperature. This caused the TSB around the fiber to be cloudy, indicating a high

population of planktonic bacteria in solution around the fiber. This is not ideal, as the presence of these cells could impact the phenotypic state of the cells in the trap, potentially altering their growth patterns and their response to external stimuli. To solve this problem, the fiber was removed from the original fabrication well following melting, which was replaced with a different well containing fresh TSB. An image of a large-stitched cylinder prior to fabrication and after overnight growth can be seen in Figure 4.12. Note that no planktonic cells are visible outside the structure. SEM images of a stitched cylinder can be seen in Figure 4.13.

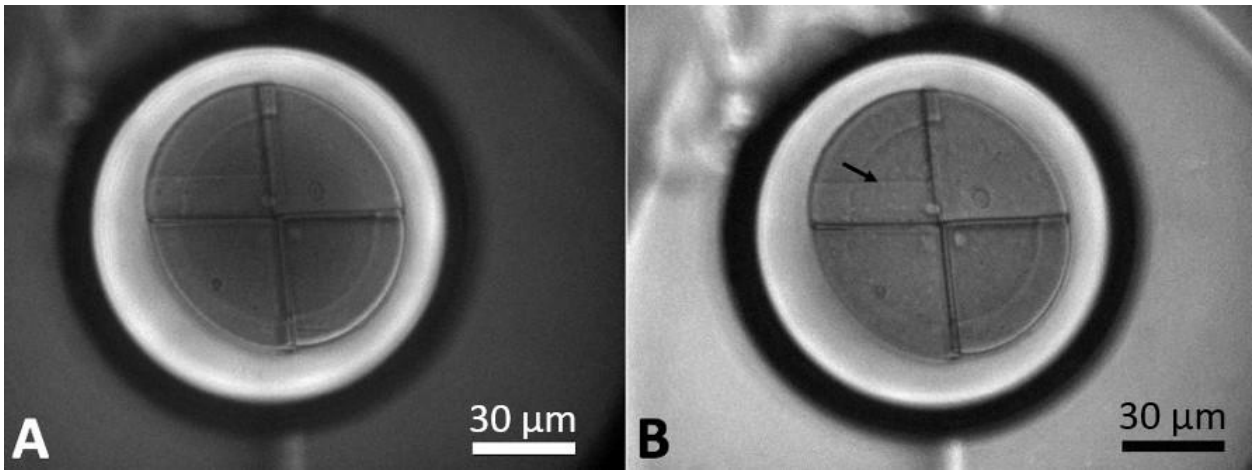

Figure 4.12: Large Stitched Structure Before and After Overnight Bacterial Growth

Large, stitched structure was fabricated from hydrogel containing dense population of P. aeruginosa cells. Following melting, Teflon well used during fabrication was replaced with new well containing fresh TSB. Cells were allowed to grow overnight (~16 hours) at room temperature, ~20 ºC. (A) Structure following melting of hydrogel and replacement of Teflon well used during fabrication. (B) Structure following overnight growth. Cells can be seen as white dots inside structure, one of which is identified with a black arrow. Cell culture was dense and highly motile.

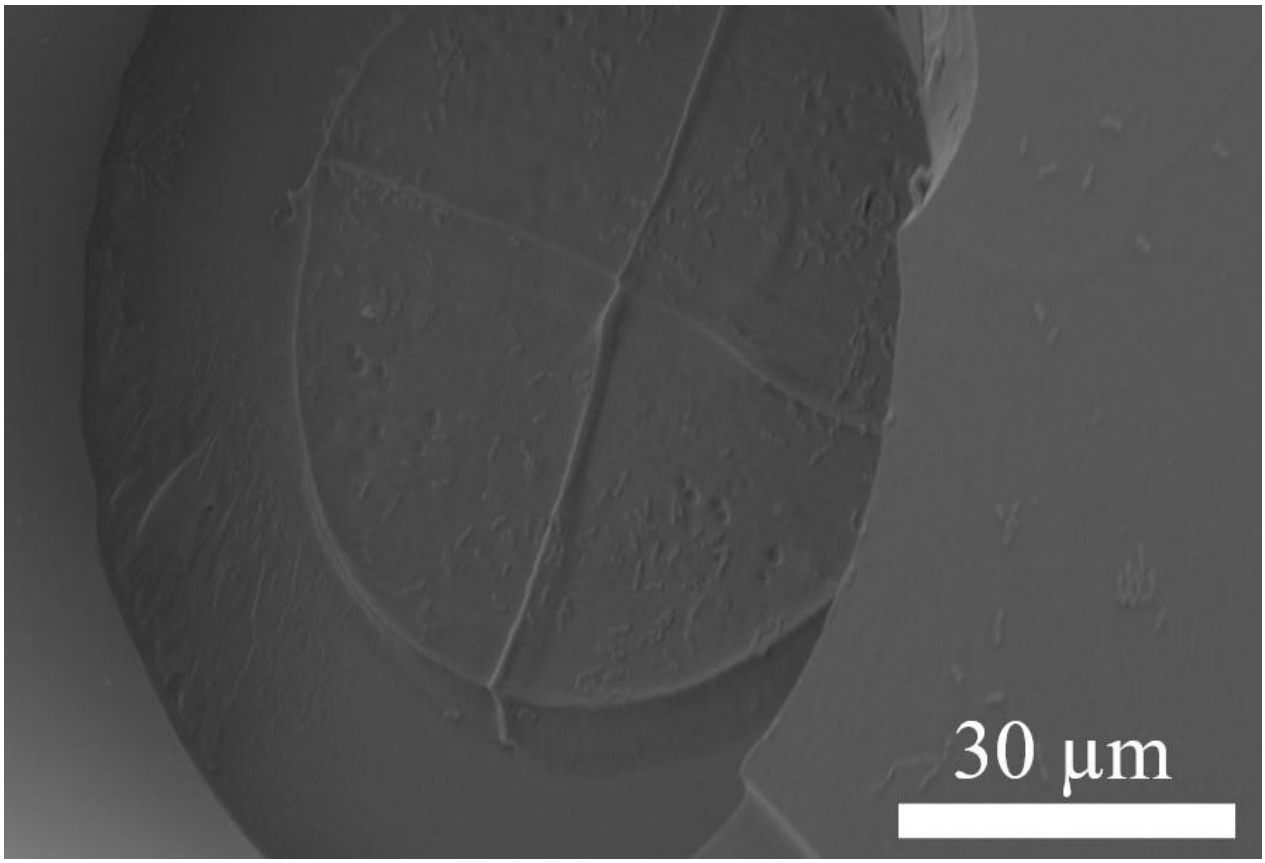

Figure 4.13: SEM of Large, Stitched Cylinder on Core of Optical Fiber

Large, stitched cylinder on fiber core. Raised seams crossing over structure represent where stitching occurred between sections. P. aeruginosa cells can be seen stuck to top of structure and coating of fiber, indicating that planktonic cells were present and dividing in solution during the growth period for trapped cells. Recession of fiber core believed to be an artifact of SEM prep, no discernible effects were visualized regarding fabricated structure.

4.3.8 Comparison of Small Cylinder to Large, Stitched Cylinder

As detailed above, both small and large cylinders are capable of being repeatedly and reproducibly fabricated on the core of an optical fiber, either with or without cells present. However, when considering future experiments, these two cylinders serve very

different purposes. When a single, monoclonal population is desired, the small cylinder is best suited in conjunction with a hydrogel containing a fairly low density of the desired bacteria. While it is possible to fabricate multiple small cylinders on a fiber core, as seen in Figures 4.7 and 4.10, a single small cylinder can also be fabricated around a cell with high accuracy when using fluorescence to locate bacteria prior to fabrication. This prevents multiple bacterial colonies from communicating with one another, which depending on what is being tested, could potentially skew results due to phenotypic changes triggered by nearby cell populations.

When a more diverse population of bacteria within the same strain is desired, the large cylinder is capable of trapping many cells at once. This also allows the final colony to more closely mimic physiological ailments, as bacterial infections rarely stem from a single bacteria. Lastly, this larger structure allows a much greater overall population of cells to grow due to an over 10-fold increase in cavity volume compared to the small cylinder. This could play an important role in future experiments where fluorescence data is collected through the fiber core. Depending on the sensitivity of the detector being used, a larger colony may be desired to generate the strongest fluorescence signal possible.

4.4 CONCLUSIONS

This chapter discussed utilizing the multiphoton lithography technique previously developed by the Shear lab to fabricate protein-based microstructures on optical fiber tips. During initial attempts to translate this technology from glass coverslip substrates to fiber tips, many challenges were faced, including fiber stabilization, cell location prior to fabrication, and maintained adherence of fabricated structures to the fiber tip. To solve these problems, a number of modifications to traditionally used techniques were made. This included the creation of a custom stage, use of a fluorescence imaging for cell location prior to fabrication, and customization of fabrication hydrogels. Using information gathered from the research detailed in Chapter 2 of this dissertation, fabrication hydrogel was optimized to secure maximum structural adherence while minimizing cytotoxicity to the bacterium being studied, *P. aeruginosa*.

Successful capture and growth of P. aeruginosa on optical fiber tips presents an exciting advancement in the fields of both micro-3D printing and bacterial study. While fabrication on optical fiber tips and microbial biosensors are both well researched topics, this is the first demonstration combining the two technologies. The ability to trap bacterial clusters of discrete population and density on a fiber tip opens up a vast array of research possibilities with regards to dynamic distance studies between bacterial populations, as well as microbial biosensors in which the density and phenotypic state of the sensing bacteria can be highly tuned and controlled. This technology will allow advanced study in both *in vivo* and *in vitro* environments through the precise delivery of well-defined microbial populations to remote environments.

4.5 REFERENCES

1. Kao, C.K. and Hockham, G.A. *Dielectric-fiber surface waveguides for optical frequencies.* Proc. IEE, 1966. **133**: p. 1151-1158.
2. Kapron, F.P., Keck, D.B., and Maurer, R.D. *Radiation losses in glass optical waveguides*. Appl. Phys. Lett., 1970. **17**: p. 144-153.
3. Gloge, D. and Marcatelli, A.J. Multimode theory of graded-core fibers. Bell Sys. Tech. J., 1973. 52(9): p. 1563-1579.
4. Jacomme, L. Wavelength dependent propagation in optical multimode fibers. Optics Comm., 1978. 24(2): p. 213-216.
5. Ballato, J. and Dragic, P. *Glass: the carrier of light – a brief history of optical fiber*. Int. J. Appl. Glass Sci., 2016. **7**(4): p. 413-422.
6. Kepler, J. *Dioptrice*. 1611.
7. Huygens, C. *Traite de la Lumiere*. 1690.
8. Keck, D.B., Maurer, R.D., and Shultz, P.C. *On the ultimate lower limit of attenuation in glass optical waveguides.* Appl. Phys. Lett., 1973. **22**(7): p. 307-309.
9. Payne, D.N. and Gambling, W.A. *New silica-based low-loss optical fibre.* Electron. Lett., 1974. **10**(15): p. 289-290.
10. Horiguchi, M. and Osanai, H. *Spectral losses of low-OH-content optical fibers*. Electron. Lett., 1976. 12: p. 310-312.
11. Mitra, P.P., and Stark, J.B. *Nonlinear limits to the information capacity of optical fibre communications.* Nature, 2001. **411**(6841): p. 1027-1030.
12. Sanchez, D.M., Gresil, M., and Soutis, C. *Distributed internal strain measurement during composite manufacturing using optical fibre sensors*. Composites Sci. Tech., 2015. **120**: p. 49-57.
13. Russo, V. *Optical fibre delivery systems for laser angioplasty and laser treatment of tumours.* Lasers in Medical Sci., 1988. **3**(1): p. 207-211.
14. Correia, R., James, S., Lee, S.W., Morgan, S.P. and Korposh, S. *Biomedical application of optical fibre sensors*. J. Optics., 2018. **20**(7): p. 1-25.
15. Macchi, E.G., *et al. Optical fiber sensors-based temperature distribution measurement in ex vivo radiofrequency ablation with submillimeter resolution*. J. Biomed. Opt., 2014. **19**(11): p. 1-7.
16. Petrova, E., Liopo, A., Nadvoretskiy, V., and Ermilov, S. *Imaging technique for real-time temperature monitoring during cryotherapy of lesions*. J. Biomed. Opt. 2016. **21**(11): p. 1-10.

17. Biran, I., Rissen, D.M., Ron, E.Z., and Walt, D.R. *Optical imaging fiber-based live bacterial cell array biosensor.* Anal. Biochem., 2003. **315**(1): p. 106-113.

18. Kano, H. and Hamaguchi, H. *In-vivo multi-nonlinear optical imaging of a living cell using a supercontinuum light source generated from a photonic crystal fiber.* Optics Express, 2006. **14**(7): p. 2798-2804.

19. Singh, A., Hugall, J.T., Calbris, G., and van Hulst, N.F. *Fiber-based optical nanoantennas for single-molecule imaging and sensing*. J. Lightwave Tech., 2015. **33**(12): p. 2371-2377.

20. Fang, X. and Tan, W. *Imaging single fluorescent molecules at the interface of an optical fiber probe by evanescent wave excitation.* Anal. Chem., 1999. **71**(15): p. 3101-3105.

21. Polyak, B., Bassis, E. Novodvorets, A., Belkin, S., and Marks, R.S. *Bioluminescent whole cell optical fiber sensor to genotoxicants: system optimization.* Sensors and Actuators B: Chem., 2001. **74**(1): p. 18-26.

22. Polyak, B., Bassis, E., Novodvorets, A., Belkin, S., and Marks, R.S. *Optical fiber bioluminescent whole-cell microbial biosensors to genotoxicants.* Water Sci. Technol., 2000. **42**(1): p. 305-311.

23. Yaliang, S., Ticho, Z., Jianli, G., and Yiyong, L. *Dark variants of luminous bacteria whole cell bioluminescent optical fiber sensor to genotoxicants.* J. Huazhong Univ. Sci. Technol., 2004. **24**(5): p. 507-59.

24. Kumar, J., Jha, S.K., and D'Souza, S.F. *Optical microbial biosensor for detection of methyl parathion pesticide using Flavobacterium sp. whole cells adsorbed on glass fiber filters as disposable biocomponent.* Biosens. Bioelect., 2006. **21**(11): p. 2100-2105.

25. Eltzov, E. and Marks, R.S. *Whole-cell aquatic biosensors*. Anal. Bioanal. Chem., 2011. **400**(4): p. 895-913.

26. Futra, D., Heng, L.Y., Ahmad, A., Surif, S., Ling, T.L. *An optical biosensor from green fluorescent Escherichia coli for the evaluation of single and combined heavy metal toxicities.* Sensors, 2015. **15**(6): p. 12668-12681.

27. Kalabova, H., Pospisilova, M., Siroka, R., and Kuncova, G. *A biosensor with encapsulated bioreporters – optical fiber element for enhanced detection of bioluminescence.* Measurement Sci. Technol., 2018. **29**(7): p. 1-7.

28. Connell, J.L., Ritschdorff, E.T., and Shear, J.B. *Three-dimensional printing of photoresponsive biomaterials for control of bacterial microenvironments*. Anal. Chem., 2016. **88**: p. 12264-12271.

29. Connell, J.L., Ritschdorff, E.T., Whiteley, M., and Shear, J.B. *3D printing of microscopic bacterial communities*. PNAS, 2013. **110**(46): p. 18380-18385.

30. Wessel, A.K., *et al*. *Oxygen limitation within a bacterial aggregate*. mBio, 2014. **5**(2): p. 1-9.

31. Connell, J.L., Whiteley, M. and Shear, J.B. *Sociomicrobiology in engineered landscapes*. Nature Chem. Bio., 2012. **8**(1): p. 10-13.

32. Connell, J.L. *et al. Probing prokaryotic social behaviors with bacterial "lobster traps."* mBio, 2010. **1**(4): p. 1-8.

Chapter 5: Review and Future Directions

5.1 Review of Work

This dissertation describes my efforts towards the characterization and application of customizable hydrogels, as well as the advancement of our current micro-3D printing technology from a static to a dynamic platform. As discussed previously, hydrogels have been utilized and manipulated in a variety of different scenarios due to their tunable [1-4] and biomimetic properties, [5-7] making them highly desirable for use in the study of biological systems. [7-13] While hydrogels have been used extensively in the Shear lab, [7, 12-16] few efforts have been made to specifically characterize the impact that changes in key components, including BSA, gelatin, and RB have on overall hydrogel properties.

The development of customizable hydrogels allowed for immediate breakthroughs to be made with regards to applications such as layered hydrogels and fabrication on optical fiber tips. Using the information gathered regarding the effects gelatin concentration has on hydrogel melting temperature, two hydrogels of markedly different melting temperatures were created and used in layering studies on the tip of a glass rod. With the assistance of a PDMS mold, two hydrogels of distinctly different gelatin concentration were reproducibly layered on a mobile glass rod. With the assistance of microbeads, the hydrogel-hydrogel interface was located and structures were successfully micro-3D printed in such a way that each structure was anchored in the high-melting-temperature hydrogel layer. This allowed for proof of concept experiments to be done regarding controlled delivery of protein microstructures via thermal manipulation.

Technology surrounding structures attached to a moveable substrate was further expanded by successfully fabricating protein microstructures on the silica core of optical fiber tips. The transition of fabrication on an optical fiber was not without challenges, with many experimental modifications made including creation of a custom stage, location of bacterial cells on the core surface, and customization of hydrogel to encourage maximum adherence with minimal cell toxicity. To begin, both solid structures as well as those with a hollow inner cavity were fabricated on the silica fiber core to test reproducibility of structural integrity and adherence. Then, proof of concept studies were completed showing the successful capture and growth of bacteria in structures of varying size on fiber tips.

5.2 FUTURE WORK

5.2.1 Study of "Unculturable" Bacteria

It is widely known in microbiology that the vast majority of bacteria cannot be grown using current laboratory culture methods. [17-18] This is largely due to difficulties in creating culture mediums that mimic the wide array of bacterial hosts, such as soil, [19] seawater, [20] and the human gut. [21] Therefore, there is a pressing need to design a technology that provides environmentally-sensitive bacteria with favorable growth conditions. By successfully culturing previously "unculturable" bacteria, we will be able to better understand their functionality and dynamics through the use of genetic sequencing, antibiotic testing, and more.

The results presented in all three chapters of this dissertation can be applied towards solving this scientific query. Using the hydrogel customization methods discussed in Chapter 2, hydrogels can be created to closely match a bacterial strains' optimal melting temperature and susceptibility to photosensitizer, thus maximizing bacterial tolerance to the hydrogel in which they are suspended. These tailored hydrogels can then be used for either gel layering or capture of bacteria on fiber tips. Using the gel layering techniques detailed in Chapter 3 of this dissertation, bacteria could be captured at the hydrogel-hydrogel interface. Following melting and rinsing away of the low-melting-temperature layer (thus rinsing away all excess, uncaptured bacteria), the captured bacteria could be released back into their native environments via thermally-driven controlled release. Alternatively, bacteria could also be captured in structures secured to optical fiber tips, after which the fiber tip could be re-submersed in the bacteria's native environment (i.e. a marine water sample) to allow for bacterial growth to take place.

5.2.2 Dynamic Distance Studies

Prior to the research detailed in Chapter 4 of this dissertation, significant limitations were present regarding the ability to conduct dynamic studies of bacterial interactions. By fabricating structures on a static substrate such as a coverslip, resulting bacterial clusters were immobile with respect to their surrounding environment. When attempts were made to study polymicrobial interactions, one of two situations occurred – either bacterial cultures were "nested," which allowed close contact but restricted bacteria from establishing the precise distance required for maximum synergistic activity, [13] or free bacterial clusters suspended in a viscous matrix such as mucin were deposited surrounding a fabricated structure holding a bacterial population of the desired volume and phenotypic state, which allowed for "calling distances" to be established, but maintained no control over the placement of free bacterial clusters in relation to the fabricated trap. [22]

Through capture and growth of bacterial clusters on a moveable fiber tip, precisely controlled dynamic distance studies can be conducted in a number of ways, using one or more optical fibers. For example, traps can be fabricated on both a static coverslip and the tip of an optical fiber, after which the fiber tip is slowly manipulated with respect to the trap on the coverslip. Alternatively, traps could also be fabricated on multiple fiber tips, each of which can be individually manipulated in one common environment, from simple growth media to a more complex *in vitro* biological system such as an excised wound. While the use of a coverslip and single fiber would allow for simpler experiments to be conducted, such as what distance between two species of bacteria causes a change from synergistic to adversarial behavior, the use of multiple fibers would allow for more intricate polymicrobial studies to take place in which there is simultaneous manipulation of multiple bacterial clusters and/or species.

5.2.3 Real-Time Fluorescence Sensing

Lastly, the work presented in Chapter 4 of this dissertation, in which bacteria are trapped on the silica core of a fiber, can be expanded further to take advantage of the inherent data transmission capabilities of optical fibers themselves. As mentioned previously, optical fiber technology has grown significantly in the past few decades, resulting in the creation of low-loss multimode optical fibers capable of carrying multiple modes of light across long distances. This technology combined with the ease with which bacterial strains can be genetically altered to allow for constitutive or strictly-responsive fluorescence/luminescence presents exciting opportunities in the field of microbial sensors. While microbial sensors are not a new phenomenon, [23-28] the ability to trap bacteria while precisely controlling their population and density is a previously unforeseen technique.

Using the technology detailed in Chapter 4 of this dissertation combined with a light-sensitive detector such as a photomultiplier tube (PMT), a real-time, deployable sensor could be developed for use in both *in vitro* and *in vivo* studies. For example, a bacterial strain genetically modified to exclusively fluoresce in the presence of quorum sensing (QS) could be trapped on an optical fiber and introduced to a remote location such as a chronic wound. Upon detection of QS molecules (thus indicating communication occurring between different bacterial populations), the captured cells would begin to fluoresce via a gfp expressor gene, and the light produced by this fluorescence would be transmitted through the optical fiber core and collected as photon counts by the PMT.

Real-time microbial sensors containing bacterial microclusters of physiologically relevant size and density present exciting future capabilities regarding the dynamic study of polymicrobial interactions. Due to the increasing prevalence of bacteria-induced medical issues such as antibiotic resistance, chronic wounds, and diseases like cystic fibrosis, there has never been a more important time to investigate the unique behaviors of bacteria and further our understanding of phenomena such as QS and formation of biofilms. The minimally invasive nature of optical fibers coupled with advances in multiphoton lithography create a unique experimental process that will allow for dynamic sensing to take place in a wide variety of scenarios. Combined with the customizable, biomimetic hydrogels presented in Chapter 2 of this dissertation, sensors can be created and customized for a wide variety of biological applications, occurring in both physiological (i.e. chronic wounds) and environmental (i.e. seawater) conditions.

5.4 REFERENCES

1. Tong, M.H., *et al*. *Multiphoton photochemical crosslinking-based fabrication of protein micropatterns with controllable mechanical properties for single cell traction force measurements*. Scientific Reports, 2016. **6**(1): 1-12.
2. Wust, S., Godla, M.E., Muller, R., and Hofmann, S. *Tunable hydrogel composite with two-step processing in combination with innovative hardware upgrade for cell-based three-dimensional bioprinting*. Acta Biomaterialia, 2014. **10**(2): 630-640.
3. Skardal, A., *et al*. *A tunable hydrogel system for long-term release of cell-secreted cytokines and bioprinted in situ wound cell delivery*. J. of Biomed. Mat. Res. Part B: App. Biomat., 2016. **105**(7): p. 1986-2000.
4. Kaehr, B. and Shear, J.B. *Multiphoton fabrication of chemically responsive protein hydrogels for microactuation*. PNAS, 2008. **105**(26): p. 8850-8854.
5. Chia, H.N. and Wu, B.W., *Recent advances in 3D printing of biomaterials*. J. or Biological Eng., 2015. **9**(4): p. 1-14.
6. Klouda, L., and Mikos, A.G. *Thermoresponsive hydrogels in biomedical applications*. Euro. J. of Pharm. And Biopharm., 2008. **68**(1): p. 34-45.
7. Connell, J.L., Ritschdorff, E.T., and Shear, J.B. *Three-dimensional printing of photoresponsive biomaterials for control of bacterial microenvironments*. Anal. Chem., 2016. **88**: p. 12264-12271.
8. Yan, H., Saiani, A., Gough, J.E., and Miller, A.F. *Thermoreversible protein hydrogel as cell scaffold*. Biomacromolecules, 2006. **7**(10): p. 2776-2782.
9. Ziv, K., *et al. A tunable silk-alginate hydrogel scaffold for stem cell culture and transplantation.* Biomaterials, 2014. **35**(12): p. 3736-3743.
10. Barry III, R.A., *et al. Direct-write assembly of 3D hydrogel scaffolds for guided cell growth*. Adv. Mat., 2009. **21**(23): p. 2407-2410.
11. Gao, M., *et al*. *A crucial role for spatial distribution in bacterial quorum sensing*. Scientific Reports, 2016. **6**: p. 1-10.
12. Connell, J.L., Whiteley, M. and Shear, J.B. *Sociomicrobiology in engineered landscapes*. Nature Chem. Bio., 2012. **8**(1): p. 10-13.
13. Connell, J.L., Ritschdorff, E.T., Whiteley, M., and Shear, J.B. *3D printing of microscopic bacterial communities*. PNAS, 2013. **110**(46): p. 18380-18385.
14. Spivey, E.C., *et al. Multiphoton lithography of unconstrained three-dimensional protein microstructures.* Adv. Func. Mat., 2013. **23**: p. 333-339.

15. Seidlits, S.K., Schmidt, C.E., and Shear, J.B. *High-resolution patterning of hydrogels in three dimensions using direct-write photofabrication for cell guidance*. Adv. Func. Mat., 2009. **19**: p. 3543-3551.

16. Connell, J.L., Kim, J., Shear, J.B., Bard, A.J., and Whiteley, M. *Real-time monitoring of quorum sensing in 3D-printed bacterial aggregates using scanning electrochemical microscopy.* PNAS, 2014. **111**(51): p. 18255-18260.

17. Stewart, E.J. *Growing unculturable* bacteria. J. Bacteriology, 2012. **194**(16): p. 4151-4160.

18. Schloss, P.D. and Handelsman, J. *Metagenomics for studying unculturable microorganisms: cutting the Gordian knot.* Genome Biol, 2005. **6**(8): p. 1-4.

19. Pham, V.H.T., and Kim, J. Cultivation of unculturable soil bacteria. Trends in Biotech., 2012. 30(9): p. 475-484.

20. Eilers, H., Pernthaler, J., Glockner, O. and Amann, R. *Culturability and in situ abundance of pelagic bacteria from the North Sea.* App. Environ. Microbiol., 2000. **66**(7): p. 3044-3051.

21. Tanaka, Y. and Benno, Y. *Application of a single-colony coculture technique to the isolation of hitherto unculturable gut bacteria*. Microbiol. Immunol., 2015. **59**: p. 63-70.

22. Darch, S.E., *et al. Spatial determinants of quorum signaling in a Pseudomonas aeruginosa infection model*. PNAS, 2018. **115**(18): p. 4779-4784.

23. Polyak, B., Bassis, E. Novodvorets, A., Belkin, S., and Marks, R.S. Bioluminescent whole cell optical fiber sensor to genotoxicants: system optimization. Sensors and Actuators B: Chem., 2001. 74(1): p. 18-26.

24. Polyak, B., Bassis, E., Novodvorets, A., Belkin, S., and Marks, R.S. Optical fiber bioluminescent whole-cell microbial biosensors to genotoxicants. Water Sci. Technol., 2000. 42(1): p. 305-311.

25. Yaliang, S., Ticho, Z., Jianli, G., and Yiyong, L. *Dark variants of luminous bacteria whole cell bioluminescent optical fiber sensor to genotoxicants.* J. Huazhong Univ. Sci. Technol., 2004. **24**(5): p. 507-59.

26. Kumar, J., Jha, S.K., and D'Souza, S.F. *Optical microbial biosensor for detection of methyl parathion pesticide using Flavobacterium sp. whole cells adsorbed on glass fiber filters as disposable biocomponent.* Biosens. Bioelect., 2006. **21**(11): p. 2100-2105.

27. Eltzov, E. and Marks, R.S. *Whole-cell aquatic biosensors*. Anal. Bioanal. Chem., 2011. **400**(4): p. 895-913.

28. Futra, D., Heng, L.Y., Ahmad, A., Surif, S., Ling, T.L. *An optical biosensor from green fluorescent Escherichia coli for the evaluation of single and combined heavy metal toxicities.* Sensors, 2015. **15**(6): p. 12668-12681.

Bibliography

1. Ahmed, E.M. *Hydrogel: preparation, characterization, and applications: a review*. J. Adv. Research, 2015. **6**(2): p. 105-121.

2. Anjum, S., Arora, A., Alam, M.S., and Gupta, B. *Development of antimicrobial and scar preventive chitosan hydrogel would dressings*. Int. J. Pharma. **508**(1): p. 92-101.

3. Antunes, L.C.M., Ferreira, R.B.R., Buckner, M.M.C., and Finlay, B.B. *Quorum sensing in bacterial virulence*. Microbio., 2010. **156**: p. 2271-2282.

4. Ashley, G.W., Henise, J., Reid, R., Santi, D.V. *Hydrogel drug delivery system with predictable and tunable drug release and degradation rates*. PNAS, 2013. **110**(6): p. 2318-2323.

5. Balakrishnan, B., Mohanty, M., Umashankar, P.R., and Jayakrishnan, A. *Evaluation of an in situ forming hydrogel would dressing based on oxidized alginate and gelatin.* Biomaterials, 2005. **26**(32): p. 6335-6342.

6. Ballato, J. and Dragic, P. *Glass: the carrier of light – a brief history of optical fiber*. Int. J. Appl. Glass Sci., 2016. **7**(4): p. 413-422.

7. Barry III, R.A., *et al. Direct-write assembly of 3D hydrogel scaffolds for guided cell growth*. Adv. Mat., 2009. **21**(23): p. 2407-2410.

8. Basu, S., Banerjee, D., Chowdhury, R. and Bhattacharya, P. *Controlled release of microencapsulated probiotics in food matrix*. J. Food Eng., 2018. **238**: p. 6169.

9. Basu, S. and Campagnola, P.J. *Properties of crosslinked protein matrices for tissue engineering applications synthesized by multiphoton excitation*. J. of Biomed. Mat. Research, 2004. **71A**(2): p 359-368.

10. Biran, I., Rissen, D.M., Ron, E.Z., and Walt, D.R. *Optical imaging fiber-based live bacterial cell array biosensor.* Anal. Biochem., 2003. **315**(1): p. 106-113.

11. Bjarnsholt, T., et al. *Quorum sensing and virulence of Pseudomonas aeruginosa during lung infection of cystic fibrosis patients*. PLoS One, 2010. **5**(4): p. 1-11.

12. Bosman, W.M.P.F., *et al*. *Treatment of types II-IV endoleaks by injecting biocompatible elastomer (PDMS) in the aneurysm sac: an in vitro study*. J. Endovasc. Therapy, 2011. **18**: p. 205-213.

13. Calafiore, G., *et al. Campanile Near-field probes fabricated by nanoimprint lithography on the facet of an optical fiber*. Sci. Rep., 2017. **7**: p. 1-7

14. Castaneda-Tamez, P., *et al. Pyocyanin restricts social cheating in Pseudomonas aeruginosa.* Front. Microbiol., 2018. **9**: p. 1-10.

15. Chenari, Z., Latifi, H., Ghamari, S., Hashemi, R.S., and Doroodmand, F. *Adiabatic tapered optical fiber fabrication in two step etching.* Optics Laser Tech., 2016. **76**: p. 91-95.

16. Chia, H.N. and Wu, B.W., *Recent advances in 3D printing of biomaterials*. J. or Biological Eng., 2015. **9**(4): p. 1-14.

17. Childs, A., *et al. Fabricating customized hydrogel contact lens*. Sci. Rep., 2016. **6**(1): p. 1-9.

18. Cho, H., *et al. Self-organization in high density bacterial colonies: efficient crowd control*. PLoS Biology, 2007. **5**: p. 2614-2623.

19. Cho, K., *et al. Enhanced two-photon excited fluorescence in three-dimensinally crosslinked bovine serum albumin microstructures.* Optics Express, 2011. **19**(12): p. 11732-11739.

20. Chou, S., Luo, L., Lai, J., and Ma, D.H. *On the importance of bloom number of gelatin to the development of biodegradable in situ gelling copolymers for intracameral drug delivery*. Int. J. Pharmaceutics, 2016. **511**: p. 30-43.

21. Cojoc, G., *et al. Optical micro-structures fabricated on top of optical fibers by means of two-photon photopolymerization*. Microelectronic Eng., 2010. **87**: p. 876-879.

22. Connell, J.L., *et al. Probing prokaryotic social behaviors with bacterial "lobster traps."* mBio, 2010. **4**: p. 202-210.

23. Connell, J.L., Kim, J., Shear, J.B., Bard, A.J., and Whiteley, M. *Real-time monitoring of quorum sensing in 3D-printed bacterial aggregates using scanning electrochemical microscopy.* PNAS, 2014. **111**(51): p. 18255-18260.

24. Connell, J.L., Ritschdorff, E.T., Whiteley, M., and Shear, J.B. *3D printing of microscopic bacterial communities*. PNAS, 2013. **110**(46): p. 18380-18385.

25. Connell, J.L., Ritschdorff, E.T., and Shear, J.B. *Three-dimensional printing of photoresponsive biomaterials for control of bacterial microenvironments*. Anal. Chem., 2016. **88**: p. 12264-12271.

26. Connell, J.L., Whiteley, M., and Shear, J.B. *Sociomicrobiology in engineered landscapes*. Nature Chem. Bio., 2012. **8**(1): p. 10-13.

27. Correia, R., James, S., Lee, S.W., Morgan, S.P. and Korposh, S. *Biomedical application of optical fibre sensors*. J. Optics., 2018. **20**(7): p. 1-25.

28. Dang, T., Kim, Y.H., Choi, J.H., and Kim, G. *A novel simple preparation method of a hydrogel mold for PDMS micro-fluidic device fabrication*. J. Micromech. And Microeng., 2011. **22**: p. 1-8.

29. Darch, S.E., *et al. Spatial determinants of quorum signaling in a Pseudomonas aeruginosa infection model*. PNAS, 2018. **115**(18): p. 4779-4784.

30. Davidson, H.J. and Kuonen, V.J. *The tear film and ocular mucins*. Veterinary Ophtham., 2004. **7**(2): p. 71-77.

31. DeLeon, S., *et al. Synergistic interactions of Pseudomonas aeruginosa and Staphylococcus aureus in an in vitro would model*. Infection and Immunity, 2014. **82**: p. 4718-4728.

32. Duan, B., Hockaday, L.A., Kang, K.H., and Butcher, J.T. *3D bioprinting of heterogeneous aortic valve conduits with alginate/gelatin hydrogels.* J. of Biomed. Mat. Res. Part A, 2013. **101A**: p. 1255-1264.

33. Dunn, A.C., *et al*. *Lubricity of surface hydrogel layers.* Tribol. Lett., 2013. **49**: p. 371-378.

34. Eilers, H., Pernthaler, J., Glockner, O. and Amann, R. *Culturability and in situ abundance of pelagic bacteria from the North Sea.* App. Environ. Microbiol., 2000. **66**(7): p. 3044-3051.

35. El-Ghaffar, M.A.A., Hashem, M.S., El-Awady, M.K. and Rabie, A.M. *pH-sensitive sodium alginate hydrogels for riboflavin controlled release.* Carbohydrate Polymers, 2012. **89**: p. 667-675.

36. Elliott, J., Simoska, O., Karasik, S., Shear, J.B., and Stevenson, K.J. *Transparent carbon ultramicroelectrode arrays for the electrochemical detection of a bacterial warfare toxin, pyocyanin.* Anal. Chem., 2017. **89**(12): p. 6285-6289.

37. Eltzov, E., and Marks, R.S. *Whole-cell aquatic biosensors.* Anal. Bioanal. Chem., 2011. **400**(4): p. 895-913.

38. Ergaieg, K. and Seux, R. *A comparative study of the photoinactivation of bacteria by meso-substituted cationic porphyrin, rose bengal, and methylene blue*. Desalination, 2009. **246**: p. 353-362.

39. Fang, X. and Tan, W. *Imaging single fluorescent molecules at the interface of an optical fiber probe by evanescent wave excitation.* Anal. Chem., 1999. **71**(15): p. 3101-3105.

40. Favre-Bonte, S., Kohler, T., and Van Delden, C. *Biofilm formation by Pseudomonas aeruginosa: role of the C4-HSL cell-to-cell signal and inhibition by azithromycin.* J. Antimicrobial Chemotherapy, 2003. **52**(4): p. 598-604.

41. Foote, C.S. *Definition of type I and type II photosensitized oxidation.* Photochem. and Photobio., 1991. **54**: p. 659.

42. Futra, D., Heng, L.Y., Ahmad, A., Surif, S., Ling, T.L. *An optical biosensor from green fluorescent Escherichia coli for the evaluation of single and combined heavy metal toxicities.* Sensors, 2015. **15**(6): p. 12668-12681.

43. Gao, M., *et al*. *A crucial role for spatial distribution in bacterial quorum sensing*. Scientific Reports, 2016. **6**: p. 1-10.

44. Gaowa, A., *et al*. *Combination of hybrid peptide with biodegradable gelatin hydrogel for controlled release and enhancement of anti-tumor activity in vivo*. J. Controlled Release, 2014. **176**: p. 1-7.

45. Gloge, D. and Marcatelli, A.J. Multimode theory of graded-core fibers. Bell Sys. Tech. J., 1973. 52(9): p. 1563-1579.

46. Guvendiren, M., and Burdick, J.A. *Engineering sythentic hydrogel microenvironments to instruct stem cells*. Curr. Opin. Biotech., 2013. **24**(5): p. 841-846.

47. Hardy, J.G., *et al*. *Multiphoton microfabrication of conducting polymer-based biomaterials*. J. Mat. Chem. B, 2015. **3**(25): p. 5001-5004.

48. Helary, C., *et al. Concentrated collagen hydrogels as dermal substitutes.* Biomat., 2010. **31**(3): p. 481-490.

49. Hindmarsh, J.P., Prasad, J., Gopal, P., and Singh, H. *NMR measurement of bacteria death kinetics during heat stress*. LWT Food Sci. Tech., 2015. **60**(2): p. 876-880.

50. Hoare, T.R. and Kohane, D.S. *Hydrogels in drug delivery: progress and challenges*. Polymer, 2008. **49**(8): p. 1993-2007.

51. Hori, Y., Argueso, P., Spurr-Michaud, S., and Gipson, I.K. *Mucins and contact lens wear*. Cornea, 2006. **25**(2): p. 176-181.

52. Horiguchi, M. and Osanai, H. *Spectral losses of low-OH-content optical fibers*. Electron. Lett., 1976. 12: p. 310-312.

53. Hu, X., *et al. A novel method to prepare homogeneous biocompatible graphene-based PDMS composites with enhanced mechanical, thermal, and antibacterial properties.* Polymer Composites, 2018. **0**(0): p. 1-10.

54. Hu, X., Li, D., Zhou, F., and Gao, C. *Biological hydrogel synthesized from hyaluronic acid, gelatin and chondroitin sulfate by click chemistry*. Acta Biomaterialia, 2011. **7**(4): p. 1618-1626.

55. Huygens, C. Traite de la Lumiere. 1690.

56. Huynh, C.T., Nguyen, M.K., and Lee, D.S. *Biodegradable pH/temperature-sensitive oligo(β-amino ester urethane) hydrogels for controlled release of doxorubicin.* Acta Biomaterialia, 2011. **7**: p. 3123-3130.

57. Hwang, Y., Paydar, O.H., and Candler, R.N. *3D printed molds for non-planar PDMS microfluidic channels*. Sensors and Actuators A: Phys., 2015. **226**: p. 137-142.

58. Jacomme, L. Wavelength dependent propagation in optical multimode fibers. Optics Comm., 1978. 24(2): p. 213-216.

59. Jayaseelan, S., Ramaswamy, D., Dharmaraj, S. *Pyocyanin: production, applications, challenges and new insights*. World J. Microbiol. Biotech., 2014. **30**(4): p. 1159-1168.

60. Jeon, O., Bouhadir, K.H., Mansour, J.M., and Alsberg, E. *Photocrosslinked alginate hydrogels with tunable biodegradation rates and mechanical properties.* Biomat., 2009. **30**(14): p. 2724-2734.

61. Jin, M., *et al*. *Super-hydrophobic PDMS surface with ultra-low adhesive force.* Macromol. Rapid Comm., 2005. **26**(22): p. 1805-1809.

62. Kaehr, B. and Shear, J.B. *Multiphoton fabrication of chemically responsive protein hydrogels for microactuation*. PNAS, 2008. **105**(26): p. 8850-8854.

63. Kaehr, B. and Shear, J.B. *High-throughput design of microfluidics based on directed bacterial motility.* Lab on a Chip, 2009. **18**: p. 2632-2637.

64. Kalabova, H., Pospisilova, M., Siroka, R., and Kuncova, G. *A biosensor with encapsulated bioreporters – optical fiber element for enhanced detection of bioluminescence.* Measurement Sci. Technol., 2018. **29**(7): p. 1-7.

65. Kanamori, Y., Okochi, M., and Hane, K. *Fabrication of antireflection subwavelength gratings at the tips of optical fibers using UV nanoimprint lithography*. Optics Express, 2013. **21**(1): p. 322-328.

66. Kano, H. and Hamaguchi, H. *In-vivo multi-nonlinear optical imaging of a living cell using a supercontinuum light source generated from a photonic crystal fiber.* Optics Express, 2006. **14**(7): p. 2798-2804.

67. Kao, C.K. and Hockham, G.A. *Dielectric-fiber surface waveguides for optical frequencies.* Proc. IEE, 1966. **133**: p. 1151-1158.

68. Kapron, F.P., Keck, D.B., and Maurer, R.D. *Radiation losses in glass optical waveguides*. Appl. Phys. Lett., 1970. **17**: p. 144-153.

69. Kariminik, A., Baseri-Salehi, M., and Kheirkhah, B. *Pseudomonas aeruginosa quorum sensing modulates immune responses: an updated review article*. Immun. Lett., 2017. **190**: p. 1-6.

70. Keck, D.B., Maurer, R.D., and Shultz, P.C. *On the ultimate lower limit of attenuation in glass optical waveguids.* Appl. Phys. Lett., 1973. **22**(7): p. 307-309.

71. Kepler, J. *Dioptrice*. 1611.

72. Khademohosseini, A. and Langer, R. *Microengineered hydrogels for tissue engineering*. Biomat., 2007. **28**(34): p. 5087-5092.

73. Khmel, I.A. *Quorum-sensing regulation of gene expression: fundamental and applied aspects and the role in bacteria communication*. Microbiol., 2006. **75**(4): p. 390-397.

74. Kim, H.J., Boedicker, J.Q., Choi, J.W., and Ismagilov, R.F. *Defined spatial structure stabilizes a synthetic multispecies bacterial community*. PNAS, 2008. **105**: p. 18188-18193.

75. Kim, J., Conway, A., and Chauhan, A. *Extended delivery of ophthalmic drugs by silicone hydrogel contact lenses*. Biomaterials, 2008. **29**(14): p. 2259-2269.

76. Kim, J., Connell, J.L., Whiteley, M., and Bard, A.J. *Development of a versatile in vitro platform for studying biological systems using micro-3D printing and scanning electrochemical microscopy*. Anal. Chem., 2014. **86**(24): p. 12327-12333.

77. Kim, K., *et al. HHQ and PQS, two Pseudomonas aeruginosa quorum-sensing molecules, down regulate the innate immune responses through the nuclear factor-κB pathway.* Immunology, 2010. **129**(4): p. 578-588.

78. Kiyonaka, S., Sugiyasu, K., Shinkai, S., and Hamachi, I. *First thermally responsive supramolecular polymer based on glycosylated amino acid.* J. Amer. Chem. Soc., 2012. **124**(37): p. 10964-10955.

79. Klouda, L., and Mikos, A.G. *Thermoresponsive hydrogels in biomedical applications*. Euro. J. of Pharm. And Biopharm., 2008. **68**(1): p. 34-45.

80. Koehler, J., Brandl, F.P., and Goepferich, A.M. *Hydrogel wound dressings for bioactive treatment of acute and chronic wounds*. Euro. Polymer J., 2018. **100**: p. 1-11.

81. Kumar, J., Jha, S.K., and D'Souza, S.F. *Optical microbial biosensor for detection of methyl parathion pesticide using Flavobacterium sp. whole cells adsorbed on glass fiber filters as disposable biocomponent.* Biosensors and Bioelectronics, 2006. **21**(11): p. 2100-2105.

82. Kusters, I., *et al*. *Taming membranes: functional immobilization of biological membranes in hydrogels*. PLoS One, 2011. **6**(5): p. 1-9.

83. Lacin, N.T. *Development of biodegradable antibacterial cellulose based hydrogel membranes for would healing*. Int. J. Bio. Macromol., 2014. **67**: p. 2-27.

84. Ladet, S.G. Tahiri, K., Montembault, A.S., Domard, A.J. and Corvol, M.T.M. *Multi-membrane chitosan hydrogels as condrocytic cell bioreactors.* Biomaterials, 2011. **32**(23): p. 5354-5364.

85. LaFratta, C.N., Fourkas, J.T., Baldacchini, T., and Farrer, R.A. *Multiphoton fabrication*. Angew. Chem. Int. Ed., 2007. **46**: p. 6238-6258.

86. Lai, J. *The role of bloom index of gelatin on the interaction with retinal pigment epithelial cells*. Int. J. Molec. Sci., 2009. **10**: p. 3442-3456.

87. Lai, J., *et al*. *Low bloom strength gelatin as a carrier for potential use in retinal sheet encapsulation and transplantation*. Biomacromolecules, 2009. **10**: p. 310-319.

88. Lax, S. and Gilbert, J.A. *Hospital-associated microbiota and implications for nosocomial infections.* Trends in Molec. Med., 2015. **21**: p. 427-432.

89. Lee, K.Y. and Mooney, D.J. *Hydrogels for tissue engineering*. Chemical Reviews, 2001. **101**(7): p. 1869-1880.

90. Li, P. *et al. Autoinducer sensing microarrays by reporter bacteria encapsulated in hybrid supramolecular-polysaccharide hydrogels*. Macromolec. Biosci., 2017. **17**(1700176): p. 1-13.

91. Lieleg, O. and Ribbeck, K. *Biological hydrogels as selective diffusion barriers*. Trends in Cell Biology, 2011. **21**(9): p. 543-551.

92. Lin, C., *et al. Investigation of two-photon excited fluorescence increment via crosslinked bovine serum albumin.* Optics Express, 2012. **20**(13): p. 13669-13676.

93. Lin, C., and Metters, A.T. *Hydrogels in controlled release formulations: network design and mathematical modeling*. Adv. Drug Delivery Rev., 2006. **58**(12): p. 1379-1408.

94. Lin, Y., et al. *Preparation and evaluation of chitosan biocompatible electronic skin*. Computers in Industry, 2018. **100**: p. 1-6.

95. Lin, Y., Zou, Y., Mo, Y., Guo, J., and Lindquist, R.G. *E-beam patterned gold nanodot arrays on optical fiber tips for localized surface plasmon resonance biochemical sensing.* Snesors, 2010. **10**(10): p. 9397-9406.

96. Lopes, S.P., Azevedo, N.F., and Pereira, M.O. *Developing a model for cystic fibrosis sociomicrobiology based on antibiotic and environmental stress*. Int. J. Med. Microbio., 2017. **307**(8): p. 460-470.

97. Luksiene, Z. *New approach to inactivation of harmful and pathogenic microorganisms by photosensitization*. Food Technol. Biotechnol., 2005. **43**(4): p. 411-418

98. Lutolf, M.P., Raeber, G.P., Zisch, A.H., Tirelli, N., and Hubbell, J.A. *Cell-responsive synthetic hydrogels.* Adv. Mat., 2003. **15**: p. 888-892.

99. Ma, J., *et al. Multiphoton fabrication of fibronectin-functionalized protein micropatterns: stiffness-induced maturation of cell-matrix adhesions in human*

mesenchymal stem cells. ACS Appl. Mater. Interfaces, 2017. **9**(35): p. 29469-29480.

100. Macchi, E.G., *et al. Optical fiber sensors-based temperature distribution measurement in ex vivo radiofrequency ablation with submillimeter resolution*. J. Biomed. Opt., 2014. **19**(11): p. 1-7.

101. Marra, A.R., Bearman. G.M.L., Wenzel, R.P., and Edmond, M.B. *Comparison of the systemic inflammatory response syndrome between monomicrobial and polymicrobial Pseudomonas aeruginosa nosocomial bloodstream infections*. BMC Infect. Diseases, 2005. **5**:94, p. 1-7.

102. McCain, M.L., Agarwal, A., Nesmith, H.W., Nesmith, A.P., and Parker, K.K. *Micromolded gelatin hydrogels for extended culture of engineered cardiac tissues.* Biomaterials, 2014. **35**(21): p. 5462-5471.

103. Mellbye, B. and Schuster, M. *The sociomicrobiology of antivirulence drug resistance: a proof of concept.* mBio, 2011. **2**(5): p. 1-4.

104. Mendez, U., Zhou, H., and Shikanov, A. *Synthetic PEG hydrogel for engineering the environment of ovarian follicles*. Biomat. Tissue Eng., 2018. **1758**: p. 115-128.

105. Michie, K.L., Cornforth, D.M., and Whiteley, M. *Bacterial tweets and podcasts #signaling#eavesdropping#microbialfightclub.* Molec. Biochem. Parasit., **2016**. 208: p. 41-48.

106. Miller, M.B. and Bassler, B.L. *Quorum sensing in bacteria*. Ann. Rev. Microbio., 2001. **55**: p. 165-199.

107. Mitra, P.P., and Stark, J.B. *Nonlinear limits to the information capacity of optical fibre communications.* Nature, 2001. **411**(6841): p. 1027-1030.

108. Mohan, R., *et al. A microfluidic approach to study the effect of bacterial interactions on antimicrobial susceptibility in polymicrobial cultures.* RSC Adv., 2015. **5**: p. 35211-35223.

109. Moorjani, S., Nielson, R., Chang, X.A., and Shear, J.B. *Dynamic remodeling of subcellular chemical gradients using a multi-directional flow device*. Lab on a Chip, 2010. **10**: p. 2139-2146.

110. Morales-Delgado, E.E., *et al. Three-dimensional microfabrication through a multimode optical fiber.* Optics Express, 2017. **25**(6): p. 1-19.

111. Morales-Hurtado, M., Zeng, X., Gonzalez-Rodriguez, P., Ten Elshof, J.E., and van der Heide, E. *A new water absorbable mechanical epidermal skin equivalent: the combination of hydrophobic PDMS and hydrophilic PVA hydrogel*. J. Mech. Behav. Biomed. Mat., 2015. **46**: p. 305-317.

112. Mousavi, S.H., Tavakkol-Afshari, J., Brook, A., and Jafari-Anarkooli, I. *Direct toxicity of rose bengal in MCF-7 cell line: role of apoptosis.* Food Chem. Toxic., 2009. **47**: p. 855-859.

113. Nguyen, K.T. and West, J.L. *Photopolymerizable hydrogels for tissue engineering applications*. Biomat., 2002. **23**(22): p. 4307-4314.

114. Nguyen, M.K. and Alsberg, E. *Bioactive factor delivery strategies from engineered polymer hydrogels for therapeutic medicine*. Progress in Polymer Sci., 2014. **39**: p. 1235-1265.

115. Nielson, R., Kaehr, B., and Shear, J.B. *Microreplication and design of biological architectures using dynamic-mask-based multiphoton lithography*. Small, 2009. **5**: p. 120-125.

116. Ochsner, M. *Photophysical and photobiological processes in the photodynamic therapy of tumors*. J. Photochem. and Photobiol., 1997. **39**: p. 1-18.

117. Osorio, F.A., Bilbao, E., Bustos, R., and Alvarez, F. *Effects of concentration, bloom degree, and pH on gelatin melting and gelling temperatures using small amplitude oscillatory rheology*. Int. J. Food Properties, 2007. **10**: p. 841-851.

118. Parsek, M.R. and Greenberg, E.P. *Sociomicrobiology; the connections between quorum sensing and biofilms.* Trends Microbiol., 2005. **13**: p. 27-33.

119. Payne, D.N. and Gambling, W.A. *New silica-based low-loss optical fibre*. Electron. Lett., 1974. **10**(15): p. 289-290.

120. Peng, C. and Chauhan, A. *Ion transport in silicone hydrogel contact lenses*. J. Membrane Sci., 2012. **399**: p. 95-105.

121. Peng, C., and Chauhan, A. *Extended cyclosporine delivery by silicone-hydrogel contact lenses.* J. Controlled Release, 2011. **154**(3): p. 267-274.

122. Peng, X., Ren, J., Zhong, L., Peng, F., and Sun, R. *Xylan-rich hemicelluloses-graft-acrylic acid ionic hydrogels with rapid responses to pH, salt, and organic solvents*. J. of Agricultural and Food Chemistry, 2011. **59**(15): p. 8208-8215.

123. Petrova, E., Liopo, A., Nadvoretskiy, V., and Ermilov, S. *Imaging technique for real-time temperature monitoring during cryotherapy of lesions*. J. Biomed. Opt. 2016. **21**(11): p. 1-10.

124. Pham, V.H.T., and Kim, J. *Cultivation of unculturable soil bacteria.* Trends in Biotech., 2012. **30**(9): p. 475-484.

125. Phan, C., *et al*. *Effects of antifungal soaked silicone hydrogel contact lenses on Candida albicans in an agar eye model*. Eye & Contact Lens: Science and Clinical Practice, 2016. **42**(5): p. 313-317.

126. Pidwill, G.R., Rego, S., Jenkinson, H.F., Lamont, R.J. and Nobbs, A.H. *Coassociation between group B Streptococcus and Candida albicans promotes interactions with vaginal epithelium*. Infection and Immunity, 2018. **86**(4): p. 1-18.

127. Pittet, D., Li, N., and Wenzel, R.P. *Association of secondary and polymicrobial nosocomial bloodstream infections with higher mortality*. Euro. J. Clin. Microbio. Infec. Disease, 1993. **12**(11): p. 813-819.

128. Pitts, J.D., Campagnola, P.J., Epling, G.A., and Goodman, S.L. *Submicron multiphoton free-form fabrication of proteins and polymers: studies of reaction efficiencies and applications in sustained release*. Macromolecules, 2000. **33**: p. 1514-1523.

129. Polyak, B., Bassis, E., Novodvorets, A., Belkin, S., and Marks, R.S. *Optical fiber bioluminescent whole-cell microbial biosensors to genotoxicants.* Water Sci. Technol., 2000. **42**(1): p. 305-311.

130. Polyak, B., Bassis, E. Novodvorets, A., Belkin, S., and Marks, R.S. *Bioluminescent whole cell optical fiber sensor to genotoxicants: system optimization.* Sensors and Actuators B: Chem., 2001. 74(1): p. 18-26.

131. Pomeroy, L.R. and Wiebe, W.J. *Temperature and substrates as interactive limiting factors for marine heterotrophic bacteria*. Aquat. Microb. Ecol., 2001. **23**: p. 187-204.

132. Pritchard, D.I. *Immune modulation by Pseudomonas aeruginosa quorum-sensing signal molecules*. Int. J. Med. Microbio., 2006. **296**(2): p. 111-116.

133. Qiao, H., Pham, C.M., Walther, H., Subbaraman, L.N., and Jones, L. *Depth profile assessment of the early phase deposition of lysozyme on soft contact lens materials using a novel in vitro eye model*. Eye Contact Lens, 2018. **44**: S11-S18.

134. Qiu, Y. and Park, K. *Environment-sensitive hydrogels for drug delivery*. Adv. Drug Delivery Rev., 2012. **64**: p. 49-60.

135. Ramsey, M.M. and Whiteley, M. *Polymicrobial interactions stiumulate resistance to host innate immunity through metabolite perception*. PNAS, 2009. **106**(5): p. 1578-1583.

136. Rhoads, M.K., *et al*. *Incorporating LsrK AI-2 quorum quenching capability in a functionalized biopolymer capsule*. Biotech. Bioeng., 2018. **115**: 278-289.

137. Roncarati, D. and Scarlato, V. *Regulation of heat-shock genes in bacteria: from signal sensing to gene expression output*. FEMS Microbio. Rev., 2017. **41**(4): p. 549-574.

138. Ruan, W., Lian, Y., Zhen, T., Huang, L., and Qiao, J. *pH-response superabsorbent hydrogel synthesized by ultraviolet photopolymerization*. J. of App. Polymer Sci., 2006. **103**(3)1847-1852.

139. Rudy, A., *et al*. *Lubricous hydrogel surface coatings on polydimethylsiloxane (PDMS).* Tribiology Lett., 2017. **65**(3): 1-11.

140. Russo, V. *Optical fibre delivery systems for laser angioplasty and laser treatment of tumours.* Lasers in Medical Sci., 1988. **3**(1): p. 207-211.

141. Samsom, M., *et al. In vitro friction testing of contact lenses and human ocular tissues: effect of proteoglycan 4 (PRG4).* Tribology Int., 2015. **89**: p. 27-33.

142. Sanchez, D.M., Gresil, M., and Soutis, C. *Distributed internal strain measurement during composite manufacturing using optical fibre sensors*. Composites Sci. Tech., 2015. **120**: p. 49-57.

143. Sancho, S., *et al*. *Impact of nosocomial polymicrobial bloodstream infections on the outcome in critically ill patients*. Euro. J. Clin. Microbio. Infec. Disease, 2012. **31**(8): p. 1791-1796.

144. Schuetz, Y.B., Gurny, R., and Jordan, O. *A novel thermoresponsive hydrogel based on chitosan*. Euro. J. of Pharm. And Biopharm., 2008. **68**(1): p. 19-25.

145. Schloss, P.D. and Handelsman, J. *Metagenomics for studying unculturable microorganisms: cutting the Gordian knot.* Genome Biol, 2005. **6**(8): p. 1-4.

146. Seidlits, S.K., *et al. Fibronectin-hyaluronic acid composite hydrogels for three-dimensional endothelial cell culture*. Acta Biomaterialia, 2011. **7**(6): p. 2401-2409.

147. Seidlits, S.K., Schmidt, C.E., and Shear, J.B. *High-resolution patterning of hydrogels in three dimensions using direct-write photofabrication for cell guidance.* Adv. Func. Mat., 2009. **19**: p. 3543-3551.

148. Shear, J.B. *Multiphoton-excited fluorescence in bioanalytical chemistry*. Anal. Chem., 1999. **71**: p. 598A-605A.

149. Shen, H.R., Spikes, J.D., Smith, C.J., and Kopecek, J. *Photodynamic cross-linking of proteins IV. Nature of the His-His bond (s) formed in the rose bengal-photosensitized cross-linking of N-benzoyl-L-histidine.* J. Photochem. Photobiol., A: Chem., 2000. **130**: p. 1-6.

150. Singh, A., Hugall, J.T., Calbris, G., and van Hulst, N.F. *Fiber-based optical nanoantennas for single-molecule imaging and sensing*. J. Lightwave Tech., 2015. **33**(12): p. 2371-2377.

151. Singh, B., Sharma, S., and Dhiman, A. *Design of antibiotic containing hydrogel wound dressings: biomedical properties and histology study of wound healing*. Int. J. Pharma. **457**(1): p. 82-91.

152. Skardal, A., *et al*. *A tunable hydrogel system for long-term release of cell-secreted cytokines and bioprinted in situ wound cell delivery*. J. of Biomed. Mat. Res. Part B: App. Biomat., 2016. **105**(7): p. 1986-2000.

153. Skindersoe, M.E., *et al. Effects of antibiotics on quorum sensing in Pseudomonas aeruginosa.* Antimicrobial Agents and Chemotherapy, 2008. **52**(10): p. 3648-3663.

154. Sollich, M., et al. *Heat stress dictates microbial lipid composition along a thermal gradien in marine sediments*. Front. Microbiol., 2017. **8**: p. 1-19.

155. Spivey, E.C., *et al. Multiphoton lithography of unconstrained three-dimensional protein microstructures.* Adv. Func. Mat., 2013. **23**: p. 333-339.

156. Spivey, E.C., Xhemalce, B., Shear, J.B., and Finkelstein, I.J. *3D-printed microfluidic microdissector for high-throughput studies of cellular aging.* Anal. Chem., 2014. **86**(15): p. 7406-7412.

157. Srivastav, A.K., *et al*. *Photosensitized rose bengal-induced phototoxicity on human melanoma cell line under natural sunlight exposure*. J. Photochem. Photobio. B: Biology, 2016. **156**: p. 87-99.

158. Stacy, A., *et al. Bacterial fight-and-flight responses enhance virulence in a polymicrobial infection*. PNAS, 2014. **111**(21): p. 7819-7824.

159. Stacy, A., Mcnally, L., Darch, S.E., Brown, S.P. and Whiteley, M. *The biogeography of polymicrobial infection.* Nature Rev. Microbio. Nature Rev., 2016. **14**: p. 93-105.

160. Stanton, M.M., Ducker, R.E., MacDonald, J.C., Lambert, C.R., and McGimpsey, W.G. *Super-hydrophobic, highly adhesive, polydimethylsiloxane (PDMS) surfaces*. J. Colloid and Interface Sci., 2012. **367**(1): p. 502-508.

161. Stewart, E.J. *Growing unculturable* bacteria. J. Bacteriology, 2012. **194**(16): p. 4151-4160.

162. Sugiura, S., *et al. On-demand microfluidic control by micropatterned light irradiation of a photoresponsive hydrogel sheet.* Lab on a Chip, 2009. **9**(2): p. 196-198.

163. Tan, H., Xiao, C., Sun, J., Xiong, D., and Hu, X. *Biological self-assembly of injectable hydrogel as cell scaffold via specific nucleobase pairing*. Chem. Comm., 2012. **48**: p. 10289-10291.

164. Tanaka, Y. and Benno, Y. *Application of a single-colony coculture technique to the isolation of hitherto unculturable gut bacteria*. Microbiol. Immunol., 2015. **59**: p. 63-70.

165. Tong, M.H., *et al*. *Multiphoton photochemical crosslinking-based fabrication of protein micropatterns with controllable mechanical properties for single cell traction force measurements*. Scientific Reports, 2016. **6**(1): 1-12.

166. Turunen, S., *et al. Pico- and femtosecond laser-induced crosslinking of protein microstructures: evaluation of processability and bioactivity.* Biofabrication, 2011. **3**(4): p. 1-14.

167. Upadhyay, A., Kandi, R., and Rao, C.P. *Injectable, self-healing, and stress sustainable hydrogel of BSA as a functional biocompatible material for controlled drug delivery in cancer cells.* ACS Sustainable Chem. Eng., 2018. **6**(3): p. 3321-3330.

168. Vaiano, P., *et al. Lab on fiber technology for biological sensing applications*. Laser Photonics Rev., 2016. **10**(6): p. 922-961.

169. Van Derlinden, E., Bernaerts, K., and Van Impe, J.F. *Accurate estimation of cardinal growth temperatures of Escherichia coli from optimal dynamic experiments*. Int. J. Food Microbio., 2008. **128**(1): 89-100.

170. Verhulsel, M., *et al*. *A review of microfabrication and hydrogel engineering for micro-organs on chips.* Biomaterials, 2014. **35**(6): p. 1816-1832.

171. Wang, H., Tu, F., Gui, Z., Lu, X., and Chu, W. *Antibiotic resistance profiles and quorum sensing-dependent virulence factors in clinical isolates of Pseudomonas aeruginosa*. Indian J. Microbio., 2013. **53**(2): 163-167.

172. Wang, J., Yun, W., Zhao, S., Zhou, Y., and He, W. *The analysis of viability for mammalian cells treated at different temperatuers and its application in cell shipment*. PLoS One, 2017. **12**(4): p. 1-16.

173. Wang, K., Buschle-Diller, G., and Wu, Y. *Thermoresponsive hydrogels from BSA esterified with low molecular weight PEG.* J. of App. Polymer Sci., 2014. **131**(20): p. 1-8.

174. Wang, Q., *et al. 3D printing with cellulose materials.* Cellulose, 2018. **25**: p. 4275-4301.

175. Wang, X., *et al*. *Modeling growth of Pseudomonas aeruginosa single cells with temperature shifts.* J. Food Safety, 2016. **36**(2016): 442-449.

176. Wang, X., *et al*. *Gelatin-based hydrogels for organ 3D bioprinting.* Polymers, 2017. **9**(401): 1-24.

177. Wessel, A.K., *et al. Oxygen limitation within a bacterial aggregate*. mBio, 2014. **5**: p. 1-9.

178. Wessel, A.K., Hmelo, L., Parsek, M.R., and Whiteley, M. *Going local: technologies for exploring bacterial microenvironments*. Nature Rev. Microbio., 2013. **11**(5): 337-348.

179. Williams, H.E., Freppon, D.J., Kuebler, S.M., Rumpf, R.C., and Melino, M.A. *Fabrication of three-dimensional micro-photonic structures on the tip of optical fibers using SU-8.* Optics Express, 2011. **19**(23): p. 22910-22922.

180. Wong, M.J.Q., *et al. Microbial herd protection mediated by antagonistic interaction in polymicrobial communities.* Microb. Ecology, 2016. **82**(23): p. 6881-6888.

181. Wright, E., Neethirajan, S., and Weng, X. *Microfluidic would model for studying the behaviors of Pseudomonas aeruginosa in polymicrobial biofilms*. Biotechnol. Bioeng., 2015. **112**: p. 2351-2359.

182. Wu, Z., Lin, X., Zou, X., Sun, J., and He, Q. *Biodegradable protein-based rockets for drug transportation and light-triggered release*. App. Mat. Interfaces, 2014. **7**: p. 250-255.

183. Wust, S., Godla, M.E., Muller, R., and Hofmann, S. *Tunable hydrogel composite with two-step processing in combination with innovative hardware upgrade for cell-based three-dimensional bioprinting*. Acta Biomaterialia, 2014. **10**(2): 630-640.

184. Ye, Y.N., *et al. Tough and self-recoverable thin hydrogel membranes for biological applications.* Adv. Func. Mat., 2018. **28**(31): p. 1-11.

185. Xavier, J.B. *Sociomicrobiology and pathogenic bacteria*. Microbiol. Spectrum, 2016. **4**(3): p. 89-101.

186. Xu, J., Liu, Z., and Erhan, S.Z. *Viscoelastic properties of a biological hydrogel produced from soybean oil*. J. of American Oil Chemists Society, 2008. **85**(3): 285-290.

187. Yaliang, S., Ticho, Z., Jianli, G., and Yiyong, L. *Dark variants of luminous bacteria whole cell bioluminescent optical fiber sensor to genotoxicants.* J. Huazhong Univ. Sci. Technol., 2004. **24**(5): p. 507-59.

188. Yan, H., Saiani, A., Gough, J.E., and Miller, A.F. *Thermoreversible protein hydrogel as cell scaffold*. Biomacromolecules, 2006. **7**(10): p. 2776-2782.

189. Yao, M. and Fang, J. *Hydrophilic PEO-PDMS for microfluidic applications*. J. Micromech. Microeng., 2012. **22**(2): p. 1-6.

190. Yi, C., *et al*. *Electroaddressing functionalized polysaccharides as model biofilms for interrogating cell signaling*. Adv. Func. Mat., 2012. **22**: 519-528.

191. Zhang, Y., Tao, L., Li, S., and Wei, Y. *Synthesis of multiresponsive and dynamic chitosan-based hydrogels for controlled release of bioactive molecules*. Biomacromol., 2011. **12**: p. 2894-2901.

192. Zhou, C., *et al*., *High water content hydrogel with super high refractive index*. Macromolecular Bioscience, 2013. **13**(11): p. 1485-1491.

193. Zhou, X., *et al*. *A pH and magnetic dual-response hydrogel for synergistic chemo-magnetic hyperthermia tumor therapy*. RSC Advances, 2018. **8**: p. 9812-9821.

194. Ziv, K., *et al*. *A tunable silk-alginate hydrogel scaffold for stem cell culture and transplantation*. Biomat., 2014. **35**(12): p. 3736-3743.

195. Zukauskas, A., Melissinaki, V., Kaskelyte, D., Farsari, M., and Malinauskas, M. *Improvement of the fabrication accuracy of fiber tip microoptical components via mode field.* J. Laser Micro Nanoeng., 2014. **9**(1): p. 68-72.

Vita

Allison Paige Myers was born in San Antonio, TX in 1990 to Doreen and Garry Myers. She completed her secondary education in 2008 at Olympia High School in Olympia, WA. After a brief stint at George Fox University in Newberg, OR, she attended Saint Martin's University in Lacey, WA, graduating Magna Cum Laude in 2013 with a Bachelor of Science in Biology and a Bachelor of Arts in Chemistry. In the fall of 2013, she enrolled in the Chemistry graduate program at the University of Texas at Austin to pursue a doctorate in Analytical Chemistry.

Permanent email address: allison.myers@utexas.edu

This dissertation was typed by the author.